INDUCING UNCERTAINTY FOR TEST-TIME PRIVACY

Muhammad H. Ashiq, **Peter Triantafillou**, **Hung Yun Tseng**, **Grigoris G. Chrysos**
: University of Wisconsin-Madison, USA
: University of Warwick, UK
{ashiq, htseng23, chrysos}@wisc.edu, p.triantafillou@warwick.ac.uk

ABSTRACT

Unlearning is the predominant method for removing the influence of data in machine learning models. However, even after unlearning, models often continue to produce the same predictions on the unlearned data with high confidence. This persistent behavior can be exploited by adversaries using confident model predictions on incorrect or obsolete data to harm users. We call this threat model, which unlearning fails to protect against, *test-time privacy*. In particular, an adversary with full model access can bypass any naive defenses which ensure test-time privacy. To address this threat, we introduce an algorithm which perturbs model weights to induce maximal uncertainty on protected instances while preserving accuracy on the rest of the instances. Our core algorithm is based on finetuning with a Pareto optimal objective that explicitly balances test-time privacy against utility. We also provide a certifiable approximation algorithm which achieves (ε, δ) guarantees without convexity assumptions. We then prove a tight, non-vacuous bound that characterizes the privacy-utility tradeoff that our algorithms incur. Empirically, our method obtains $> 3\times$ stronger uncertainty than pretraining with $< 0.2\%$ drops in accuracy on various image recognition benchmarks. Altogether, this framework provides a tool to guarantee additional protection to end users.

1 INTRODUCTION

Data privacy is increasingly important for large-scale machine learning (ML), where models are often trained on sensitive user instances. To protect sensitive data, governments have implemented policies like the right to be forgotten (RTBF) (European Parliament and Council of the European Union, 2016) which mandates that a model provider, referred to as a *data controller*, must delete a user's data upon request. This has inspired machine unlearning (Ginart et al., 2019), which seeks to provide efficient methods to remove the influence of training data instances from a pretrained model. Furthermore, some unlearning algorithms are *certifiable*, providing formal guarantees of compliance with the RTBF (Sekhari et al., 2021).

However, while certified unlearning allows data controllers to effectively comply with the RTBF, one can attack a pretrained model despite unlearning. Specifically, recent research into unlearning has established that data in the support of the training distribution will likely still be confidently predicted with the same prediction as before, even after using state-of-the-art unlearning algorithms to unlearn them (Zhao et al., 2024). That is, denoting the pretrained model as f and the unlearned model as f_u, for typical training instances, it holds that $f = f_u$.

In particular, an adversary can leverage $f = f_u$ to harm a user. Concretely, suppose a model f is trained on criminal records to predict individual crime likelihood. Additionally, suppose the criminal record $\boldsymbol{x}_p$ of a person p is corrupted and publicly available. To remove this corrupted data from f, p invokes the RTBF. Thus, the data controller for f unlearns $\boldsymbol{x}_p$, yielding f_u. But, even after unlearning, any law enforcement agency can still access the publicly available $\boldsymbol{x}_p$ and obtain $f_u(\boldsymbol{x}_p)$. But, $f_u(\boldsymbol{x}_p) = f(\boldsymbol{x}_p)$, and thus the law enforcement agency incorrectly labels person p as a criminal. An adversarial law enforcement agency, or even a prospective employer, may ignore or be unaware of warnings about the data being corrupted, rendering a dangerous scenario for person p.

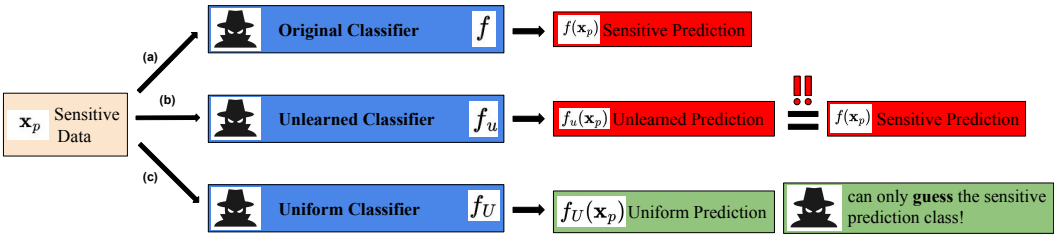

Figure 1: An adversary, like a law enforcement agency seeking to label person p as a criminal using corrupted criminal history $\boldsymbol{x}_p$, can use model outputs to endanger person p–we call this threat model test-time privacy (TTP), as illustrated in (a). Next, as demonstrated in (b), unlearning does not suffice, since an adversary can recover a confident prediction (Zhao et al., 2024). However, as demonstrated in (c), after inducing uniformity on the sensitive data, the adversary can now only guess at the prediction–this maximal uncertainty offers optimal protection against such an adversary.

A dominant viewpoint is that model f cannot be blamed in this scenario, as it has learned something underlying about nature (Mcsherry, 2016); (Bun et al., 2021). Furthermore, the privacy leakage occurred when $\boldsymbol{x}_p$ became public (Kamath, 2020). This view misses the point: ML models are often trained and applied on freely available data. For example, training data could be scraped from the web or social media platforms. Subsets of this data can be incorrect, corrupted, or confidential. With such data as input, model f presents a clear and present danger for safe ML which unlearning falls short of addressing, as the above example showed. In parallel, as humans, we learn to not act upon certain kinds of knowledge. For example, when we read confidential documents or learn that previously obtained knowledge is incorrect, we are not allowed to share or act on this knowledge.

Importantly, we do not place blame on the data controller for this privacy violation; they complied with all laws, like the RTBF, and did not release information about $\boldsymbol{x}_p$ in a way that p did not consent to. Therefore, the threat models addressed by unlearning and other privacy-preserving frameworks like differential privacy (Dwork et al., 2006) or homomorphic encryption (Brakerski et al., 2014) –which are different than ours–are still mitigated. However, an adversary can still clearly take advantage of model outputs in a way that unlearning, differential privacy, or homomorphic encryption *cannot* protect against, since they still result in confident classification.

Therefore, we seek to ensure *test-time privacy* (TTP): obtain a method which renders model outputs no longer confident for particular training instances, protecting against adversaries which seek to take advantage of model predictions. Furthermore, we aim to maintain high model utility, continuing to provide confident and correct classifications on the remaining instances.

A naive way to solve this is to simply mask particular outputs. However, an adversary with white-box access, i.e. access to the model architecture and parameters, can easily remove such a mask. To make this clear, we provide a threat model in Sec. A. To that end, we ask the following question:

Can we ensure test-time privacy against white-box adversaries?

We answer affirmatively, providing:

1. A method to finetune a pretrained model with a Pareto optimal objective, rendering the model maximally uncertain over protected instances while preserving accuracy on others;
2. Several principled (ε, δ)-certified full-batch and sequential algorithms which approximate the Pareto objective, derived without assumptions of convexity;
3. A theoretical analysis of the privacy-utility tradeoff that our algorithms incur, establishing a tight, non-vacuous bound;
4. Empirical studies, in which we observe that after applying our algorithms we can maintain high uniformity on the protected instances while guaranteeing excellent utility on the rest.

Importantly, we do **not** propose an unlearning algorithm, which would need to be aligned with the goals of unlearning. Instead, we aim to address an entirely new threat scenario—test time privacy—that (certified) unlearning cannot solve. What may constitute a privacy violation in unlearning, e.g. revealing that an instance is in the forget set, does *not* constitute a violation in our framework.

Due to space constraints, we provide a detailed related work section in Sec. B. Critically, we describe how methods like label differential privacy (LabelDP) (Ghazi et al., 2021) and private aggregation of teacher ensembles (PATE) (Papernot et al., 2018) differ from our setting, and also why misclassification-based methods for unlearning (Cha et al., 2024) are suboptimal in addressing our threat model. We detail our motivation; why unlearning fails; and why our method succeeds in Fig. 1. The code for our experiments is available for reproducibility at `https://github.com/ashiqwisc/test_time_privacy/blob/main/README.md`.

2 Approaches and Algorithms

Notation: Let $\mathcal{X} \subset \mathbb{R}^d$ be a sample space and let $\mathcal{Y} \subset \mathbb{R}^o$ be a label space. Denote $\mathcal{Z} = \mathcal{X} \times \mathcal{Y}$ as the space of feature-label pairs. Let $\mathcal{Z}^n$ be the n-fold Cartesian product of $\mathcal{Z}$ such that a dataset $\mathcal{D} \subset \mathcal{Z}^n$ is a collection of n feature-label pairs. Following the unlearning literature, we subset $\mathcal{D}$ as a "forget set" $\mathcal{D}_f$, containing instances to protect, and a retain set $\mathcal{D}_r = \mathcal{D} \setminus \mathcal{D}_f$. Then, suppose we have a (randomized) learning algorithm $\mathcal{A} : \mathcal{Z}^n \to \mathcal{W}$, where $\mathcal{W} \subset \mathbb{R}^z$ is a parameter space. Let the set of hypotheses parameterized with respect to this parameter space be $\mathcal{H}_\mathcal{W}$. Let $f_{\boldsymbol{w}} \in \mathcal{H}_\mathcal{W}$ be the hypothesis parameterized by $\boldsymbol{w} \in \mathcal{W}$, defined as $f_{\boldsymbol{w}} : \mathcal{X} \to \Delta_{|\mathcal{Y}|}$, where $\Delta_{|\mathcal{Y}|}$ is the probability simplex $\{p_1, ..., p_\gamma : p_i \geq 0, \sum_{i=1}^{\gamma} p_i = 1\}$. When $\boldsymbol{A}$ is a matrix, $||\boldsymbol{A}||_2$ is the 2 operator norm. When $\boldsymbol{v}$ is a vector, $||\boldsymbol{v}||_2$ is the ℓ_2 norm. Furthermore, let $\lambda_{\min}(\boldsymbol{A})$ denote the minimum eigenvalue of $\boldsymbol{A}$. Finally, when for sets $\mathcal{S}, \mathcal{F} \subset \mathcal{N}$ and $\mathcal{R}$ and mechanisms $\mathcal{M}, \mathcal{M}' : \mathcal{N} \to \mathcal{R}$, we have $\Pr(\mathcal{M}(\mathcal{S}) \in \mathcal{R}) \leq e^\varepsilon \Pr(\mathcal{M}'(\mathcal{F}) \in \mathcal{R}) + \delta$, we will denote $\mathcal{M}(\mathcal{S}) \approx_{\varepsilon,\delta,\mathcal{R}} \mathcal{M}'(\mathcal{F})$. We provide a symbol table in Sec. L.

In order to prevent test-time privacy violations, it suffices to have the model output a uniform distribution over the forget set, rendering the model maximally uncertain. Then, as illustrated in Fig. 1, an adversary can only guess at the original sensitive prediction. We also would like to preserve retain set accuracy; to that end, we present an algorithm that finetunes the pretrained model with a Pareto optimal objective. To make this algorithm concrete, we define a *uniform learner*, which we prove to be realizable for many common hypothesis classes. Then, we use this concept in order to construct a Pareto objective.

2.1 The Exact Pareto Learner

For a dataset $\mathcal{D} \subset \mathcal{Z}^n$, we denote the pretrained model as $\mathcal{A}(\mathcal{D})$. Then, to make $\mathcal{A}(\mathcal{D})$ uniform over the forget set, we introduce our core concept of a *uniform learner*:

Definition 2.1 (Uniform learner)**.** *Suppose we have a (randomized) learning algorithm $\mathcal{K} : \mathcal{Z}^n \to \mathcal{W}$ that, given $\mathcal{D} \subset \mathcal{Z}^n$, yields the parameter $\mathcal{K}(D) = \boldsymbol{w}_\mathcal{D}$. We say $\mathcal{K}$ is a uniform learner if $\forall \mathcal{D} \in \mathcal{Z}^n$, $\boldsymbol{w}_\mathcal{D}$ parametrizes $f_{\boldsymbol{w}_\mathcal{D}} \in \mathcal{H}_\mathcal{W}$ and satisfies:*

$$||f_{\boldsymbol{w}_\mathcal{D}} - \underbrace{(\frac{1}{|\mathcal{Y}|}, ..., \frac{1}{|\mathcal{Y}|})}_{|\mathcal{Y}| \text{ times}}||_{\infty,\mathcal{X}} = 0. \tag{1}$$

That is, $\mathcal{K}$ is a uniform learner if its parameterized outputs yield the uniform distribution $U[0, |\mathcal{Y}|]$ for all inputs across all datasets. Furthermore, $\mathcal{K}$ is realizable for many common hypothesis spaces:

Proposition 2.2. *Suppose we have a hypothesis space $\mathcal{H}_\mathcal{W}$ consisting of functions where the ultimate layer is an affine transformation and the outputs are passed through a softmax. Let $\mathcal{K}$ be a uniform learner. Then, $f_{\mathcal{K}(\mathcal{D})} \in \mathcal{H}_\mathcal{W}$ $\forall \mathcal{D} \subset \mathcal{Z}^n$.*

Proof Sketch: Setting the weights in the ultimate affine layer to 0 yields uniform outputs. See Sec. E.2 for a full proof.

Most classifiers built and deployed in ML recently, including multilayer perceptrons (MLP), residual networks (ResNets) (He et al., 2016), and transformers (Vaswani et al., 2017) satisfy the premise of Prop. 2.2, making it widely applicable.

Next, we assume $\mathcal{A}$ and $\mathcal{K}$ are obtained through empirical risk minimization (ERM) to a local or global minima. That is, let $\mathcal{A}(\mathcal{D}) = \text{argmin}_{\boldsymbol{w} \in \mathcal{W}} \mathcal{L}_\mathcal{A}(\boldsymbol{w}, \mathcal{D})$ and $\mathcal{K}(\mathcal{D}) = \text{argmin}_{\boldsymbol{w} \in \mathcal{W}} \mathcal{L}_\mathcal{K}(\boldsymbol{w}, \mathcal{D})$. One choice of $\mathcal{L}_\mathcal{K}$ is the KL divergence (Kullback and Leibler, 1951) between the softmax outputs

and the uniform distribution. This loss has been previously used to penalize highly confident classifier predictions (Pereyra et al., 2017); we thus adapt this loss to our setting. Furthermore, by Prop. 2.2, this loss can be completely minimized over $\mathcal{W}$.

Critically, we seek the optimal tradeoff between uniformity over the forget set and utility over the retain set. That is, we should produce a learner that is Pareto optimal with respect to $\mathcal{L}_\mathcal{K}$ and $\mathcal{L}_\mathcal{A}$. This learner can be characterized as follows:

Proposition 2.3. *Let $\theta \in (0,1)$. Fix $\mathcal{D} \subset \mathcal{Z}^n$ and consider the forget set $\mathcal{D}_f \subset \mathcal{D}$ and the retain set $\mathcal{D}_r = \mathcal{D} \setminus \mathcal{D}_f$. Then, if $\mathcal{M}_\theta(\mathcal{D}) = \text{argmin}_{\boldsymbol{w}\in\mathcal{W}}\ \theta\mathcal{L}_\mathcal{K}(\boldsymbol{w}, \mathcal{D}_f) + (1-\theta)\mathcal{L}_\mathcal{A}(\boldsymbol{w}, \mathcal{D}_r)$ is a global minimizer, it is globally Pareto optimal with respect to $\mathcal{L}_\mathcal{K}(\boldsymbol{w}, \mathcal{D}_f)$ and $\mathcal{L}_\mathcal{A}(\boldsymbol{w}, \mathcal{D}_r)$. Similarly, if $\mathcal{M}_\theta(\mathcal{D})$ is a local minimizer, it is locally Pareto optimal.*

Proof Sketch: This holds by contradiction. If the solution to the minimized objective was not globally (locally) Pareto optimal, since $\theta \in (0,1)$, it could not be the global (local) minimizer. See Sec. E.3 for a full proof. Definitions of Pareto optimality are included in Sec. E.3 as well.

As shown in Prop. 2.3, $\mathcal{M}_\theta$ yields a parameter that, given $\theta \in (0,1)$, presents a Pareto optimal tradeoff between uniformity over the forget set and utility over the retain set. One can adjust θ to vary over many Pareto optimal solutions, yielding different tradeoffs between uniformity and utility. This yields Alg. 1, in which we finetune a pretrained model by using it as initialization for $\mathcal{M}_\theta(\mathcal{D})$.

2.2 The Certified Pareto Learner

While the exact algorithm discussed above works well in practice, it is not *certifiable*. That is, there is no certificate that a third party can inspect to verify that test-time privacy has been protected. Thus, to design a certified approximation algorithm, we take inspiration from certified unlearning (Zhang et al., 2024), which aims to add a small amount of structured noise such that the pretrained model becomes indistinguishable from the retrained model. In our setting, we would like to make the pretrained model indistinguishable from the solution to the Pareto objective. To do so, we define a new notion of (ε, δ)-indistinguishability and use this definition to design multiple certifiable algorithms.

Firstly, to motivate our definition, recall the definition of differential privacy (Dwork et al., 2006):

Definition 2.4 ((ε,δ)-differential privacy)**.** *Suppose we have privacy budgets $\varepsilon \in (0,1)$ and $\delta > 0$. A randomized algorithm $\mathcal{M} : \mathbb{N}^n \to \mathcal{R}$ satisfies (ϵ, δ)-differential privacy if $\forall \mathcal{T} \subset$ range$(\mathcal{M})$ and $\forall \boldsymbol{x}, \boldsymbol{y} \in \mathbb{N}^n$ s.t. $||\boldsymbol{x} - \boldsymbol{y}|| \leq 1$:*

$$\mathcal{M}(x) \approx_{\varepsilon,\delta,\mathcal{T}} \mathcal{M}(y) \tag{2}$$

This guarantees that the algorithm $\mathcal{M}$ applied on a dataset is statistically indistinguishable from the same algorithm applied on all datasets different by one instance. One can leverage this definition to formalize certified unlearning (Sekhari et al., 2021):

Definition 2.5 ((ε,δ)-certified unlearning)**.** *Suppose we have privacy budgets $\varepsilon \in (0,1)$ and $\delta > 0$. Consider $\mathcal{D} \subset \mathcal{Z}^n$ and let $\mathcal{D}_f \subset \mathcal{D}$ be the forget set to be unlearned, and $\mathcal{D}_r = \mathcal{D} \setminus \mathcal{D}_f$ be the retain set. $\mathcal{U} : \mathcal{Z}^n \times \mathcal{Z}^n \times \mathcal{W} \to \mathcal{W}$ is an (ε, δ)-certified unlearning algorithm if $\forall \mathcal{T} \subset \mathcal{W}$, we have:*

$$\mathcal{U}(\mathcal{D}, \mathcal{D}_f, \mathcal{A}(\mathcal{D})) \approx_{\varepsilon,\delta,\mathcal{T}} \mathcal{A}(\mathcal{D}_r) \tag{3}$$

$$\mathcal{A}(\mathcal{D}_r) \approx_{\varepsilon,\delta,\mathcal{T}} \mathcal{U}(\mathcal{D}, \mathcal{D}_f, \mathcal{A}(\mathcal{D})) \tag{4}$$

This formalizes making $\mathcal{A}(\mathcal{D})$ indistinguishable from $\mathcal{A}(\mathcal{D}_r)$. In light of Def. 2.5, we seek to make $\mathcal{A}(\mathcal{D})$ indistinguishable from $\mathcal{M}_\theta(\mathcal{D})$. Thus, we provide the following new definition:

Definition 2.6 ($(\varepsilon,\delta,\theta)$-certified Pareto learner)**.** *Suppose we have privacy budgets $\varepsilon \in (0,1)$ and $\delta > 0$ with $\mathcal{D} \subset \mathcal{Z}^n$. Let $\mathcal{D}_f \subset \mathcal{D}$ be the forget set and let $\mathcal{D}_r = \mathcal{D} \setminus \mathcal{D}_f$ be the retain set. Suppose we have $\theta \in (0,1)$ and $\mathcal{M}_\theta(\mathcal{D}) = \text{argmin}_{\boldsymbol{w}\in\mathcal{W}}\ \theta\mathcal{L}_\mathcal{K}(\boldsymbol{w}, \mathcal{D}_f) + (1-\theta)\mathcal{L}_\mathcal{A}(\boldsymbol{w}, \mathcal{D}_r)$, where $\mathcal{K}$ is a uniform learner and $\mathcal{A}$ is a learning algorithm both obtained through ERM. An algorithm $\mathcal{G} : \mathcal{Z}^n \times \mathcal{Z}^n \times \mathcal{W} \to \mathcal{W}$ is a $(\varepsilon, \delta, \theta)$-certified Pareto learner if $\forall \mathcal{T} \subset \mathcal{W}$:*

$$\mathcal{G}(\mathcal{D}, \mathcal{D}_f, \mathcal{A}(\mathcal{D})) \approx_{\varepsilon,\delta,\mathcal{T}} \mathcal{M}_\theta(\mathcal{D}) \tag{5}$$

$$\mathcal{M}_\theta(\mathcal{D}) \approx_{\varepsilon,\delta,\mathcal{T}} \mathcal{G}(\mathcal{D}, \mathcal{D}_f, \mathcal{A}(\mathcal{D})) \tag{6}$$

Algorithm 1 $\mathcal{M}_\theta$ Finetuning

Require: Dataset $\mathcal{D}$; forget set $\mathcal{D}_f$; pretrained model $\boldsymbol{w}^* = \mathcal{A}(\mathcal{D})$; uniformity-utility tradeoff coefficient θ; e epochs
Use $\boldsymbol{w}^*$ as initialization for the Pareto learner $\mathcal{M}_\theta(\mathcal{D})$
Optimize the Pareto learner $\mathcal{M}_\theta(\mathcal{D})$ for e epochs with e.g. stochastic gradient descent to yield $\boldsymbol{w}^-$
return $\boldsymbol{w}^-$

Algorithm 2 $(\epsilon, \delta, \theta)$-Certified Uniformity with Exact Inverse Hessian

Require: Dataset $\mathcal{D}$; forget set $\mathcal{D}_f$; pretrained model $\boldsymbol{w}^* = \mathcal{A}(\mathcal{D})$; privacy budgets ε and δ; uniformity-utility tradeoff coefficient θ; local convex coefficient λ; norm upper bound C
$\tilde{\boldsymbol{w}} \leftarrow \boldsymbol{w}^* - (\boldsymbol{H}_{\boldsymbol{w}^*,\mathcal{K},\mathcal{A}} + \lambda \boldsymbol{I})^{-1} \nabla_{\boldsymbol{w}^*,\mathcal{K},\mathcal{A}}$
Compute Δ as the bound in Eq. (20)
$\sigma = \frac{\Delta}{\epsilon}\sqrt{2\ln(1.25/\delta)}$
$\boldsymbol{w}^- \leftarrow \tilde{\boldsymbol{w}} + Y$ where $Y \sim \mathcal{N}(\boldsymbol{0}, \sigma^2 \boldsymbol{I})$
return $\boldsymbol{w}^-$

Discussion: Qualitatively, what the conditions in Def. 2.6 mean is that the model obtained by algorithm $\mathcal{G}$ is statistically indistinguishable from a model that is Pareto optimal between utility over the retain set and uniformity over the forget set. Here, we consider the classical setting[1] of $\varepsilon \in (0, 1)$.

Inspired by Sekhari et al. (2021), we can design an algorithm which satisfies Def. 2.6 by taking a Newton step towards the Pareto model and applying structured Gaussian noise; this yields Alg. 2, which is certifiable as described in Sec. D. Using local convex approximation (Nocedal and Wright, 1999), in which we add a regularization term to the objective of the Pareto learner, we design Alg. 2 without any assumptions of convexity on the component loss functions. However, Alg. 2 requires inverting a Hessian, which is computationally infeasible for practical neural networks e.g. ResNets, even after employing conjugate gradient methods (Nocedal and Wright, 1999) and Hessian vector product techniques (Pearlmutter, 1994).

To resolve this issue, we also derive Alg. 3 in Sec. D, which computes an efficient estimator for the inverse Hessian, inspired by the techniques of Zhang et al. (2024). Furthermore, this algorithm does not assume convergence to even a local minima for $\mathcal{A}(\mathcal{D})$, handling e.g. early stopping. An online version is presented in Sec. F as Alg. 4. While Alg. 2 to 4 have more hyperparameters than Alg. 1, they offer a certificate which can be used to verify use of our method by a third party. Additionally, we present ways to reduce hyperparameters in Sec. G.

3 Theoretical Analysis

Firstly, we seek to understand how we can choose θ to guarantee uniformity over the forget set. To do so, we provide a constraint to be satisfied to ensure uniformity. Then, we provide an appropriate lower bound on θ to ensure the constraint is satisfied. In doing so, one obtains a bound on the privacy of our algorithm.

We next want to obtain a bound on the utility of our algorithm. To that end, we upper bound the difference between the retain loss of the locally optimal learned model $\mathcal{A}(\mathcal{D}_r)$ and the locally optimal solution to the Pareto objective $\mathcal{M}_\theta(\mathcal{D})$. We obtain a tight, non-vacuous bound with respect to θ and characterize it asymptotically. Incorporating the two bounds provides a concrete characterization of the privacy-utility tradeoffs that occur when our algorithms are used.

Across all algorithms, we make the pretrained model indistinguishable from:

[1]Notably, Balle and Wang (2018) provide a way to achieve (ε, δ)-indistinguishability for $\varepsilon > 1$, and their technique can be adapted without loss of generality to our setting.

$$\mathcal{M}_\theta(\mathcal{D}) = \arg \min_{||\boldsymbol{w}||_2 \leq C, \boldsymbol{w} \in \mathcal{W}} \theta \mathcal{L}_\mathcal{K}(\boldsymbol{w}, \mathcal{D}_f) + (1-\theta)\mathcal{L}_\mathcal{A}(\boldsymbol{w}, \mathcal{D}_r) + \frac{\lambda}{2}||\boldsymbol{w}||_2^2, \tag{7}$$

$$= \arg \min_{||\boldsymbol{w}||_2 \leq C, \boldsymbol{w} \in \mathcal{W}} \theta \sum_{i=1}^{|\mathcal{D}_f|} \ell_\mathcal{K}(\boldsymbol{w}, \mathcal{D}_f^{(i)}) + (1-\theta) \sum_{i=1}^{|\mathcal{D}_r|} \ell_\mathcal{A}(\boldsymbol{w}, \mathcal{D}_r^{(i)}) + \frac{\lambda}{2}||\boldsymbol{w}||_2^2. \tag{8}$$

where $\ell_\mathcal{K}^{(i)}$ and $\ell_\mathcal{A}^{(i)}$ are component loss functions corresponding to individual data instances in the forget and retain sets, respectively. Note that λ is present either as weight decay in the Pareto learning in Alg. 1 or as part of the local convex approximation in Alg. 2 or Alg. 3. Furthermore, note that the objective is constrained by $||\boldsymbol{w}||_2 \leq C$; we use this as a part of our local convex approximation when deriving our algorithms, and unlearning methods assume this either implicitly or explicitly (Zhang et al., 2024). One can use projected gradient descent (Nocedal and Wright, 1999) during optimization to satisfy this constraint.

Note that Alg. 1 has $\lambda \approx 0$. For Alg. 2 and Alg. 3, by Lemma E.9, our models $f_{\boldsymbol{w}^-}$ and $f_{\mathcal{M}_\theta(\mathcal{D})}$ have approximately the same outputs over $\mathcal{D}_f$. Hence, for any of our algorithms, to ensure indistinguishability from uniformity over $\mathcal{D}_f$, it suffices to ensure that $\mathcal{M}_\theta$ satisfies the following constraint:

$$||f_{\mathcal{M}_\theta(\mathcal{D})}(\mathcal{D}_f) - U[0, |\mathcal{Y}|]||_\infty \leq \varepsilon. \tag{9}$$

We then have the following bound on Eq. (9) with respect to θ:

Proposition 3.1. *Let $\mathcal{M}_\theta(\mathcal{D})$ be the global solution to the Pareto objective. Choose, as surrogate losses, $\ell_\mathcal{K}^{(i)}(\boldsymbol{w}, \mathcal{D}_f^{(i)}) = D_{KL}(f_{\boldsymbol{w}}(\mathcal{D}_f^{(i)})||U[0, |\mathcal{Y}|)$, the KL divergence between the model outputs over the forget set and the uniform distribution, and $\ell_\mathcal{A}^{(i)}(\boldsymbol{w}, \mathcal{D}_r^{(i)}) = \mathbb{H}_{CE}(\mathcal{D}_r^{(i,\mathcal{Y})}, f_{\boldsymbol{w}}(\mathcal{D}_r^{(i,\mathcal{X})}))$, the cross entropy between model predictions and labels over the retain set. Then, $||f_{\mathcal{M}_\theta(\mathcal{D})}(\mathcal{D}_f) - U[0, |\mathcal{Y}|]||_\infty \leq \sqrt{2(\frac{1-\theta}{\theta}|\mathcal{D}_r| \ln |\mathcal{Y}|)}$.*

Proof Sketch: By using Prop. 2.2 and the fact that $\mathcal{M}_\theta(\mathcal{D})$ is a global minimizer, we can yield a bound on $\mathcal{L}_\mathcal{K}$. Then, we can apply standard inequalities relating the ℓ_∞ norm, ℓ_1 norm, the total variation distance, and the KL divergence. See Sec. E.10 for a full proof.

Then, we can choose θ as follows to guarantee Eq. (9):

Corollary 3.2. *For any $\varepsilon > 0$, choosing $\theta \geq \frac{2|\mathcal{D}_r| \ln |\mathcal{Y}|}{\varepsilon^2 + 2|\mathcal{D}_r| \ln |\mathcal{Y}|}$ guarantees that $||f_{\mathcal{M}_\theta(\mathcal{D})}(\mathcal{D}_f) - U[0, |\mathcal{Y}|]||_\infty \leq \varepsilon$.*

Proof See Sec. E.11.

Discussion: Note that Cor. 3.2 does not yield that $\theta \geq 1$, i.e. $\theta \in (0, 1)$ given this constraint, as desired. Furthermore, Cor. 3.2 restricts $\mathcal{M}_\theta(\mathcal{D})$ to a subset of Pareto optimal solutions, but this does not render it no longer Pareto optimal; thus, our formulation as in Sec. D still holds in its entirety. Importantly, this is a sufficient but not necessary condition to satisfy Eq. (9).

Similarly, by Lemma E.9, we can reason about how our choice of θ in $\mathcal{M}_\theta(\mathcal{D})$ affects the (empirical) retain error, i.e. the empirical loss over $\mathcal{D}_r$, after our algorithms are applied. To provide this bound, we require two key assumptions:

Assumption 3.3. *The gradients of $\ell_\mathcal{K}$ and $\ell_\mathcal{A}$ are Lipschitz in $\boldsymbol{w}$ with Lipschitz constants $\frac{L_\mathcal{K}}{|\mathcal{D}_f|}$ and $\frac{L_\mathcal{A}}{|\mathcal{D}_r|}$.*

Assumption 3.4. *The Hessians of $\ell_\mathcal{K}$ and $\ell_\mathcal{A}$ are Lipschitz in $\boldsymbol{w}$ with Lipschitz constants $\frac{M_\mathcal{K}}{|\mathcal{D}_f|}$ and $\frac{M_\mathcal{A}}{|\mathcal{D}_r|}$.*

Discussion: Note that these assumptions are only used to prove theorem 3.5 and in Sec. D; we do not require them to prove all previously mentioned theorems. These assumptions, similar to those studied by Zhang et al. (2024), are less restrictive than those typically studied in certified unlearning Sekhari et al. (2021); importantly, we do not assume (strong) convexity of the losses.

We then present a tight, non-vacuous bound on the retain error after applying any of our algorithms:

Theorem 3.5. *Suppose Assumptions 3.3 and 3.4 hold, and let $L_{\mathcal{K}}, L_{\mathcal{A}}, M_{\mathcal{K}}, M_{\mathcal{A}}$ be as defined in Assumptions 3.3 and 3.4. Let $\alpha^* := \mathcal{L}_{\mathcal{A}}(\mathcal{A}(\mathcal{D}_r), \mathcal{D}_r)$ be the locally optimal (empirical) retain loss, achieved by $\mathcal{M}_\theta(\mathcal{D})$ when $\theta = 0$. Let $\alpha(\theta) := \mathcal{L}_{\mathcal{A}}(\mathcal{M}_\theta(\mathcal{D}), \mathcal{D}_r)$ be the locally optimal retain loss obtained by $\mathcal{M}_\theta(\mathcal{D})$ when $\theta \in (0, 1)$. Suppose all weights used throughout are bounded by $||\boldsymbol{w}||_2 \leq C$. Additionally, denote by $M := \theta M_{\mathcal{K}} + (1-\theta) M_{\mathcal{A}}$ and $L := \theta L_{\mathcal{K}} + (1-\theta) L_{\mathcal{A}}$. Consider regularization coefficient $\lambda \geq L + 2\theta CM + \sqrt{2\theta CM(L + 2\theta CM + 8L_{\mathcal{K}})}$. Then, we have the following bound:*

$$|\alpha^* - \alpha(\theta)| \leq \frac{L_{\mathcal{A}}}{2}\left(\frac{\lambda - L - \sqrt{(\lambda - L)^2 - 4\theta CM(2L_{\mathcal{K}} + \lambda)}}{2M}\right)^2 + \tag{10}$$

$$\lambda C\left(\frac{\lambda - L - \sqrt{(\lambda - L)^2 - 4\theta CM(2L_{\mathcal{K}} + \lambda)}}{2M}\right). \tag{11}$$

Proof Sketch: We subtract the first order conditions yielded by the definitions of α^* and $\alpha(\theta)$ to get an expression with respect to the gradients; plugging in an equivalent path integral expression and applying Lemma E.2 yields our desired result. See Sec. E.12 for a full proof.

Discussion: Note that when $\theta = 0$, the bound simplifies to 0, indicating that it is tight near 0. We demonstrate that it is tight near 1 in Sec. J. Additionally, in the case of Alg. 1, since $\lambda = 0$, we do not need the condition on λ and obtain a clearer characterization. Furthermore, we can obtain a more concise bound with simpler techniques, but such a bound is vacuous and does not incorporate information about θ; we elaborate on this in Sec. E.12.

Additionally, this bound yields the following asymptotic characterization of the error:

Corollary 3.6. *Let α^*, $\alpha(\theta)$, L, and M be defined as above. Consider $\lambda \geq L + 2\theta CM + \sqrt{2\theta CM(L + 2\theta CM + 8L_{\mathcal{K}})}$. We then have the following asymptotic characterizations of the error:*

$$|\alpha^* - \alpha(\theta)| \leq \mathcal{O}(\theta) \text{ as } \theta \to 0, |\alpha^* - \alpha(\theta)| \leq \mathcal{O}(1) \text{ as } \theta \to 1. \tag{12}$$

Discussion: This yields that as we emphasize the retain loss in $\mathcal{M}_\theta$, the retain accuracy improves linearly with θ. Obtaining algorithms which result in softer degradation e.g. $O(\sqrt{\theta})$ is left to future work. In contrast, as we emphasize the forget loss in $\mathcal{M}_\theta$, the retain accuracy degrades to a constant distance from optimality, reflecting the maximal penalty in enforcing uniformity.

4 Empirical Analysis

In what follows, we provide empirical results for Alg. 1 and Alg. 2. We firstly discuss our experimental setup and baselines. Then, we provide a metric by which we measure uniformity throughout. Next, we provide our core results across Alg. 1, Alg. 2, and our baselines for several architectures and benchmarks. We also comment on the Pareto frontier and optimization dynamics of Alg. 1 and Alg. 2, providing additional insight into the structure of our problem. Additional experiments on test-time privacy attacks, robustness of the finetuned classifier on neighboring test instances, inducing uniformity on test instances, and other ablations can be found in Sec. J. Code for reproducibility is available at `https://github.com/ashiqwisc/test_time_privacy/blob/main/README.md`.

Setup and Baselines: We use PyTorch with ADAM (Kingma and Ba, 2014) to implement the algorithms, with details deferred to Sec. I. For most of our experiments, we optimize the Pareto objective in Alg. 1 with gradient surgery (Yu et al., 2020), which corrects interfering gradients for competing objectives. Our primary results on Alg. 1 are for ResNet50 (He et al., 2016) over SVHN (Netzer et al., 2011), CIFAR10, and CIFAR100 (Krizhevsky et al., 2009). We also provide results for logistic regression on MNIST (Deng, 2012) to evaluate Alg. 2. We compare results with the pretrained model and the model retrained without the forget set, which constitutes exact unlearning (Bourtoule et al., 2021). We also compare our methods to LabelDP (Ghazi et al., 2021) and a synthetic baseline that assigns random labels to instances neighboring the forget set and retrains. Across methods, we compare retain accuracy, test accuracy, and forget uniformity. In Sec. J, we provide additional comparisons with a uniformity baseline based on generating a synthetic dataset and label differential privacy (Ghazi et al., 2021). We also include additional experiments with more complicated datasets

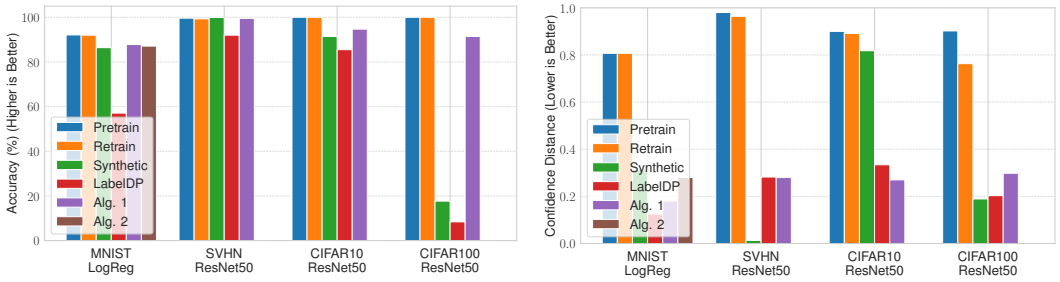

(a) Accuracy on retain set for baselines as well as Alg. 1 and Alg. 2 with $\theta = 0.75$.

(b) Confidence distance on forget set for baselines as well as Alg. 1 and Alg. 2 with $\theta = 0.75$..

Figure 2: We observe a significant drop in confidence distance, where lower is better, for both our algorithms. We also observe that both algorithms provide strong accuracy on the retain set. We observe similar behavior for the test set in Sec. J.

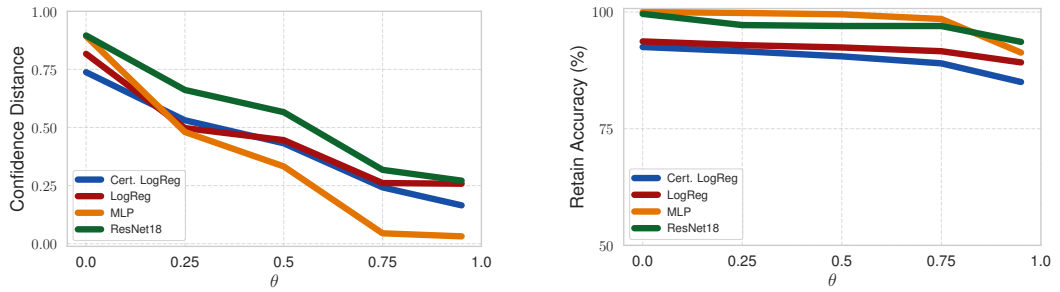

(a) Confidence Distance vs. θ, MNIST

(b) Retain Accuracy vs. θ, MNIST

Figure 3: From Fig. 3a we observe that the confidence distance decreases roughly linearly as θ increases. Furthermore, from Fig. 3b, as demonstrated in theorem 3.5, we observe a linear increase in retain accuracy in a neighborhood of $\theta = 0$ and convergence to a constant error as $\theta \to 1$.

and models, as well as ablation studies on our hyperparameters, in Sec. J. We find that we guarantee similar retain accuracy to retraining while obtaining the same or better uniformity than our baselines. We provide more details and the rationale for our baselines in Sec. I.

Providing a Uniformity Metric: We require a metric to compare uniformity over the forget set in an interpretable manner. Thus, we define the "confidence distance" as $\max\{0, f(\boldsymbol{x})_t - \frac{1}{|\mathcal{Y}|}\}$ for $\boldsymbol{x} \in \mathcal{D}_f$, where $f(\boldsymbol{x})_t$ is the max confidence score. In our experiments, we use this as the primary metric for uniformity, reporting the average confidence distance over the forget set. We discuss why this is reasonable in Sec. C and compare it to alternative metrics in Sec. J.

Overall Results: The results for Alg. 1 are presented in Fig. 2, in which we were able to achieve a $> 3\times$ decrease in confidence distance with only a 0.01% and 0.04% decrease in retain and test accuracy, respectively, for a ResNet50 pretrained on SVHN. We obtain similar results for MNIST, CIFAR10, and CIFAR100: retain and test set accuracies remain high, while forget confidence distance is significantly reduced. Results for the test set are deferred to Sec. J. We additionally find that our synthetic baseline can induce uniformity well for SVHN, but catastrophically fails in terms of retain and test accuracy for CIFAR100. This holds similarly for LabelDP, which also undesirably reduces the confidence distance on retain and test sets, while our method does not, as demonstrated in Sec. J. Furthermore, we confirm the results of Zhao et al. (2024), observing that unlearned models still produce confident predictions on deleted instances.

We observe similar results for logistic regression and MLP, obtaining confidence distances as low as 0.04 while obtaining 92% retain accuracy, as demonstrated in Fig. 3. Furthermore, as illustrated by Fig. 2, we find that Alg. 2 also induces uniformity well, while marginally improving retain and test accuracy. Thus, this algorithm produces a certificate through which test-time privacy can be verified while still obtaining a good privacy-utility tradeoff. For both algorithms, tables are included in Sec. J.

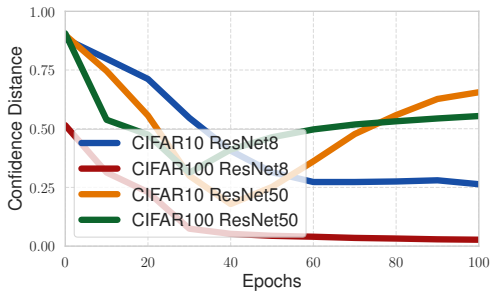

(a) Confidence Distance vs. Epochs, $\theta = 0.75$

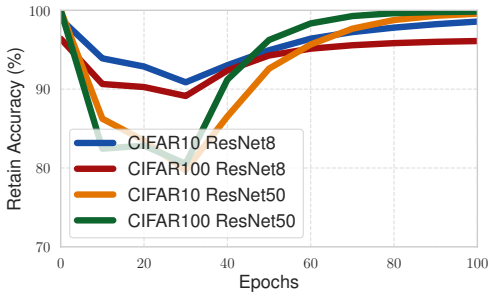

(b) Retain Accuracy vs. Epochs, $\theta = 0.75$

Figure 4: For CIFAR10 and CIFAR100 ResNet50, we observe a sharp drop in confidence distance followed by a sharp increase in Fig. 4a, in line with the drops and increases for retain accuracy in Fig. 4b. Test accuracy is similar. This highlights the need for early stopping when using Alg. 1 for large models, since otherwise one escapes from a good privacy-utility tradeoff. For smaller models, e.g. MNIST MLP, this issue does not persist–we obtain good uniformity after an initial drop in accuracy, but then increase accuracy and decrease confidence distance simultaneously.

Pareto Frontiers: To better understand the structure of our problem, we explore the Pareto frontier in Fig. 3. We observe that for simple datasets like MNIST, various θ can provide good retain accuracy, albeit at the cost of uniformity. In general, we find that $\theta \approx 0.75$ offers a solid privacy-utility tradeoff. Thus, the ε in Prop. 3.1 can be chosen fairly large while ensuring a small confidence distance.

Optimization Dynamics: Upon using Alg. 1, we observe that logistic regression fails to induce uniformity for more complex benchmarks than MNIST, e.g. KMNIST. These models have poor test accuracy; we thus conclude that a model must be large enough to generalize well in order to have uniformity induced over it without a large cost to retain accuracy. We hypothesize that this is because a model with more parameters has many more subspaces where two task losses can coexist in a way that provides a good tradeoff.

However, when using Alg. 1 on larger models, we observe that we need early stopping. After achieving a good uniformity-utility tradeoff, large models e.g. ResNet50 on CIFAR10 will powerfully increase accuracy at the cost of uniformity. This is undesired behavior when compared to, for example, a ResNet8 trained on CIFAR10, where we initially increase uniformity at the cost of accuracy but slowly regain accuracy without critically damaging uniformity. We illustrate this in Fig. 4. Altogether, our method works best for large models with early stopping during finetuning. We characterize this mathematically in Sec. H.

5 Discussion

We present *test-time privacy*, a threat model in which an adversary seeks to directly use a confident prediction to harm a user. This contrasts with existing work like PATE and LabelDP, which focus on protecting against model inversion and leakage of ground truth labels. To protect against a test-time privacy adversary, we present four algorithms to induce uniformity on a subset of the training data while preserving utility on the rest data. This can be used to prevent adversaries from taking advantage of model outputs, overcoming the limitations of unlearning found by Zhao et al. (2024). Furthermore, we prove a privacy-utility tradeoff for our algorithms, providing a tight bound which is empirically verified. We hope our test-time privacy can further inspire the community to explore the impact of large models around sensitive data.

Limitations and Future Directions: Notably, our presented method only applies to classification. Extending this to generative models e.g. diffusion models for image generation (Song et al., 2021) or autoregressive transformers for sequence-to-sequence generation (Vaswani et al., 2017) remains as future work.

From an algorithmic perspective, in Alg. 1, we use linear scalarization to design our objective (Hwang and Masud, 2012). One can instead design an objective using ε-constraints (Miettinen, 1999), which can then be solved by an augmented Lagrangian method (Nocedal and Wright, 1999). For the certified

methods, one could obtain Hessian-free algorithms by using the structure of SGD updates during pretraining, taking inspiration from (Qiao et al., 2025) or (Mu and Klabjan, 2025). Additionally, using recent techniques (Koloskova et al., 2025), one can certify finetuning-based algorithms without relying on the pretraining dynamics or storing additional information, which is especially promising for our approach.

ACKNOWLEDGEMENTS

The authors would like to thank Kangwook Lee for feedback on the early idea and proposing the synthetic baseline.

REFERENCES

Martin Abadi, Andy Chu, Ian Goodfellow, H Brendan McMahan, Ilya Mironov, Kunal Talwar, and Li Zhang. Deep learning with differential privacy. *Proceedings of the Conference on on Computer and Communiscations Security (CCS)*, pages 308–318, 2016.

Naman Agarwal, Brian Bullins, and Elad Hazan. Second-order stochastic optimization in linear time. *stat*, 1050:15, 2016.

Mohammad Al-Rubaie and J Morris Chang. Privacy-preserving machine learning: threats and solutions. *IEEE Security & Privacy*, 17(2):49–58, 2019.

Kareem Amin, Alex Kulesza, and Sergei Vassilvitskii. Practical considerations for differential privacy, 2024. URL `https://arxiv.org/abs/2408.07614`.

Anastasios N Angelopoulos, Michael I Jordan, and Ryan J Tibshirani. Gradient euilibrium in online learning: theory and applications. *arXiv preprint arXiv:2501.08330*, 2025.

Yoshinori Aono, Takuya Hayashi, Lihua Wang, Shiho Moriai, et al. Privacy-preserving deep learning via additively homomorphic encryption. *IEEE Transactions on Information Forensics and Security*, 13(5):1333–1345, 2017.

Borja Balle and Yu-Xiang Wang. Improving the gaussian mechanism for differential privacy: analytical calibration and optimal denoising. *International Conference on Machine Learning (ICML)*, 2018.

Lucas Bourtoule, Varun Chandrasekaran, Christopher A Choquette-Choo, Hengrui Jia, Adelin Travers, Baiwu Zhang, David Lie, and Nicolas Papernot. Machine unlearning. *IEEE Symposium on Security and Privacy (SP)*, pages 141–159, 2021.

Zvika Brakerski, Craig Gentry, and Vinod Vaikuntanathan. (leveled) fully homomorphic encryption without bootstrapping. *Transactions on Computation Theory (TOCT)*, 6(3):1–36, 2014.

Mark Bun, Damien Desfontaines, Cynthia Dwork, Naor Moni, Kobbi Nissim, Aaron Roth, Adam Smith, Thomas Steinke, Jonathan Ullman, and Salil Vadhan. Statistical inference is not a privacy violation, 2021.

Robert Istvan Busa-Fekete, Umar Syed, Sergei Vassilvitskii, et al. On the pitfalls of label differential privacy. In *NeurIPS Workshops*, 2021.

Sungmin Cha, Sungjun Cho, Dasol Hwang, Honglak Lee, Taesup Moon, and Moontae Lee. Learning to unlearn: instance-wise unlearning for pre-trained classifiers. *AAAI Conference on Artificial Intelligence*, 38(10):11186–11194, 2024.

Kamalika Chaudhuri and Claire Monteleoni. Privacy-preserving logistic regression. *Advances in Neural Information Processing Systems (NeurIPS)*, 21, 2008.

Kamalika Chaudhuri, Claire Monteleoni, and Anand D Sarwate. Differentially private empirical risk minimization. *Journal of Machine Learning Research*, 12(3), 2011.

Lynn Chua, Badih Ghazi, Pritish Kamath, Ravi Kumar, Pasin Manurangsi, Amer Sinha, and Chiyuan Zhang. Scalable dp-sgd: shuffling vs. poisson subsampling. *Advances in Neural Information Processing Systems (NeurIPS)*, 37:70026–70047, 2024.

Tarin Clanuwat, Mikel Bober-Irizar, Asanobu Kitamoto, Alex Lamb, Kazuaki Yamamoto, and David Ha. Deep learning for classical japanese literature. *Advances in Neural Information Processing Systems (NeurIPS)*, 2018.

Li Deng. The mnist database of handwritten digit images for machine learning research. *IEEE Signal Processing*, 29(6):141–142, 2012.

Irit Dinur and Kobbi Nissim. Revealing information while preserving privacy. *Proceedings of the Symposium on Principles of Databases (PODS)*, pages 202–210, 2003.

Alexey Dosovitskiy, Lucas Beyer, Alexander Kolesnikov, Dirk Weissenborn, Xiaohua Zhai, Thomas Unterthiner, Mostafa Dehghani, Matthias Minderer, Georg Heigold, Sylvain Gelly, Jakob Uszkoreit, and Neil Houlsby. An image is worth 16x16 words: Transformers for image recognition at scale. *International Conference on Learning Representations (ICLR)*, 2021.

Cynthia Dwork, Frank McSherry, Kobbi Nissim, and Adam Smith. Calibrating noise to sensitivity in private data analysis. *Proceedings of the Theory of Cryptography Conference (TCC)*, pages 265–284, 2006.

Cynthia Dwork, Aaron Roth, et al. The algorithmic foundations of differential privacy. *Foundations and Trends® in Theoretical Computer Science*, 9(3-4):211–407, 2014.

European Parliament and Council of the European Union. Regulation (EU) 2016/679 of the European Parliament and of the Council, 2016. URL `https://data.europa.eu/eli/reg/2016/679/oj`.

Matt Fredrikson, Somesh Jha, and Thomas Ristenpart. Model inversion attacks that exploit confidence information and basic countermeasures. In *Proceedings of the Conference on on Computer and Communiscations Security (CCS)*, pages 1322–1333, 2015.

Badih Ghazi, Noah Golowich, Ravi Kumar, Pasin Manurangsi, and Chiyuan Zhang. Deep learning with label differential privacy. *Advances in Neural Information Processing Systems (NeurIPS)*, 34: 27131–27145, 2021.

Antonio Ginart, Melody Guan, Gregory Valiant, and James Y Zou. Making ai forget you: data deletion in machine learning. *Advances in Neural Information Processing Systems (NeurIPS)*, 32, 2019.

Ian J Goodfellow, Jonathon Shlens, and Christian Szegedy. Explaining and harnessing adversarial examples. *International Conference on Learning Representations (ICLR)*, 2015.

Kaiming He, Xiangyu Zhang, Shaoqing Ren, and Jian Sun. Deep residual learning for image recognition. *Conference on Computer Vision and Pattern Recognition (CVPR)*, pages 770–778, 2016.

C-L Hwang and Abu Syed Md Masud. *Multiple objective decision making—methods and applications: a state-of-the-art survey*, volume 164. Springer Science & Business Media, 2012.

Gautam Kamath. Lecture 12: what is privacy? *Lectures on private ml and stats*, 2020.

Diederik P Kingma and Jimmy Ba. Adam: A method for stochastic optimization. *arXiv preprint arXiv:1412.6980*, 2014.

Anastasia Koloskova, Youssef Allouah, Animesh Jha, Rachid Guerraoui, and Sanmi Koyejo. Certified unlearning for neural networks. *International Conference on Machine Learning (ICML)*, 2025.

Alex Krizhevsky, Geoffrey Hinton, et al. Learning multiple layers of features from tiny images. *Technical Report from the University of Toronto*, 2009.

Solomon Kullback and Richard A Leibler. On information and sufficiency. *The Anals of Mathematical Statistics*, 22(1):79–86, 1951.

Meghdad Kurmanji, Peter Triantafillou, Jamie Hayes, and Eleni Triantafillou. Towards unbounded machine unlearning. *Advances in Neural Information Processing Systems (NeurIPS)*, 2023.

Joon-Woo Lee, HyungChul Kang, Yongwoo Lee, Woosuk Choi, Jieun Eom, Maxim Deryabin, Eunsang Lee, Junghyun Lee, Donghoon Yoo, Young-Sik Kim, et al. Privacy-preserving machine learning with fully homomorphic encryption for deep neural network. *IEEE Access*, 10:30039–30054, 2022.

Ninghui Li, Wahbeh Qardaji, and Dong Su. On sampling, anonymization, and differential privacy or, k-anonymization meets differential privacy. *Proceedings of the Conference on on Computer and Communiscations Security (CCS)*, pages 32–33, 2012.

Aleksander Madry, Aleksandar Makelov, Ludwig Schmidt, Dimitris Tsipras, and Adrian Vladu. Towards deep learning models resistant to adversarial attacks. *International Conference on Learning Representations (ICLR)*, 2018.

Günter Mayer. On the convergence of the neumann series in interval analysis. *Linear algebra and its applications*, 65:63–70, 1985.

Frank Mcsherry. Statistical inference considered harmful, 2016. URL `https://github.com/frankmcsherry/blog/blob/master/posts/2016-06-14.md`.

Kaisa Miettinen. *Nonlinear multiobjective optimization*, volume 12. Springer Science & Business Media, 1999.

Siqiao Mu and Diego Klabjan. Rewind-to-delete: certified machine unlearning for nonconvex functions, 2025. URL `https://arxiv.org/abs/2409.09778`.

Yuval Netzer, Tao Wang, Adam Coates, Alessandro Bissacco, Baolin Wu, Andrew Y Ng, et al. Reading digits in natural images with unsupervised feature learning. *NeurIPS Workshops*, page 4, 2011.

Thanh Tam Nguyen, Thanh Trung Huynh, Zhao Ren, Phi Le Nguyen, Alan Wee-Chung Liew, Hongzhi Yin, and Quoc Viet Hung Nguyen. A survey of machine unlearning. *arXiv preprint arXiv:2209.02299*, 2022.

Jorge Nocedal and Stephen J Wright. *Numerical optimization*. Springer, 1999.

Nicolas Papernot, Shuang Song, Ilya Mironov, Ananth Raghunathan, Kunal Talwar, and Úlfar Erlingsson. Scalable private learning with pate. *International Conference on Learning Representations (ICLR)*, 2018.

Panos M Pardalos, Antanas Žilinskas, Julius Žilinskas, et al. *Non-convex multi-objective optimization*. Springer, 2017.

Barak A Pearlmutter. Fast exact multiplication by the hessian. *Neural computation*, 6(1):147–160, 1994.

Gabriel Pereyra, George Tucker, Jan Chorowski, Łukasz Kaiser, and Geoffrey Hinton. Regularizing neural networks by penalizing confident output distributions. *International Conference on Learning Representations (ICLR)*, 2017.

Mark S Pinsker. Information and information stability of random variables and processes. *Holden-Day*, 1964.

Xinbao Qiao, Meng Zhang, Ming Tang, and Ermin Wei. Hessian-free online certified unlearning. *International Conference on Learning Representations (ICLR)*, 2025.

Ayush Sekhari, Jayadev Acharya, Gautam Kamath, and Ananda Theertha Suresh. Remember what you want to forget: algorithms for machine unlearning. *Advances in Neural Information Processing Systems (NeurIPS)*, 34:18075–18086, 2021.

Congzheng Song, Thomas Ristenpart, and Vitaly Shmatikov. Machine learning models that remember too much. *Proceedings of the Conference on on Computer and Communiscations Security (CCS)*, pages 587–601, 2017.

Yang Song, Jascha Sohl-Dickstein, Diederik P Kingma, Abhishek Kumar, Stefano Ermon, and Ben Poole. Score-based generative modeling through stochastic differential equations. *International Conference on Learning Representations (ICLR)*, 2021.

Ashish Vaswani, Noam Shazeer, Niki Parmar, Jakob Uszkoreit, Llion Jones, Aidan N Gomez, Łukasz Kaiser, and Illia Polosukhin. Attention is all you need. *Advances in Neural Information Processing Systems (NeurIPS)*, 30, 2017.

Roman Vershynin. *High-dimensional probability: An introduction with applications in data science*, volume 47. Cambridge university press, 2018.

Ruihan Wu, Jin Peng Zhou, Kilian Q Weinberger, and Chuan Guo. Does label differential privacy prevent label inference attacks? *International Conference on Artificial Intelligence and Statistics (AISTATS)*, 2023.

Samuel Yeom, Irene Giacomelli, Matt Fredrikson, and Somesh Jha. Privacy risk in machine learning: Analyzing the connection to overfitting. *2018 IEEE Symposium on Computer Security Foundations (CSF)*, pages 268–282, 2018.

Da Yu, Saurabh Naik, Arturs Backurs, Sivakanth Gopi, Huseyin A Inan, Gautam Kamath, Janardhan Kulkarni, Yin Tat Lee, Andre Manoel, Lukas Wutschitz, et al. Differentially private fine-tuning of language models. *International Conference on Learning Representations (ICLR)*, 2022.

Tianhe Yu, Saurabh Kumar, Abhishek Gupta, Sergey Levine, Karol Hausman, and Chelsea Finn. Gradient surgery for multi-task learning. *Advances in Neural Information Processing Systems (NeurIPS)*, 33:5824–5836, 2020.

Binchi Zhang, Yushun Dong, Tianhao Wang, and Jundong Li. Towards certified unlearning for deep neural networks. *International Conference on Machine Learning (ICML)*, 2024.

Kairan Zhao, Meghdad Kurmanji, George-Octavian Bărbulescu, Eleni Triantafillou, and Peter Triantafillou. What makes unlearning hard and what to do about it. *Advances in Neural Information Processing Systems (NeurIPS)*, 2024.

Mingyi Zhou, Xiang Gao, Jing Wu, John Grundy, Xiao Chen, Chunyang Chen, and Li Li. Modelobfuscator: obfuscating model information to protect deployed ml-based systems. *Proceedings of the Symposium on Software Testing and Analysis*, pages 1005–1017, 2023.

Appendix

Table of Contents

A THREAT MODEL

To be clear, we say an adversary has *black-box access* if they can only input data into a model and obtain a prediction. We say an adversary has *white-box access* if they have access to the model parameters, learned representations, and architecture as well. In our paper, we focus on designing attacks for an adversary with white-box access.

Concretely, let $f_{\mathcal{A}(\mathcal{D})}$ be the original model pretrained over $\mathcal{D}$. In our setting, a white box adversary has access to the following information:

- The instances $\mathcal{D}_f$; they do not, however, have access to their ground truth labels, but rather $\mathcal{D}_f$ restricted to $\mathcal{X}$.
- The model $f_{\mathcal{A}(\mathcal{D})}$. The adversary has full access to the model architecture, including parameters, learned representations, and all other components.

Then, the adversary seeks to test $f_{\mathcal{A}(\mathcal{D})}$ with the inputs in $\mathcal{D}_f$ in order to obtain a warrant by which they can harm the owners of the instances in $\mathcal{D}_f$.

Given this, an algorithm $\mathcal{G}$ satisfies *test-time privacy* if the adversary can only guess at the model output for all instances in $\mathcal{D}_f$.

Thus, it does not suffice to simply mask the outputs. For example, suppose one adds an "if" statement to $f_{\mathcal{A}(\mathcal{D})}$: if $\boldsymbol{x} \in \mathcal{D}_f$ is the input, output a uniform distribution over all possible labels i.e. $f_{\mathcal{A}(\mathcal{D})}(\boldsymbol{x}) \approx \mathcal{U}(0, |\mathcal{Y}|)$. Then, an adversary with white-box model access can detect this type of protection and remove it, again obtaining the original prediction of $f_{\mathcal{A}(\mathcal{D})}(\boldsymbol{x})$ for any $\boldsymbol{x} \in \mathcal{D}_f$, since they have access to all model components. As such, to defend against such a white-box adversary, one must perturb the model weights in a non-invertible manner, motivating our approach.

B RELATED WORK

Data Privacy: Data leakage is a persistent danger for large information systems (Al-Rubaie and Chang, 2019). In the context of ML, data privacy is ubiquitous (Fredrikson et al., 2015); (Song et al., 2017); (Yeom et al., 2018). Approaches to privacy-preserving ML include differential privacy (Dwork et al., 2006); (Balle and Wang, 2018); (Amin et al., 2024), homomorphic encryption (Brakerski et al., 2014); (Lee et al., 2022); (Aono et al., 2017), and model obfuscation (Zhou et al., 2023). Notably, these methods protect against various privacy violations, like reconstruction attacks (Dinur and Nissim, 2003) due to failures of anonymization (Li et al., 2012). However, existing methods do not prevent confidently correct classification, and thus fail to protect against the attacks we consider in our setting.

Importantly, the privacy-preserving ML literature does not view a model's correct operation–e.g. producing accurate predictions–as a privacy breach by the data controller (Bun et al., 2021); (Mcsherry, 2016); (Kamath, 2020). In our threat model, we likewise do not fault the data controller for issuing accurate predictions on $\boldsymbol{x}_p$. Nonetheless, even correct predictions can be weaponized against a user. Therefore, we propose a mechanism that enables controllers to guard against such attacks, strengthening user privacy.

Differential Privacy: Specifically, differential privacy has widely been studied in the ML community in order to ensure privacy-preservation (Chaudhuri and Monteleoni, 2008); (Chaudhuri et al., 2011); (Abadi et al., 2016); (Chua et al., 2024). There also exist methods to finetune pretrained models to satisfy differential privacy (Yu et al., 2022). Furthermore, there are also ways to aggregate label noise to preserve privacy (Papernot et al., 2018).

However, differential privacy is designed to address an entirely different threat model than ours. In particular, in the threat model of differential privacy, an adversary seeks to use model outputs to recover private information about data instance $\boldsymbol{x}_p$ corresponding to person p. A differentially private classifier generally results in confident, accurate predictions. This does not address our threat model, where an adversary may use model outputs to violate the privacy of person p in a different manner, taking advantage of them directly to cause harm to person p. Notably, such an adversary is not necessarily gleaning private information about $\boldsymbol{x}_p$, or its associated label y_p.

Label Differential Privacy: Similarly, our formulation differs from label differential privacy (LabelDP) (Ghazi et al., 2021), which seeks to protect an adversary from learning the true labels of the instances in the training data. Given an instance, even after computing $f(\boldsymbol{x}_p)$, under LabelDP an adversary cannot be confident that $f(\boldsymbol{x}_p) = y$. However, LabelDP is applied to the entire dataset; our threat model involves only a particular subset of the training data. Furthermore, we do not need to protect the user's ground truth label, necessarily. In our law enforcement example in Sec. 1, the agency does not care about the ground truth label. Instead, they want any confirmation such that they have a warrant to act adversarially towards person p; for this, a prediction by model f suffices, and they can rely on the model's softmax confidence output. Thus, one must induce uniformity over the softmax outputs, which LabelDP does not do while preserving utility for CIFAR-scale datasets as presented in Tab. 1.

Furthermore, from the perspective of protecting the privacy of the labels themselves, rather than protecting against any confident prediction, Busa-Fekete et al. (2021) demonstrate that testing a model, trained with LabelDP, on the training dataset allows an adversary to recover the labels of the label-private data with high probability. Since our algorithms induce uniformity, an adversary cannot infer the correct forget set labels by testing the model on the training dataset; thus, we provide better privacy against this threat model than LabelDP as well. Wu et al. (2023) argue that, under this threat model where one seeks to protect the labels, any model that generalizes must leak the accurate labels when tested on the training data. However, as we demonstrate by inducing uniformity while maintaining high test accuracy, this only holds when the model is to be tested on the *entire* training data, not a *subset* of the training data, as in our setting.

Machine Unlearning: Machine unlearning (Sekhari et al., 2021); (Bourtoule et al., 2021); (Kurmanji et al., 2023) is inspired by the right to be forgotten (RBTF), mandating that data controllers delete user data upon request (European Parliament and Council of the European Union, 2016). In practice, data controllers must remove user data and its effects from trained models and algorithms. A naive approach is to retrain the model from scratch without the user's data. However, this is prohibitively expensive for large models. Thus, various methods have been developed to comply without retraining from scratch, including resource-efficient retraining (Bourtoule et al., 2021) and heuristic methods like finetuning through student-teacher knowledge distillation (Kurmanji et al., 2023).

While these methods are largely heuristic and do not come with formal guarantees, there exist *certified* unlearning methods (Sekhari et al., 2021) which formally guarantee that after applying structured noise, the pretrained model will be statistically indistinguishable from retraining. However, whether certified or not, as demonstrated by Zhao et al. (2024), all state-of-the-art unlearning methods result in instances common in the training distribution to result in the same classification after unlearning with high confidence. Thus, certified unlearning does not protect against the attacks we seek to defend against.

Misclassification & Relabeling in Unlearning: Recently, methods have emerged to finetune a model to misclassify rather than mimicking retraining from scratch (Cha et al., 2024). There are other similar relabeling methods in the debiasing literature which could be used for this purpose (Angelopoulos et al., 2025). However, these methods often achieve poor performance on the remaining training data and fail to provide protection against our threat model in all cases. In particular, a purposefully incorrect classification can also be used to endanger an individual. For example, in the police example in Sec. 1, it may still be problematic to classify the user as "low risk" instead of "high risk". Furthermore, in the binary classification case, if an adversary knows that $\boldsymbol{x}_p$ is in the forget set, they can recover the true $f(\boldsymbol{x}_p)$ by taking complements, if an unlearning method which seeks to induce misclassification is used. They can also use the information that learned representations are markedly different than other similar examples to understand the method used. Additionally, in the multiclass setting, they can still take complements of this class, yielding a probability of recovering the true class which is better than choosing uniformly at random. Instead, it is fairer and more robust to have an output that is maximally uncertain.

C Uniformity Metric

The confidence distance quantifies the adversary's confidence in their final prediction, i.e. the difference between the argmax softmax score and the uniform softmax score. Importantly, our

method aims to have the adversary lack confidence in their final prediction. Thus, our metric captures what we aim to measure and is interpretable.

Furthermore, confidence distance allows us to quantify how uncertain the model is without relying on accuracy, since a drop in forget set accuracy is not the goal of our formulation. Next, if the maximum confidence score is very close to the uniform distribution, the probability mass of the output distribution must be distributed over the other softmax outputs, clearly yielding that the higher our uniformity metric, the more confident our model is, and the lower our uniformity metric, the less confident our model is. Additionally, it takes the dataset into account; for example, in CIFAR10, one would expect a uniformity score of ≈ 0.2 to be reasonable, as then the adversary can only be $\approx 30\%$ confident that they have a useful prediction. However, for CIFAR100, a uniformity score of ≈ 0.2 is much better, as it implies that an adversary can only be $\approx 21\%$ confident that they have a useful prediction.

One objection to the use of this metric may be that it does not indicate uniformity if it is low. For example, on CIFAR10, one could have a confidence score of 0.2, which yields that the max softmax output is 0.35. There could be three other nonzero softmax outputs of 0.3, 0.3, 0.1, 0.05; this clearly is not uniform. However, this ensures test-time privacy; a test-time privacy adversary now has little confidence in their prediction, even if they choose the first one, rendering their warrant for misuse of sensitive data useless.

We compare our confidence distance metric to other similar metrics in Sec. J.

D Designing Certified Algorithms

In our setting, the original model is obtained using ERM over some loss function $\mathcal{L}_{\mathcal{A}}$, some dataset $\mathcal{D}$, and some parameter space $\mathcal{W}$. Furthermore, we consider the common scenario where the cumulative loss $\mathcal{L}_{\mathcal{A}}$ over the dataset is a finite sum of individual losses $\ell_{\mathcal{A}}$. Thus, we denote the pretrained model as:

$$\boldsymbol{w}^* = \mathcal{A}(D) := \arg\min_{\boldsymbol{w}\in\mathcal{W}} \mathcal{L}_{\mathcal{A}}(\boldsymbol{w}, \mathcal{D}) = \arg\min_{\boldsymbol{w}\in\mathcal{W}} \sum_{i=1}^{|\mathcal{D}|} \ell_{\mathcal{A}}(\boldsymbol{w}, \mathcal{D}^{(i)}). \tag{13}$$

By Prop. 2.2, we can similarly obtain a uniform learner through ERM with respect to some loss function $\mathcal{L}_{\mathcal{K}}$. Furthermore, in our setting, we have the forget set $\mathcal{D}_f$ and retain set $\mathcal{D}_r = \mathcal{D} \setminus \mathcal{D}_f$. Thus, the uniform learner over the retain set can be characterized as:

$$\mathcal{K}(\mathcal{D}_f) := \arg\min_{\boldsymbol{w}\in\mathcal{W}} \mathcal{L}_{\mathcal{K}}(\boldsymbol{w}, \mathcal{D}) = \sum_{i=1}^{|\mathcal{D}_f|} \ell_{\mathcal{K}}(\boldsymbol{w}, \mathcal{D}_f^{(i)}). \tag{14}$$

Let $\theta \in (0, 1)$ be a tradeoff parameter between uniformity over the forget set and utility over the retain set. This yields a concrete characterization of $\mathcal{M}_\theta$ as:

$$\tilde{\boldsymbol{w}}^* = \mathcal{M}_\theta(D) := \arg\min_{\boldsymbol{w}\in\mathcal{W}} \theta\mathcal{L}_{\mathcal{K}}(\boldsymbol{w}, \mathcal{D}_f) + (1-\theta)\mathcal{L}_{\mathcal{A}}(\boldsymbol{w}, \mathcal{D}_r), \tag{15}$$

$$= \arg\min_{\boldsymbol{w}\in\mathcal{W}} \theta \sum_{i=1}^{|\mathcal{D}_f|} \ell_{\mathcal{K}}(\boldsymbol{w}, \mathcal{D}_f^{(i)}) + (1-\theta) \sum_{i=1}^{|\mathcal{D}_r|} \ell_{\mathcal{A}}(\boldsymbol{w}, \mathcal{D}_r^{(i)}). \tag{16}$$

as in Eq. (8).

To design an algorithm which takes in $\mathcal{D}, \mathcal{D}_r$, and $\boldsymbol{w}^*$ and outputs a parameter which satisfies Def. 2.6, we follow the methodology of certified unlearning, which seeks to satisfy Def. 2.5. Specifically, given our setup, we extend the state-of-the-art algorithm of Zhang et al. (2024) to our setting.

First, we simplify the problem of deriving a model that satisfies Def. 2.6:

Theorem D.1. *(Certification Guarantee) Let $\tilde{\boldsymbol{w}} := \mathcal{F}(\mathcal{D}, \mathcal{D}_f, \boldsymbol{w}^*)$ be an approximation to $\tilde{\boldsymbol{w}}^*$. Suppose $||\tilde{\boldsymbol{w}} - \tilde{\boldsymbol{w}}^*||_2 \leq \Delta$. Then, $\mathcal{U}(\mathcal{D}, \mathcal{D}_f, A(D)) = \boldsymbol{w}^- = \tilde{\boldsymbol{w}} + \boldsymbol{Y}$ is a $(\epsilon, \delta, \theta)$ certified uniformity algorithm, where $Y \sim \mathcal{N}(0, \sigma^2 \boldsymbol{I})$ and $\sigma \geq \frac{\Delta}{\epsilon}\sqrt{2\ln(1.25/\delta)}$.*

Proof: See Sec. E.4.

Thus, it then suffices to find an approximation of $\tilde{\boldsymbol{w}}^*$, i.e. a form for $\mathcal{F}(\mathcal{D}, \mathcal{D}_f, \boldsymbol{w}^*)$ and its associated Δ. To do so, we consider the two assumptions Asm. 3.3 and Asm. 3.4.

For any $\boldsymbol{w} \in \mathcal{W}$, denote $\nabla_{\boldsymbol{w},\mathcal{K},\mathcal{A}} := \nabla_{\boldsymbol{w}}(\theta\mathcal{L}_{\mathcal{K}}(\boldsymbol{w}, \mathcal{D}_f) + (1-\theta)\mathcal{L}_{\mathcal{A}}(\boldsymbol{w}, \mathcal{D}_r))$, the gradient of the objective of $\mathcal{M}_\theta$ with respect to $\boldsymbol{w}$, and $\boldsymbol{H}_{\boldsymbol{w},\mathcal{K},\mathcal{A}} := \nabla^2_w(\theta\mathcal{L}_{\mathcal{K}}(\boldsymbol{w}, \mathcal{D}_f) + (1-\theta)\mathcal{L}_{\mathcal{A}}(\boldsymbol{w}, \mathcal{D}_r))$, the Hessian of the objective of $\mathcal{M}_\theta$ with respect to $\boldsymbol{w}$. We thus have $\nabla_{\boldsymbol{w},\mathcal{K},\mathcal{A}} = \theta\nabla_{\boldsymbol{w},\mathcal{K}} + (1-\theta)\nabla_{\boldsymbol{w},\mathcal{A}}$, and similarly for the Hessian.

Next, letting $g(\boldsymbol{w}) := \nabla_{\boldsymbol{w},\mathcal{K},\mathcal{A}}$, by Taylor's theorem, expanding $g(\tilde{\boldsymbol{w}}^*)$ around $\boldsymbol{w}^*$, we have that:

$$g(\tilde{\boldsymbol{w}}^*) \approx g(\boldsymbol{w}^*) + Dg|_{\boldsymbol{w}^*}(\tilde{\boldsymbol{w}}^* - \boldsymbol{w}^*). \tag{17}$$

.

Note that $g(\tilde{\boldsymbol{w}}^*) = 0$, since $\tilde{\boldsymbol{w}}^*$ is the minimizer of the objective in $\mathcal{M}_\theta$. Isolating $\tilde{\boldsymbol{w}}^*$ and using the definition of g, we then have that:

$$\tilde{\boldsymbol{w}}^* \approx \boldsymbol{w}^* - \boldsymbol{H}^{-1}_{\boldsymbol{w}^*,\mathcal{K},\mathcal{A}}\nabla_{\boldsymbol{w}^*,\mathcal{K},\mathcal{A}}. \tag{18}$$

.

Thus, we let $\tilde{\boldsymbol{w}} = \boldsymbol{w}^* - \boldsymbol{H}^{-1}_{\boldsymbol{w}^*,\mathcal{K},\mathcal{A}}\nabla_{\boldsymbol{w}^*,\mathcal{K},\mathcal{A}}$. This yields the following general form of Δ:

Proposition D.2. *Suppose Asm. 3.3 and Asm. 3.4 hold. Suppose $\tilde{\boldsymbol{w}} = \boldsymbol{w}^* - \boldsymbol{H}^{-1}_{\boldsymbol{w}^*,\mathcal{K},\mathcal{A}}\nabla_{\boldsymbol{w}^*,\mathcal{K},\mathcal{A}}$. Then,*

$$||\tilde{\boldsymbol{w}}^* - \tilde{\boldsymbol{w}}||_2 \leq \frac{\theta M_{\mathcal{K}} + (1-\theta)M_{\mathcal{A}}}{2}||\boldsymbol{H}^{-1}_{\boldsymbol{w}^*,\mathcal{K},\mathcal{A}}||_2||\boldsymbol{w}^* - \tilde{\boldsymbol{w}}^*||_2^2. \tag{19}$$

Proof: See Sec. E.5.

We then use local convex approximation (Nocedal and Wright, 1999) to bound $||\boldsymbol{H}^{-1}_{\boldsymbol{w}^*,\mathcal{K},\mathcal{A}}||_2$. To that end, we let the objective of $\mathcal{M}_\theta$ have a regularization term $\frac{\lambda}{2}||\boldsymbol{w}||_2^2$, yielding the inverse Hessian $||(\boldsymbol{H}_{\boldsymbol{w}^*,\mathcal{K},\mathcal{A}} + \lambda\boldsymbol{I})^{-1}||_2$; thus, in Prop. D.2, the norm of the inverse Hessian is replaced by $||(\boldsymbol{H}_{\boldsymbol{w}^*,\mathcal{K},\mathcal{A}} + \lambda\boldsymbol{I})^{-1}||_2$. It then suffices to bound this term.

Additionally, note that since the objective of $\mathcal{M}_\theta$ is nonconvex, the Hessian may not be invertible, i.e. $\lambda_{\min}(\boldsymbol{H}_{\boldsymbol{w}^*,\mathcal{K},\mathcal{A}}) < 0$. However, $\lambda_{\min}(\boldsymbol{H}_{\boldsymbol{w}^*,\mathcal{K},\mathcal{A}} + \lambda\boldsymbol{I}) = \lambda_{\min}(\boldsymbol{H}_{\boldsymbol{w}^*,\mathcal{K},\mathcal{A}}) + \lambda$. Thus, for λ sufficiently large, we can make $\boldsymbol{H}_{\boldsymbol{w}^*,\mathcal{K},\mathcal{A}} + \lambda\boldsymbol{I}$ positive definite and hence invertible, resolving this issue. In particular, we can take $\lambda > ||\boldsymbol{H}_{\boldsymbol{w}^*,\mathcal{K},\mathcal{A}}||_2$.

Furthermore, we let $||\boldsymbol{w}||_2 \leq C$ in $\mathcal{M}_\theta$ and $\mathcal{A}$, i.e. $\mathcal{M}_\theta = \arg\min_{||\boldsymbol{w}||_2 \leq C, \boldsymbol{w}\in\mathcal{W}} \theta\mathcal{L}_{\mathcal{K}}(\boldsymbol{w}, \mathcal{D}_f) + (1-\theta)\mathcal{L}_{\mathcal{A}}(\boldsymbol{w}, \mathcal{D}_{\mathcal{A}}) + \frac{\lambda}{2}||\boldsymbol{w}||_2^2$ and $\mathcal{A}(\mathcal{D}) = \arg\min_{\boldsymbol{w}\in\mathcal{W}, ||\boldsymbol{w}||\leq C} \mathcal{L}_{\mathcal{A}}(\boldsymbol{w}, \mathcal{D})$. Note that, as mentioned in (Zhang et al., 2024), unlearning methods implicitly assume this.

Together, these two methods yield a tractable form of Δ:

Proposition D.3. *Suppose Asm. 3.3 and Asm. 3.4 hold. Suppose $\tilde{\boldsymbol{w}} = \boldsymbol{w}^* - (\boldsymbol{H}_{\boldsymbol{w}^*,\mathcal{K},\mathcal{A}} + \lambda\boldsymbol{I})^{-1}\nabla_{\boldsymbol{w}^*,\mathcal{K},\mathcal{A}}$ where $||\boldsymbol{w}^*||_2, ||\tilde{\boldsymbol{w}}^*||_2 \leq C$. Let $\lambda_{\min} := \lambda_{\min}(\boldsymbol{H}_{\boldsymbol{w}^*,\mathcal{K},\mathcal{A}})$. Suppose $\lambda > ||\boldsymbol{H}_{\boldsymbol{w}^*,\mathcal{K},\mathcal{A}}||_2$. Then,*

$$||\tilde{\boldsymbol{w}}^* - \tilde{\boldsymbol{w}}||_2 \leq \frac{2C((\theta M_K + (1-\theta)M_A)C + \lambda)}{\lambda + \lambda_{\min}}. \tag{20}$$

Proof: See Sec. E.6.

While Prop. D.3 does yield a form of $\mathcal{F}$ and Δ, the computation of $\tilde{\boldsymbol{w}}$ requires obtaining the exact inverse Hessian, which has runtime $\mathcal{O}(dz^2 + z^3)$, where z is the number of learnable parameters. Furthermore, computing the gradient product with the inverse Hessian is $\mathcal{O}(z^2)$. Finally, computing the gradient $\nabla_{\boldsymbol{w}^*,\mathcal{K},\mathcal{A}}$ is $\mathcal{O}(|\mathcal{D}|z)$. Thus, the algorithm yielded by Prop. D.3 has a runtime complexity of $\mathcal{O}(dz^2 + z^3 + z^2 + |\mathcal{D}|z)$.

If we consider the additional assumption of convexity, we can take λ very small to ensure the Hessian is invertible, since we have $\lambda_{\min} = 0$. Thus, for convex models e.g. logistic regression with a mean-square uniform loss, this is tractable. This yields Alg. 2.

However, for nonconvex models e.g. large scale neural networks, this is computationally intractable. Thus, to provide better runtime, we derive an asymptotically unbiased estimator of the inverse Hessian. However, the estimator in Zhang et al. (2024) does not trivially extend to our case. In particular, we cannot glean Hessian samples using sampled i.i.d. data from the retain set, because the Hessian in our setting is defined over the forget set as well. Thus, we must derive an unbiased estimator while sampling Hessians from *both* the retain and forget set. As such, following the techniques of (Agarwal et al., 2016), we design an unbiased estimator as follows:

Theorem D.4. *Suppose we have n i.i.d. data samples $(X_1, ..., X_n)$ drawn from D_f and D_r, uniformly at random, with probabilities θ and $1-\theta$ respectively. Then, suppose $||\boldsymbol{H}_{w^*,\mathcal{K},\mathcal{A}} + \lambda I||_2 \leq H$. For $t = 1, ..., n$, if $X_t \sim D_f$ let $\boldsymbol{H}_{t,\lambda} = \boldsymbol{H}_{w^*,\mathcal{K},t} + \frac{\lambda I}{2\theta}$ and if $X_t \sim D_r$ let $\boldsymbol{H}_{t,\lambda} = \boldsymbol{H}_{w^*,\mathcal{A},t} + \frac{\lambda I}{2(1-\theta)}$. Suppose $\lambda > ||\boldsymbol{H}_{\boldsymbol{w}^*,\mathcal{K},\mathcal{A}}||_2$. Then, compute:*

$$\tilde{\boldsymbol{H}}_{t,\lambda}^{-1} = \boldsymbol{I} + (\boldsymbol{I} - \frac{\boldsymbol{H}_{t,\lambda}}{H})\tilde{\boldsymbol{H}}_{t-1,\lambda}^{-1},\ \tilde{\boldsymbol{H}}_{0,\lambda} = \boldsymbol{I}. \tag{21}$$

Then, $\frac{\tilde{\boldsymbol{H}}_{n,\lambda}^{-1}}{H}$ is an asymptotically unbiased estimator for $(\boldsymbol{H}_{\boldsymbol{w}^*,\mathcal{K},\mathcal{A}} + \lambda \boldsymbol{I})^{-1}$

Proof: See Sec. E.7

One simple choice of H is $H = 2\lambda$, by Lemma E.1. However, we let H be free. The computation of the estimator in theorem D.4 has a runtime complexity of $\mathcal{O}(nz^2)$, a great speedup over the original $\mathcal{O}(dz^2 + z^3)$. Furthermore, with Hessian vector product (HVP) techniques (Pearlmutter, 1994), we obtain a space complexity of $\mathcal{O}(z)$ instead of $\mathcal{O}(z^2)$, since we do not have to compute the sample Hessians explicitly. Furthermore, computing $\tilde{\boldsymbol{H}}_{n,\lambda}^{-1}\nabla_{\boldsymbol{w}^*,\mathcal{K},\mathcal{A}}$ recursively reduces $\mathcal{O}(z^2)$ to $\mathcal{O}(nz)$.

Additionally, following Agarwal et al. (2016), we can average b unbiased estimators $\frac{\tilde{\boldsymbol{H}}_{t,\lambda}^{-1}}{H}$ as $\frac{1}{b}\sum_{i=1}^{b}\frac{\tilde{\boldsymbol{H}}_{t,\lambda}^{-1,(i)}}{H}$ to achieve better concentration. Altogether, we achieve a final runtime complexity of $\mathcal{O}(bnz^2 + bnz + |\mathcal{D}|z)$.

Furthermore, we relax the assumption that $\boldsymbol{w}^*$ and $\tilde{\boldsymbol{w}}^*$ are the global minimizers of $\mathcal{L}_{\mathcal{A}}$ and $\theta\mathcal{L}_{\mathcal{A}} + (1-\theta)\mathcal{L}_{\mathcal{K}}$. We do so because, in practice, it is possible that the data controller trained their model with early stopping, i.e. they did not reach the global minimizer. Altogether, this yields a final form of Δ as:

Theorem D.5. *Let $\tilde{\boldsymbol{w}}^*$ and $\boldsymbol{w}^*$ not be empirical risk minimizers of their respective losses, but rather approximations thereof. Suppose Asm. 3.3 and Asm. 3.4 hold. Suppose $||\boldsymbol{w}^*||_2, ||\tilde{\boldsymbol{w}}^*||_2 \leq C$. Let $\lambda_{\min} := \lambda_{\min}(\boldsymbol{H}_{\boldsymbol{w}^*,\mathcal{K},\mathcal{A}})$. Suppose $\lambda > ||\boldsymbol{H}_{\boldsymbol{w}^*,\mathcal{K},\mathcal{A}}||_2$. Let $\tilde{\boldsymbol{w}} = \boldsymbol{w}^* - \frac{\tilde{\boldsymbol{H}}_{t,\lambda}^{-1}}{H}\nabla_{\boldsymbol{w}^*,\mathcal{K},\mathcal{A}}$. Let b be the number of inverse Hessian estimators we average. Letting n be the number of steps taken during unbiased estimation of the inverse Hessian, require $n \geq 2\frac{B}{\lambda+\lambda_{\min}}\ln(\frac{B}{\lambda+\lambda_{\min}}b)$ where $B = \max\{\frac{\theta L_{\mathcal{K}}+\lambda}{|\mathcal{D}_f|}, \frac{(1-\theta)L_{\mathcal{A}}+\lambda}{|\mathcal{D}_r|}\}$. Suppose $||\nabla_{\boldsymbol{w}^*,\mathcal{K},\mathcal{A}}||_2, ||\nabla_{\tilde{\boldsymbol{w}}^*,\mathcal{K},\mathcal{A}}||_2 \leq G$, With probability larger than $1-\rho$, we have that:*

$$||\tilde{\boldsymbol{w}}^* - \tilde{\boldsymbol{w}}||_2 \leq \frac{2C((\theta M_{\mathcal{K}} + (1-\theta)M_{\mathcal{A}})C + \lambda) + G}{\lambda + \lambda_{\min}} \tag{22}$$

$$+ (16\frac{B}{\zeta_{\min}}\sqrt{\frac{\ln(\frac{d}{\rho})}{b}} + \frac{1}{16})(2C(\theta L_{\mathcal{K}} + (1-\theta)L_{\mathcal{A}}) + G). \tag{23}$$

Algorithm 3 $(\epsilon, \delta, \theta)$-Certified Uniformity with Inverse Hessian Estimator

Require: Dataset $\mathcal{D}$; forget set $\mathcal{D}_f$; pretrained model $\boldsymbol{w}^* = \mathcal{A}(\mathcal{D})$; privacy budgets ϵ and δ; uniformity-utility tradeoff coefficient θ; estimator concentration b; sample size n; local convex coefficient λ; norm upper bound C; cumulative Hessian upper bound H; individual Hessian minimum eigenvalue upper bound $\zeta_{\min}$; gradient norm upper bound G; bound looseness probability ρ.

$\boldsymbol{P}_{0,\lambda}^{(0)} \leftarrow \nabla_{\boldsymbol{w}^*,\mathcal{K},\mathcal{A}}$
for $j = 1, ..., b$ **do**
  for $t = 1, ..., n$ **do**
    Sample X_t from D_f uniformly with probability θ or,
    sample X_t from D_r uniformly with probability $1 - \theta$.
    if $X_t \sim D_f$ **then**
      $\boldsymbol{H}_{t,\lambda}^{(j)} \leftarrow \nabla_{\boldsymbol{w}}^2 \mathcal{L}_{\mathcal{K}}(\boldsymbol{w}^*, X_i) + \frac{\lambda \boldsymbol{I}}{2\theta}$.
    else if $X_t \sim D_r$ **then**
      $\boldsymbol{H}_{t,\lambda}^{(j)} \leftarrow \nabla_{\boldsymbol{w}}^2 \mathcal{L}_{\mathcal{A}}(\boldsymbol{w}^*, X_i) + \frac{\lambda \boldsymbol{I}}{2(1-\theta)}$.
    end if
  $\boldsymbol{P}_{t,\lambda}^{(j)} = \boldsymbol{P}_{0,\lambda}^{(0)} + (\boldsymbol{I} - \frac{\boldsymbol{H}_{t,\lambda}^{(j)}}{H}) \boldsymbol{P}_{t-1,\lambda}^{(j)}$.
  end for
end for
$\boldsymbol{P}_{n,\lambda} \leftarrow \frac{1}{b} \sum_{j=1}^{b} \boldsymbol{P}_{n,\lambda}^{(j)}$.
$\tilde{\boldsymbol{w}} \leftarrow \boldsymbol{w}^* - \frac{\boldsymbol{P}_{n,\lambda}}{H}$.
Compute Δ as the bound in Eq. (23).
$\sigma = \frac{\Delta}{\epsilon} \sqrt{2 \ln(1.25/\delta)}$
$\boldsymbol{w}^- \leftarrow \tilde{\boldsymbol{w}} + Y$ where $Y \sim \mathcal{N}(\boldsymbol{0}, \sigma^2 \boldsymbol{I})$.
return $\boldsymbol{w}^-$.

where $\zeta_{\min} \geq \min_i \lambda_{\min}(\nabla_{\boldsymbol{w}}^2 \tilde{\ell}_{\mathcal{K},\mathcal{A}}(\boldsymbol{w}, \mathcal{D}^{(i)}))$.

Proof: See Sec. E.8.

Note that if we let $\boldsymbol{w}^*$ be an ERM in theorem D.5, we can use $\nabla_{\boldsymbol{w},\mathcal{K},\mathcal{A}}$ and obtain the same result. Altogether, this yields Alg. 3.

E PROOFS

E.1 HELPFUL LEMMAS

Lemma E.1. *Given Asm. 3.3, the gradients $\nabla_{\boldsymbol{w},\mathcal{K}}$ and $\nabla_{\boldsymbol{w},\mathcal{A}}$ exist and are Lipschitz with constants $L_{\mathcal{K}}$ and $L_{\mathcal{A}}$, respectively. Furthermore, given Asm. 3.4, the Hessians $\boldsymbol{H}_{\boldsymbol{w},\mathcal{K}}$ and $\boldsymbol{H}_{\boldsymbol{w},\mathcal{A}}$ exist and are Lipschitz with constants $M_{\mathcal{K}}$ and $M_{\mathcal{A}}$, respectively.*

Proof.

$$||\nabla_{\boldsymbol{w}_1,\mathcal{K}} - \nabla_{\boldsymbol{w}_2,\mathcal{K}}||_2 = ||\sum_{i=1}^{|\mathcal{D}_f|} \nabla^2 \ell_{\mathcal{K}}^{(i)}(\boldsymbol{w}_1, \mathcal{D}_f^{(i)}) - \sum_{i=1}^{|\mathcal{D}_f|} \nabla^2 \ell_{\mathcal{K}}^{(i)}(\boldsymbol{w}_2, \mathcal{D}_f^{(i)})||_2 \tag{24}$$

$$\leq \sum_{i=1}^{|\mathcal{D}_f|} ||\nabla^2 \ell_{\mathcal{K}}^{(i)}(\boldsymbol{w}_1, \mathcal{D}_f^{(i)}) - \nabla^2 \ell_{\mathcal{K}}^{(i)}(\boldsymbol{w}_2, \mathcal{D}_f^{(i)})||_2, \text{ triangle inequality} \tag{25}$$

$$\leq \sum_{i=1}^{|\mathcal{D}_f|} \frac{L_{\mathcal{K}}}{|\mathcal{D}_f|} ||\boldsymbol{w}_1 - \boldsymbol{w}_2||_2, \text{Asm. 3.3} \tag{26}$$

$$= L_{\mathcal{K}} ||\boldsymbol{w}_1 - \boldsymbol{w}_2||_2 \tag{27}$$

This follows similarly for $\nabla_{\boldsymbol{w},\mathcal{A}}$, $\boldsymbol{H}_{\boldsymbol{w},\mathcal{K}}$, and $\boldsymbol{H}_{\boldsymbol{w},\mathcal{A}}$. □

Lemma E.2. *Given Asm. 3.3, for any dataset $\mathcal{D} \subset \mathcal{Z}^n$, $\mathcal{L}_\mathcal{A}$ satisfies:*

$$|\mathcal{L}_A(\boldsymbol{w}_1, \mathcal{D}) - \mathcal{L}_\mathcal{A}(\boldsymbol{w}_2, \mathcal{D})| \leq \frac{L_\mathcal{A}}{2}||\boldsymbol{w}_1 - \boldsymbol{w}_2||_2^2 + ||\nabla_{\boldsymbol{w}_2,\mathcal{A}}||_2||\boldsymbol{w}_1 - \boldsymbol{w}_2||_2 \tag{28}$$

Proof. By the fundamental theorem of calculus, we have the path integral:

$$\int_0^1 \langle \nabla_{\boldsymbol{w}_2 + t(\boldsymbol{w}_1 - \boldsymbol{w}_2),\mathcal{A}}, \boldsymbol{w}_1 - \boldsymbol{w}_2 \rangle dt = \mathcal{L}_A(\boldsymbol{w}_1, \mathcal{D}) - \mathcal{L}_\mathcal{A}(\boldsymbol{w}_2, \mathcal{D}) \tag{29}$$

We have that:

$$\int_0^1 \langle \nabla_{\boldsymbol{w}_2 + t(\boldsymbol{w}_1 - \boldsymbol{w}_2),\mathcal{A}}, \boldsymbol{w}_1 - \boldsymbol{w}_2 \rangle dt = \int_0^1 \langle \nabla_{\boldsymbol{w}_2,\mathcal{A}} - \nabla_{\boldsymbol{w}_2,\mathcal{A}} + \nabla_{\boldsymbol{w}_2 + t(\boldsymbol{w}_1 - \boldsymbol{w}_2),\mathcal{A}}, \boldsymbol{w}_1 - \boldsymbol{w}_2 \rangle dt \tag{30}$$

$$= \int_0^1 \langle \nabla_{\boldsymbol{w}_2,\mathcal{A}}, \boldsymbol{w}_1 - \boldsymbol{w}_2 \rangle dt \tag{31}$$

$$+ \int_0^1 \langle \nabla_{\boldsymbol{w}_2 + t(\boldsymbol{w}_1 - \boldsymbol{w}_2),\mathcal{A}} - \nabla_{\boldsymbol{w}_2,\mathcal{A}}, \boldsymbol{w}_1 - \boldsymbol{w}_2 \rangle dt \tag{32}$$

The first term can be bounded by Cauchy-Schwarz as:

$$\int_0^1 \langle \nabla_{\boldsymbol{w}_2,\mathcal{A}}, \boldsymbol{w}_1 - \boldsymbol{w}_2 \rangle dt \leq ||\nabla_{\boldsymbol{w}_2,\mathcal{A}}||_2||\boldsymbol{w}_1 - \boldsymbol{w}_2||_2 \tag{33}$$

and similarly the second term can be bounded by Cauchy-Schwarz as:

$$\int_0^1 \langle \nabla_{\boldsymbol{w}_2 + t(\boldsymbol{w}_1 - \boldsymbol{w}_2),\mathcal{A}} - \nabla_{\boldsymbol{w}_2,\mathcal{A}}, \boldsymbol{w}_1 - \boldsymbol{w}_2 \rangle dt \leq \int_0^1 ||\nabla_{\boldsymbol{w}_2 + t(\boldsymbol{w}_1 - \boldsymbol{w}_2),\mathcal{A}} - \nabla_{\boldsymbol{w}_2,\mathcal{A}}||_2||\boldsymbol{w}_1 - \boldsymbol{w}_2||_2 dt \tag{34}$$

$$\leq \int_0^1 L_\mathcal{A} t||\boldsymbol{w}_1 - \boldsymbol{w}_2||_2, \text{by Lemma E.1} \tag{35}$$

$$\leq \frac{L_\mathcal{A}}{2}||\boldsymbol{w}_1 - \boldsymbol{w}_2||_2 \tag{36}$$

Incorporating these bounds into Eq. (32) and Eq. (29), upon applying the triangle inequality, yields:

$$|\mathcal{L}_A(\boldsymbol{w}_1, \mathcal{D}) - \mathcal{L}_\mathcal{A}(\boldsymbol{w}_2, \mathcal{D})| \leq \frac{L_\mathcal{A}}{2}||\boldsymbol{w}_1 - \boldsymbol{w}_2||_2^2 + ||\nabla_{\boldsymbol{w}_2,\mathcal{A}}||_2||\boldsymbol{w}_1 - \boldsymbol{w}_2||_2 \tag{37}$$

as desired.

□

Lemma E.3. *Given Asm. 3.4, the Hessians $\boldsymbol{H}_{\boldsymbol{w},\mathcal{K}}$, $\boldsymbol{H}_{\boldsymbol{w},\mathcal{A}}$, and $\boldsymbol{H}_{\boldsymbol{w},\mathcal{K},\mathcal{A}}$ are symmetric.*

Proof. By Lemma E.1, the Hessians $\boldsymbol{H}_{\boldsymbol{w},\mathcal{K}}$ and $\boldsymbol{H}_{\boldsymbol{w},\mathcal{A}}$ are continuous, and thus $\boldsymbol{H}_{\boldsymbol{w},\mathcal{K},\mathcal{A}}$ is continuous by linearity. Hence, all second-order partial derivatives contained in the Hessians are continuous, so by Schwartz's theorem all Hessians are symmetric. Importantly, for e.g. $\boldsymbol{H}_{\boldsymbol{w},\mathcal{K},\mathcal{A}}$, $||\boldsymbol{H}_{\boldsymbol{w},\mathcal{K},\mathcal{A}}||_2 = \max_i |\lambda_i(\boldsymbol{H}_{\boldsymbol{w},\mathcal{K},\mathcal{A}})|$, where λ_i denotes the ith eigenvalue. □

Lemma E.4. *(Corollary of Theorem A.1 in (Dwork et al., 2014)) Let $X \sim \mathcal{N}(\lambda, \sigma^2 \boldsymbol{I})$ and $\mathcal{Y} \sim \mathcal{N}(\lambda', \sigma^2 \boldsymbol{I})$. Suppose $||\lambda - \lambda'||_2 \leq \Delta$. Then for any $\delta > 0$, X and Y are (ε, δ)-indistinguishable if $\sigma \geq \frac{\Delta}{\varepsilon}\sqrt{2\ln(1.25/\delta)}$*

Lemma E.5. *Suppose we have n i.i.d. data samples $(X_1, ..., X_n)$ drawn from D_f and D_r with probabilities θ and $1-\theta$ respectively. For $t = 1, ..., n$, if $X_t \sim D_f$ let $\boldsymbol{H}_{t,\lambda} = \boldsymbol{H}_{w^*,\mathcal{K},t} + \frac{\lambda I}{2\theta}$ and if $X_t \sim D_r$ let $\boldsymbol{H}_{t,\lambda} = \boldsymbol{H}_{w^*,\mathcal{A},t} + \frac{\lambda I}{2(1-\theta)}$. Then, $\mathbb{E}[\boldsymbol{H}_{t,\lambda}] = \boldsymbol{H}_{\boldsymbol{w}^*,\mathcal{K},\mathcal{A}} + \lambda \boldsymbol{I}$ i.e. $\boldsymbol{H}_{t,\lambda}$ is an unbiased estimator of our Hessian of interest.*

Proof. At time t, we have sample X_t s.t. $X_t \sim D_r$ or $X_t \sim D_f$. Note that $\mathbb{E}_{X_t \sim D_f}[\boldsymbol{H}_{\boldsymbol{w}^*,\mathcal{K},t} + \frac{\lambda \boldsymbol{I}}{2\theta}] = \boldsymbol{H}_{\boldsymbol{w}^*,\mathcal{K}} + \frac{\lambda \boldsymbol{I}}{2\theta}$, and likewise $\mathbb{E}_{X_t \sim D_r}[\boldsymbol{H}_{\boldsymbol{w}^*,\mathcal{A},t} + \frac{\lambda \boldsymbol{I}}{2(1-\theta)}] = \boldsymbol{H}_{\boldsymbol{w}^*,\mathcal{A}} + \frac{\lambda \boldsymbol{I}}{2(1-\theta)}$.

By the law of iterated expectation, we have that:

$$\begin{aligned}
\mathbb{E}[\boldsymbol{H}_{t,\lambda}] &= \mathbb{E}[\boldsymbol{H}_{t,\lambda} | X_t \sim \mathcal{D}_f] \Pr(X_t \sim \mathcal{D}_f) + \mathbb{E}[\boldsymbol{H}_{t,\lambda} | X_t \sim \mathcal{D}_r] \Pr(X_t \sim \mathcal{D}_r) \\
&= \theta \mathbb{E}_{X_t \sim D_f}[\boldsymbol{H}_{\boldsymbol{w}^*,\mathcal{K},t} + \frac{\lambda I}{2\theta})] + (1-\theta)\mathbb{E}_{X_t \sim \mathcal{D}_r}[\boldsymbol{H}_{\boldsymbol{w}^*,\mathcal{A},t} + \frac{\lambda I}{2(1-\theta)}] \\
&= \theta(\boldsymbol{H}_{\boldsymbol{w}^*,\mathcal{K}} + \frac{\lambda I}{2\theta}) + (1-\theta)(\boldsymbol{H}_{\boldsymbol{w}^*,\mathcal{A}} + \frac{\lambda I}{2(1-\theta)}) \\
&= \theta \boldsymbol{H}_{\boldsymbol{w}^*,\mathcal{K}} + (1-\theta)\boldsymbol{H}_{\boldsymbol{w}^*,\mathcal{A}} + \lambda I \\
&= \boldsymbol{H}_{\boldsymbol{w}^*,\mathcal{K},\mathcal{A}} + \lambda \boldsymbol{I}
\end{aligned}$$

as desired. □

Lemma E.6. *Suppose Assumptions 3.3 and 3.4 hold. Let local condition number $\hat{\kappa}_l$ and maximum local condition number $\hat{\kappa}_l^{\max}$ correspond to the definitions of Agarwal et al. (2016) with respect to the Hessian of the loss of $\mathcal{M}_\theta$ after local convex approximation. Then, $\hat{\kappa}_l \leq \frac{B}{\lambda + \lambda_{\min}}$ and $\hat{\kappa}_l^{\max} \leq \frac{B}{\zeta_{\min}}$ where $B = \max\{\frac{\theta L_\mathcal{K} + \lambda}{|\mathcal{D}_f|}, \frac{(1-\theta)L_\mathcal{A} + \lambda}{|\mathcal{D}_r|}\}$ and where $\zeta_{\min} \geq \min_i \lambda_{\min}(\nabla^2_{\boldsymbol{w}} \tilde{\ell}^{(i)}_{\mathcal{K},\mathcal{A}}(\boldsymbol{w}, \mathcal{D}^{(i)}))$*

Proof. By Eq. (8) and our local convex approximation technique, we have that:

$$M_\theta(D) = \arg\min_{\boldsymbol{w} \in \mathcal{W}} \theta \sum_{i=1}^{|\mathcal{D}_f|} \ell^{(i)}_\mathcal{K}(\boldsymbol{w}, \mathcal{D}^{(i)}_f) + (1-\theta) \sum_{i=1}^{|\mathcal{D}_r|} \ell^{(i)}_\mathcal{A}(\boldsymbol{w}, \mathcal{D}^{(i)}_r) + \frac{\lambda}{2}||\boldsymbol{w}||_2^2 \tag{38}$$

$$= \arg\min_{w \in \mathcal{W}} \sum_{i=1}^{|D_f|} (\theta \ell^{(i)}_\mathcal{K}(\boldsymbol{w}, \mathcal{D}^{(i)}_f) + \frac{\lambda}{2|\mathcal{D}_f|}||\boldsymbol{w}||_2^2) + \sum_{i=1}^{|D_r|} (\theta \ell^{(i)}_\mathcal{A}(\boldsymbol{w}, \mathcal{D}^{(i)}_r) + \frac{\lambda}{2|\mathcal{D}_r|}||\boldsymbol{w}||_2^2) \tag{39}$$

$$= \arg\min_{w \in \mathcal{W}} \sum_{i=1}^{|D|} \tilde{\ell}^{(i)}_{\mathcal{K},\mathcal{A}}(\boldsymbol{w}, \mathcal{D}^{(i)}) \tag{40}$$

where

$$\tilde{\ell}^{(i)}_{\mathcal{K},\mathcal{A}}(\boldsymbol{w}, \mathcal{D}^{(i)}) = \begin{cases} \theta \ell^{(i)}_\mathcal{K}(\boldsymbol{w}, \mathcal{D}^{(i)}_f) + \frac{\lambda}{2|\mathcal{D}_f|}||\boldsymbol{w}||_2^2, \ 1 \leq i \leq |\mathcal{D}_f| \\ (1-\theta)\ell^{(i-|\mathcal{D}_f|)}_\mathcal{K}(\boldsymbol{w}, \mathcal{D}^{(i-|\mathcal{D}_f|)}_r) + \frac{\lambda}{2|\mathcal{D}_r|}||\boldsymbol{w}||_2^2, \ |\mathcal{D}_f| + 1 \leq i \leq |\mathcal{D}| \end{cases} \tag{41}$$

By the definitions provided in Agarwal et al. (2016), we have:

$$\hat{\kappa}_l = \max_{\boldsymbol{w} \in \mathcal{W}} \frac{\max_i \lambda_{\max}(\nabla^2_{\boldsymbol{w}} \tilde{\ell}_{\mathcal{K},\mathcal{A}}(\boldsymbol{w}, \mathcal{D}^{(i)}))}{\lambda_{\min}(\boldsymbol{H}_{\boldsymbol{w},\mathcal{K},\mathcal{A}} + \lambda \boldsymbol{I})} \tag{42}$$

and

$$\hat{\kappa}_l^{\max} = \max_{\boldsymbol{w}\in\mathcal{W}} \frac{\max_i \lambda_{\max}(\nabla^2_{\boldsymbol{w}} \tilde{\ell}_{\mathcal{K},\mathcal{A}}(\boldsymbol{w}, \mathcal{D}^{(i)}))}{\min_i \lambda_{\min}(\nabla^2_{\boldsymbol{w}} \tilde{\ell}_{\mathcal{K},\mathcal{A}}(\boldsymbol{w}, \mathcal{D}^{(i)}))} \tag{43}$$

We then have that, for any i,

$$\lambda_{\max}(\nabla^2_{\boldsymbol{w}} \tilde{\ell}^{(i)}_{\mathcal{K},\mathcal{A}}) \leq ||\nabla^2_{\boldsymbol{w}} \tilde{\ell}^{(i)}_{\mathcal{K},\mathcal{A}}||_2, \text{ by Lemma E.3} \tag{44}$$

$$= \max\{||\theta\nabla^2_{\boldsymbol{w}} \ell^{(i)}_{\mathcal{K}} + \frac{\lambda \boldsymbol{I}}{|\mathcal{D}_f|}||_2, ||(1-\theta)\nabla^2_{\boldsymbol{w}} \ell^{(i)}_{\mathcal{A}} + \frac{\lambda \boldsymbol{I}}{|\mathcal{D}_r|}||_2\} \tag{45}$$

$$\tag{46}$$

Furthermore, by Asm. 3.3 and the triangle inequality:

$$||\theta\nabla^2_{\boldsymbol{w}} \ell^{(i)}_{\mathcal{K}} + \frac{\lambda \boldsymbol{I}}{|\mathcal{D}_f|}||_2 \leq \frac{\theta L_{\mathcal{K}} + \lambda}{|\mathcal{D}_f|} \tag{47}$$

and

$$||(1-\theta)\nabla^2_{\boldsymbol{w}} \ell^{(i)}_{\mathcal{A}} + \frac{\lambda \boldsymbol{I}}{|\mathcal{D}_r|}||_2 \leq \frac{(1-\theta) L_{\mathcal{A}} + \lambda}{|\mathcal{D}_r|} \tag{48}$$

Taking max over all i, we obtain that

$$\max_i \lambda_{\max}(\nabla^2_{\boldsymbol{w}} \tilde{\ell}_{\mathcal{K},\mathcal{A}}(\boldsymbol{w}, \mathcal{D}^{(i)})) \leq \max\{\frac{\theta L_{\mathcal{K}} + \lambda}{|\mathcal{D}_f|}, \frac{(1-\theta) L_{\mathcal{A}} + \lambda}{|\mathcal{D}_r|}\} \tag{49}$$

which we denote by B.

Then, we obtain that $\hat{\kappa}_l \leq \frac{B}{\lambda+\lambda_{\min}}$ and $\hat{\kappa}_l^{\max} \leq \frac{B}{\zeta_{\min}}$ as desired, since

□

Lemma E.7. *(Lemma 3.6 adapted from Agarwal et al. (2016)) Suppose Asm. 3.3 and Asm. 3.4 hold. Consider the estimator $\frac{\tilde{\boldsymbol{H}}^{-1}_{\boldsymbol{n},\lambda}}{H}$ in theorem D.4. Let b be the number of inverse Hessian estimators we obtain. Suppose $n \geq 2\frac{B}{\lambda+\lambda_{\min}} \ln(\frac{B}{\lambda+\lambda_{\min}} b)$, where $B = \max\{\frac{\theta L_{\mathcal{K}}+\lambda}{|\mathcal{D}_f|}, \frac{(1-\theta)L_{\mathcal{A}}+\lambda}{|\mathcal{D}_r|}\}$. Then, we have that:*

$$\Pr[||\boldsymbol{H}_{\boldsymbol{w}^*,\mathcal{K},\mathcal{A}} + \lambda \boldsymbol{I})^{-1} - \frac{\tilde{\boldsymbol{H}}^{-1}_{n,\lambda}}{H}||_2 \leq 16\frac{B}{\zeta_{\min}}\sqrt{\frac{\ln(\frac{d}{\rho})}{b}} + \frac{1}{16}] \geq 1-\rho \tag{50}$$

where $\zeta_{\min} \geq \min_i \lambda_{\min}(\nabla^2_{\boldsymbol{w}} \tilde{\ell}^{(i)}_{\mathcal{K},\mathcal{A}}(\boldsymbol{w}, \mathcal{D}^{(i)}))$.

Proof. Note that $b = S_1$ in our setting. In our setting, following the subsequent steps of the proof in Agarwal et al. (2016) after plugging in the bounds in Lemma E.6 in place of $\hat{\kappa}_l, \hat{\kappa}_l^{\max}$, noting that we choose $n = S_2 \geq 2\frac{B}{\lambda+\lambda_{\min}} \ln(\frac{B}{\lambda+\lambda_{\min}} b)$, we obtain the exact same result for the Neumann series bound of $\frac{1}{16}$. Using the fact that $\frac{B}{\zeta_{\min}}$ is an upper bound on $\hat{\kappa}_l^{\max}$ by Lemma E.6, the rest of the proof follows similarly. □

Lemma E.8. *(Proposition 2.1 in Dwork et al. (2014)) Let $\mathcal{M} : \mathbb{N}^{|\mathcal{X}|} \to R$ be a randomized algorithm that is (ε, δ)-differentially private. Let $f : R \to R'$ be an arbitrary mapping. Then, $f \circ \mathcal{M} : \mathbb{N}^{|\mathcal{X}|} \to R'$ is (ε, δ)-differentially private.*

Note that, in the proof of Lemma E.8, one proves this fact for deterministic mappings, so this holds for both randomized and deterministic f.

Lemma E.9. *Consider the mapping $\mathcal{J} : \mathcal{W} \to R$, and suppose $\mathcal{G} : \mathcal{Z}^n \times \mathcal{Z}^n \times \mathcal{W} \to \mathcal{W}$ satisfies Def. 2.6. Then, $\forall C \subset R$:*

$$\Pr(\mathcal{J}(\mathcal{G}(\mathcal{D}, \mathcal{D}_f, \mathcal{A}(\mathcal{D}))) \in C) \leq e^{\varepsilon} \Pr(\mathcal{J}(\mathcal{M}_\theta(\mathcal{D})) \in C) + \delta \tag{51}$$

$$\Pr(\mathcal{J}(\mathcal{M}_\theta(\mathcal{D})) \in C) \leq e^{\varepsilon} \Pr(\mathcal{J}(\mathcal{G}(\mathcal{D}, \mathcal{D}_f, \mathcal{A}(\mathcal{D}))) \in C) + \delta \tag{52}$$

Proof. Immediate from Lemma E.8. □

E.2 Proof of Proposition 2.2

Proof. Fix a dataset $\mathcal{D} \subset \mathcal{Z}^n$.

Suppose we have an $K-$layer function $f_{\boldsymbol{w}} : \mathbb{R}^d \to \mathbb{R}^o$ parameterized by $\boldsymbol{w} \in \mathcal{W}$ of the form $f(\boldsymbol{x}) = L_1 \circ ... \circ L_{K-1} \circ L_K$ where $L_{K-1}(\boldsymbol{x}) = \boldsymbol{W}_{K-1}^T \boldsymbol{x} + \boldsymbol{b}_{K-1}$ and $L_K(\boldsymbol{x}) = \text{softmax}(\boldsymbol{x})$, i.e. $L_{K-1}(\boldsymbol{x})_i = \frac{e^{x_i}}{\sum_{j=1}^{|\mathcal{Y}|} e^{x_j}}$. Thus, $f_{\boldsymbol{w}} \in \mathcal{H}_{\mathcal{W}}$. Then, let $\boldsymbol{W}_{K-1} = \boldsymbol{0}$ and $\boldsymbol{b}_{K-1} = \boldsymbol{0}$.

Fix $\boldsymbol{z} \in \mathcal{D}$. This yields, for $j = 1, ..., |\mathcal{Y}|$, $f(\boldsymbol{z})_j = \frac{e^0}{\sum_{j=1}^{|\mathcal{Y}|} e^0} = \frac{e^0}{|\mathcal{Y}| e^0} = \frac{1}{|\mathcal{Y}|}$. Hence, since $\boldsymbol{z}$ was arbitrary, $f_{\boldsymbol{w}}(\boldsymbol{z}) = (\underbrace{\frac{1}{|\mathcal{Y}|}, ..., \frac{1}{|\mathcal{Y}|}}_{|\mathcal{Y}| \text{ times}})$ $\forall \boldsymbol{z} \in \mathcal{D}$. Since $\mathcal{D}$ was arbitrary, by definition of a uniform learner over $\mathcal{D}$, $f_{\mathcal{K}(\mathcal{D})} \in \mathcal{H}_{\mathcal{W}}$ $\forall \mathcal{D} \subset \mathcal{Z}^n$ as desired.

□

E.3 Proof of Proposition 2.3

We use the following definition of global Pareto optimality:

Definition E.10. *(Chapter 1 of Pardalos et al. (2017)) Suppose we have a multiobjective optimization problem $\min \boldsymbol{f}(\boldsymbol{x})$ s.t. $\boldsymbol{x} \in A$, where $\boldsymbol{f}(\boldsymbol{x}) = (f_1(\boldsymbol{x}), f_2(\boldsymbol{x}), ..., f_m(\boldsymbol{x}))$. $\boldsymbol{x}^* \in A$ with $\boldsymbol{f}(\boldsymbol{x}^*)$ is called globally Pareto optimal if and only if there exists no $\boldsymbol{x} \in A$ such that $f_i(\boldsymbol{x}) \leq f_i(\boldsymbol{x}^*)$ for all $i = 1, 2, ..., m$ and $f_j(\boldsymbol{x}) < f_j(\boldsymbol{x}^*)$ for at least one $j \in \{1, ..., m\}$.*

We can then prove the statement:

Proof. Let $\theta \in (0, 1)$. Fix $\mathcal{D} \subset \mathcal{Z}^n$, $\mathcal{D}_f \subset \mathcal{D}$, and $\mathcal{D}_r = \mathcal{D} \setminus \mathcal{D}_f$.

Suppose, for the sake of contradiction, that $\tilde{\boldsymbol{w}}^* = \mathcal{M}_\theta(\mathcal{D}) = \text{argmin}_{\boldsymbol{w}} \theta \mathcal{L}_{\mathcal{K}}(\boldsymbol{w}, \mathcal{D}_f) + (1 - \theta)\mathcal{L}_{\mathcal{A}}(\boldsymbol{w}, \mathcal{D}_r)$, a global minimizer, is not globally Pareto optimal with respect to $\mathcal{L}_{\mathcal{K}}(\boldsymbol{w}, \mathcal{D}_f)$ and $\mathcal{L}_{\mathcal{A}}(\boldsymbol{w}, \mathcal{D}_r)$. Then, exists $\boldsymbol{w}'$ s.t. $\mathcal{L}_{\mathcal{K}}(\boldsymbol{w}', \mathcal{D}_f) \leq \mathcal{L}_{\mathcal{K}}(\tilde{\boldsymbol{w}}^*, \mathcal{D}_f)$ and $\mathcal{L}_{\mathcal{A}}(\boldsymbol{w}', \mathcal{D}_r) \leq \mathcal{L}_{\mathcal{A}}(\tilde{\boldsymbol{w}}^*, \mathcal{D}_r)$, with at least one of these inequalities being strict.

Then, since $\theta \in (0, 1)$ and $(1 - \theta) \in (0, 1)$, we have that $\theta \mathcal{L}_{\mathcal{K}}(\boldsymbol{w}', \mathcal{D}_f) + (1 - \theta)\mathcal{L}_{\mathcal{A}}(\boldsymbol{w}', \mathcal{D}_r) < \theta \mathcal{L}_{\mathcal{K}}(\tilde{\boldsymbol{w}}^*, \mathcal{D}_f) + (1 - \theta)\mathcal{L}_{\mathcal{A}}(\tilde{\boldsymbol{w}}^*, \mathcal{D}_r)$, contradicting optimality of $\tilde{\boldsymbol{w}}^*$. As such, $\mathcal{M}_\theta(\mathcal{D})$ is globally Pareto optimal respect to $\mathcal{L}_{\mathcal{K}}(\boldsymbol{w}, \mathcal{D}_f)$ and $\mathcal{L}_{\mathcal{A}}(\boldsymbol{w}, \mathcal{D}_r)$ as desired.

This holds similarly for a local minimizer $\tilde{\boldsymbol{w}}^*$, where Pareto optimality similarly holds only locally in a neighborhood around the minima.

□

E.4 Proof of Theorem D.1

Proof. The proof follows similarly to Lemma 10 in Sekhari et al. (2021); for completeness, we adapt their proof to our setting.

Let $\boldsymbol{w}^* := A(D), \boldsymbol{w}^- := \mathcal{G}(\mathcal{D}, \mathcal{D}_f, \boldsymbol{w}^*), \tilde{\boldsymbol{w}} := \mathcal{F}(\mathcal{D}, \mathcal{D}_f, \boldsymbol{w}^*)$. Departing from the notation of the theorem for clarity, let $\hat{\boldsymbol{w}^*} := \mathcal{M}_\theta(\mathcal{D}), \hat{\boldsymbol{w}^-} := \mathcal{G}(\mathcal{D}, \emptyset, \hat{\boldsymbol{w}^*}), \hat{\tilde{\boldsymbol{w}}} := \mathcal{F}(\mathcal{D}, \emptyset, \hat{\boldsymbol{w}^*})$.

Note that $\hat{\tilde{\boldsymbol{w}}} = \hat{\boldsymbol{w}^*}$. We then have that $||\tilde{\boldsymbol{w}} - \hat{\tilde{\boldsymbol{w}}}||_2 = ||\tilde{\boldsymbol{w}} - \hat{\boldsymbol{w}^*}||_2 \leq \Delta$, by definition of Δ.

By definition of $\mathcal{G}$, we have that $\boldsymbol{w}^- = \tilde{\boldsymbol{w}} + Y$ and $\hat{\boldsymbol{w}^-} = \hat{\tilde{\boldsymbol{w}}} + Y$, where $Y \sim \mathcal{N}(0, \sigma^2 \boldsymbol{I})$ s.t. $\sigma \geq \frac{\Delta}{\varepsilon}\sqrt{2\ln(1.25/\delta)}$.

As such, $\boldsymbol{w}^- = \mathcal{N}(\tilde{\boldsymbol{w}}, \sigma^2 \boldsymbol{I})$ and $\hat{\boldsymbol{w}^-} \sim \mathcal{N}(\hat{\tilde{\boldsymbol{w}}}, \sigma^2 \boldsymbol{I})$.

Thus, by Lemma E.4, $\boldsymbol{w}^-, \hat{\boldsymbol{w}^-}$ are (ε, δ)-indistinguishable. In particular, since $\hat{\boldsymbol{w}^-} = \hat{\boldsymbol{w}^*}$ by construction, $\mathcal{G}(\mathcal{D}, \mathcal{D}_f, \mathcal{A}(\mathcal{D}))$ and $\mathcal{M}_\theta(\mathcal{D})$ are (ε, δ)-indistinguishable, as desired.

□

E.5 Proof of Proposition D.2

Proof. By the same token as Lemma 3.3 in (Zhang et al., 2024), we have that:

$$||\tilde{\boldsymbol{w}} - \tilde{\boldsymbol{w}}^*||_2 \leq ||\boldsymbol{H}^{-1}_{\boldsymbol{w}^*,\mathcal{K},\mathcal{A}}||_2 \int_0^1 ||\boldsymbol{H}_{\boldsymbol{w}^*,\mathcal{K},\mathcal{A}} - \boldsymbol{H}_{\boldsymbol{w}^*+t(\tilde{\boldsymbol{w}}^*-\boldsymbol{w}^*),\mathcal{K},\mathcal{A}}||_2 ||\boldsymbol{w}^* - \tilde{\boldsymbol{w}}^*||_2 dt \tag{53}$$

.

Let $\boldsymbol{w}' = \boldsymbol{w}^* + t(\tilde{\boldsymbol{w}} - \boldsymbol{w}^*)$. We have that $||\boldsymbol{w}^* - \boldsymbol{w}'||_2 = ||\boldsymbol{w}^* - \boldsymbol{w}^* + t(\tilde{\boldsymbol{w}}^* - \boldsymbol{w}^*)||_2 = t||\boldsymbol{w}^* - \tilde{\boldsymbol{w}}^*||_2$.

Furthermore, by linearity of $\boldsymbol{H}_{\boldsymbol{w}}$ and the triangle inequality, we have that:

$$\begin{aligned}
||\boldsymbol{H}_{\boldsymbol{w}^*,\mathcal{K},\mathcal{A}} - \boldsymbol{H}_{\boldsymbol{w}',\mathcal{K},\mathcal{A}}||_2 &= ||\theta \boldsymbol{H}_{\boldsymbol{w}^*,\mathcal{K}} + (1-\theta)\boldsymbol{H}_{\boldsymbol{w}^*,\mathcal{A}} - \theta \boldsymbol{H}_{\boldsymbol{w}',\mathcal{K}} - (1-\theta)\boldsymbol{H}_{\boldsymbol{w}',\mathcal{A}}||_2 && (54)\\
&\leq \theta||\boldsymbol{H}_{\boldsymbol{w}^*,\mathcal{K}} - \theta \boldsymbol{H}_{\boldsymbol{w}',\mathcal{K}}||_2 + (1-\theta)||\boldsymbol{H}_{\boldsymbol{w}^*,\mathcal{A}} - \boldsymbol{H}_{\boldsymbol{w}',\mathcal{A}}||_2 && (55)\\
&= \theta M_{\mathcal{K}}||\boldsymbol{w}^* - \boldsymbol{w}'||_2 + (1-\theta)M_{\mathcal{A}}||\boldsymbol{w}^* - \boldsymbol{w}'||_2, \text{ by Lemma E.1} && (56)\\
&= \theta t M_{\mathcal{K}}||\boldsymbol{w}^* - \tilde{\boldsymbol{w}}^*||_2 + (1-\theta)t M_{\mathcal{A}}||\boldsymbol{w}^* - \tilde{\boldsymbol{w}}^*||_2, && (57)
\end{aligned}$$

This yields that:

$$\begin{aligned}
||\tilde{\boldsymbol{w}} - \tilde{\boldsymbol{w}}^*||_2 &\leq ||\boldsymbol{H}^{-1}_{\boldsymbol{w}^*,\mathcal{K},\mathcal{A}}||_2 \int_0^1 ||\boldsymbol{H}_{\boldsymbol{w}^*,\mathcal{K},\mathcal{A}} - \boldsymbol{H}_{\boldsymbol{w}^*+t(\tilde{\boldsymbol{w}}^*-\boldsymbol{w}^*),\mathcal{K},\mathcal{A}}||_2 ||\boldsymbol{w}^* - \tilde{\boldsymbol{w}}^*||_2 dt && (58)\\
&\leq ||\boldsymbol{H}^{-1}_{\boldsymbol{w}^*,\mathcal{K},\mathcal{A}}||_2 \int_0^1 (\theta t M_{\mathcal{K}} + (1-\theta)t M_{\mathcal{A}})||\boldsymbol{w}^* - \tilde{\boldsymbol{w}}^*||_2^2 && (59)\\
&= \frac{\theta M_{\mathcal{K}} + (1-\theta)M_{\mathcal{A}}}{2} ||\boldsymbol{H}^{-1}_{\boldsymbol{w}^*,\mathcal{K},\mathcal{A}}||_2 ||\boldsymbol{w}^* - \tilde{\boldsymbol{w}}^*||_2^2 && (60)
\end{aligned}$$

as desired.

□

E.6 Proof of Proposition D.3

Proof. See the proof of theorem 3.4 in (Zhang et al., 2024), noting that in our setting $M = \theta M_{\mathcal{K}} + (1-\theta)M_{\mathcal{A}}$ by Eq. (57). □

E.7 Proof of Theorem D.4

Proof. First, we have that:

$$\mathbb{E}[\tilde{\boldsymbol{H}}_{t,\lambda}^{-1}] = \mathbb{E}[\boldsymbol{I} + \tilde{\boldsymbol{H}}_{t-1,\lambda}^{-1} - \frac{1}{H}\boldsymbol{H}_{t,\lambda}\tilde{\boldsymbol{H}}_{t-1,\lambda}^{-1}], \text{ by definition} \tag{61}$$

$$= \boldsymbol{I} + \mathbb{E}[\tilde{\boldsymbol{H}}_{t-1,\lambda}^{-1}] - \frac{1}{H}\mathbb{E}[\boldsymbol{H}_{t,\lambda}\tilde{\boldsymbol{H}}_{t-1,\lambda}], \text{ linearity of expectation} \tag{62}$$

$$= \boldsymbol{I} + \mathbb{E}[\tilde{\boldsymbol{H}}_{t-1,\lambda}^{-1}] - \frac{1}{H}\mathbb{E}[\boldsymbol{H}_{t,\lambda}]\mathbb{E}[\tilde{\boldsymbol{H}}_{t-1,\lambda}], \text{i.i.d. samples} \tag{63}$$

$$= \boldsymbol{I} + \mathbb{E}[\tilde{\boldsymbol{H}}_{t-1,\lambda}^{-1}] - \frac{\boldsymbol{H}_{\boldsymbol{w}^*,\mathcal{K},\mathcal{A}} + \lambda\boldsymbol{I}}{H}\mathbb{E}[\tilde{\boldsymbol{H}}_{t-1,\lambda}], \text{ by Lemma E.5} \tag{64}$$

Denote $\boldsymbol{H}_* := \boldsymbol{H}_{\boldsymbol{w}^*,\mathcal{K},\mathcal{A}}$ and $\boldsymbol{E}_t := \mathbb{E}[\tilde{\boldsymbol{H}}_{t,\lambda}^{-1}]$. We thus have that:

$$\boldsymbol{E}_t = \boldsymbol{I} + \boldsymbol{E}_{t-1} - \frac{\boldsymbol{H}_*}{H}\boldsymbol{E}_{t-1} \tag{65}$$

$$= \boldsymbol{I} + \boldsymbol{E}_{t-1}(\boldsymbol{I} - \frac{\boldsymbol{H}_*}{H}) \tag{66}$$

$$= \boldsymbol{I} + (\boldsymbol{I} - \boldsymbol{M})\boldsymbol{E}_{t-1}, \text{ letting } \boldsymbol{M} := \frac{\boldsymbol{H}_*}{H} \tag{67}$$

We then know that, by assumption, $\lambda > ||\boldsymbol{H}_*||_2$, where $\boldsymbol{H}_*$ is a symmetric Hessian by Lemma E.3; as such, $\boldsymbol{H}_* + \lambda\boldsymbol{I}$ is positive definite and has all positive eigenvalues. We also know that $||\boldsymbol{H}_*||_2 < H \implies ||\boldsymbol{M}||_2 < 1$, so we have that $0 < \lambda_i(\boldsymbol{M}) < 1$ for all eigenvalues λ_i. Furthermore, $\boldsymbol{I} - \boldsymbol{M}$ has eigenvalues $1 - \lambda_i(\boldsymbol{M})$, so we have that $0 < \lambda_i(\boldsymbol{I} - \boldsymbol{M}) < 1$, so $||\boldsymbol{I} - \boldsymbol{M}||_2 < 1$, since $\boldsymbol{I} - \boldsymbol{M}$ is symmetric. Since $\boldsymbol{I} - \boldsymbol{M}$ has spectral radius less than 1, the Neumann series $\sum_{k=0}^{\infty}(\boldsymbol{I} - \boldsymbol{M})^k$ converges. (Mayer, 1985). Thus, the Neumann series is Cauchy.

Fix $\varepsilon > 0$. Let $s_n = \sum_{k=0}^{n}(\boldsymbol{I} - \boldsymbol{M})^k$. We know that $\exists N \in \mathbb{N}$ s.t. $m > n \geq N \implies ||s_m - s_n||_2 = ||\sum_{k=n+1}^{m}(\boldsymbol{I} - \boldsymbol{M})^k||_2 < \varepsilon$. For $m > n \geq N$, we have that $||\boldsymbol{E}_m - \boldsymbol{E}_n||_2 = ||\sum_{k=n+1}^{m}(\boldsymbol{I} - \boldsymbol{M})^k||_2 < \varepsilon$. As such, $\{\boldsymbol{E}_n\}$ is Cauchy; since it is real, it converges. As such, $\boldsymbol{E}_\infty = \lim_{t\to\infty}\boldsymbol{E}_n$ exists.

Taking limits on both sides, we then have:

$$\mathbb{E}[\tilde{\boldsymbol{H}}_{\infty,\lambda}^{-1}] = \boldsymbol{I} + \mathbb{E}[\tilde{\boldsymbol{H}}_{\infty,\lambda}^{-1}] + \frac{\boldsymbol{H}_{\boldsymbol{w}^*,\mathcal{K},\mathcal{A}} + \lambda\boldsymbol{I}}{H}\mathbb{E}[\tilde{\boldsymbol{H}}_{\infty,\lambda}] \tag{68}$$

$$\iff \mathbb{E}[\frac{\tilde{\boldsymbol{H}}_{\infty,\lambda}^{-1}}{H}] = (\boldsymbol{H}_{\boldsymbol{w}^*,\mathcal{K},\mathcal{A}} + \lambda\boldsymbol{I})^{-1} \tag{69}$$

rearranging using linearity of expectation and noting that λ was chosen such that $\boldsymbol{H}_{\boldsymbol{w}^*,\mathcal{K},\mathcal{A}} + \lambda\boldsymbol{I}$ is invertible, as desired. □

E.8 Proof of Theorem D.5

This follows similarly to theorem 3.6 and proposition 4.1 in Zhang et al. (2024), noting that we apply Lemma E.7 instead of applying lemma 3.6 from Agarwal et al. (2016). Furthermore, note that $L = \theta L_{\mathcal{K}} + (1-\theta)L_{\mathcal{A}}$ in our setting. For completeness, we provide the full proof below.

Proof.

$$\tilde{\boldsymbol{w}} - \tilde{\boldsymbol{w}}^* = \boldsymbol{w}^* - \frac{\tilde{\boldsymbol{H}}_{n,\lambda}^{-1}}{H}\nabla_{\boldsymbol{w}^*,\mathcal{K},\mathcal{A}} - \tilde{\boldsymbol{w}}^* \tag{70}$$

$$= \boldsymbol{w}^* - \tilde{\boldsymbol{w}}^* - \frac{\tilde{\boldsymbol{H}}_{n,\lambda}^{-1}}{H}(\nabla_{\boldsymbol{w}^*,\mathcal{K},\mathcal{A}} - \nabla_{\tilde{\boldsymbol{w}}^*,\mathcal{K},\mathcal{A}}) - \frac{\tilde{\boldsymbol{H}}_{n,\lambda}^{-1}}{H}\nabla_{\tilde{\boldsymbol{w}}^*,\mathcal{K},\mathcal{A}} \tag{71}$$

By the triangle inequality, this yields:

$$||\tilde{\boldsymbol{w}} - \tilde{\boldsymbol{w}}^*||_2 \leq ||\boldsymbol{w}^* - \tilde{\boldsymbol{w}}^* - \frac{\tilde{\boldsymbol{H}}_{n,\lambda}^{-1}}{H}(\nabla_{\boldsymbol{w}^*,\mathcal{K},\mathcal{A}} - \nabla_{\tilde{\boldsymbol{w}}^*,\mathcal{K},\mathcal{A}})||_2 + ||\frac{\tilde{\boldsymbol{H}}_{n,\lambda}^{-1}}{H}\nabla_{\tilde{\boldsymbol{w}}^*,\mathcal{K},\mathcal{A}}||_2 \tag{72}$$

The first term in Eq. (72) can be bounded by the triangle inequality as:

$$||\boldsymbol{w}^* - \tilde{\boldsymbol{w}}^* - \frac{\tilde{\boldsymbol{H}}_{n,\lambda}^{-1}}{H}(\nabla_{\boldsymbol{w}^*,\mathcal{K},\mathcal{A}} - \nabla_{\tilde{\boldsymbol{w}}^*,\mathcal{K},\mathcal{A}})||_2 \tag{73}$$

$$= ||\boldsymbol{w}^* - \tilde{\boldsymbol{w}}^* - ((\boldsymbol{H}_{\boldsymbol{w}^*,\mathcal{K},\mathcal{A}} + \lambda\boldsymbol{I})^{-1} + \frac{\tilde{\boldsymbol{H}}_{n,\lambda}^{-1}}{H} - (\boldsymbol{H}_{\boldsymbol{w}^*,\mathcal{K},\mathcal{A}} + \lambda\boldsymbol{I})^{-1})(\nabla_{\boldsymbol{w}^*,\mathcal{K},\mathcal{A}} - \nabla_{\tilde{\boldsymbol{w}}^*,\mathcal{K},\mathcal{A}})||_2 \tag{74}$$

$$\leq ||\boldsymbol{w}^* - \tilde{\boldsymbol{w}}^* - (\boldsymbol{H}_{\boldsymbol{w}^*,\mathcal{K},\mathcal{A}} + \lambda\boldsymbol{I})^{-1}(\nabla_{\boldsymbol{w}^*,\mathcal{K},\mathcal{A}} - \nabla_{\tilde{\boldsymbol{w}}^*,\mathcal{K},\mathcal{A}})||_2 \tag{75}$$

$$+||((\boldsymbol{H}_{\boldsymbol{w}^*,\mathcal{K},\mathcal{A}} + \lambda\boldsymbol{I})^{-1} - \frac{\tilde{\boldsymbol{H}}_{n,\lambda}^{-1}}{H})(\nabla_{\boldsymbol{w}^*,\mathcal{K},\mathcal{A}} - \nabla_{\tilde{\boldsymbol{w}}^*,\mathcal{K},\mathcal{A}})||_2 \tag{76}$$

In the setting of Prop. D.3, we have that $\tilde{\boldsymbol{w}} - \tilde{\boldsymbol{w}}^* = \boldsymbol{w}^* - \tilde{\boldsymbol{w}}^* - (\boldsymbol{H}_{\boldsymbol{w}^*,\mathcal{K},\mathcal{A}} + \lambda\boldsymbol{I})^{-1}(\nabla_{\boldsymbol{w}^*,\mathcal{K},\mathcal{A}} - \nabla_{\tilde{\boldsymbol{w}}^*,\mathcal{K},\mathcal{A}})$. Hence, by Prop. D.3, we have that:

$$||\boldsymbol{w}^* - \tilde{\boldsymbol{w}}^* - (\boldsymbol{H}_{\boldsymbol{w}^*,\mathcal{K},\mathcal{A}} + \lambda\boldsymbol{I})^{-1}(\nabla_{\boldsymbol{w}^*,\mathcal{K},\mathcal{A}} - \nabla_{\tilde{\boldsymbol{w}}^*,\mathcal{K},\mathcal{A}})||_2 \tag{77}$$

$$\leq \frac{2C((\theta M_{\mathcal{K}} + (1-\theta)M_{\mathcal{A}})C + \lambda)}{\lambda + \lambda_{\min}} \tag{78}$$

Furthermore, we have:

$$||((\boldsymbol{H}_{\boldsymbol{w}^*,\mathcal{K},\mathcal{A}} + \lambda\boldsymbol{I})^{-1} - \frac{\tilde{\boldsymbol{H}}_{n,\lambda}^{-1}}{H})(\nabla_{\boldsymbol{w}^*,\mathcal{K},\mathcal{A}} - \nabla_{\tilde{\boldsymbol{w}}^*,\mathcal{K},\mathcal{A}})||_2 \tag{79}$$

$$\leq ||((\boldsymbol{H}_{\boldsymbol{w}^*,\mathcal{K},\mathcal{A}} + \lambda\boldsymbol{I})^{-1} - \frac{\tilde{\boldsymbol{H}}_{n,\lambda}^{-1}}{H})||_2||(\nabla_{\boldsymbol{w}^*,\mathcal{K},\mathcal{A}} - \nabla_{\tilde{\boldsymbol{w}}^*,\mathcal{K},\mathcal{A}})||_2, \text{property of op norm} \tag{80}$$

$$\leq (16\frac{B}{\zeta_{\min}}\sqrt{\frac{\ln\frac{d}{\rho}}{b}} + \frac{1}{16})||(\nabla_{\boldsymbol{w}^*,\mathcal{K},\mathcal{A}} - \nabla_{\tilde{\boldsymbol{w}}^*,\mathcal{K},\mathcal{A}})||_2, \text{ Lemma E.7} \tag{81}$$

$$\leq (16\frac{B}{\zeta_{\min}}\sqrt{\frac{\ln\frac{d}{\rho}}{b}} + \frac{1}{16})2C(\theta L_{\mathcal{K}} + (1-\theta)L_{\mathcal{A}}, \text{ Lemma E.1} \tag{82}$$

with probability at least 1 - ρ. Incorporating this into equation Eq. (76), we have that:

$$||\boldsymbol{w}^* - \tilde{\boldsymbol{w}}^* - \frac{\tilde{\boldsymbol{H}}_{n,\lambda}^{-1}}{H}(\nabla_{\boldsymbol{w}^*,\mathcal{K},\mathcal{A}} - \nabla_{\tilde{\boldsymbol{w}}^*,\mathcal{K},\mathcal{A}})||_2 \leq \frac{2C((\theta M_{\mathcal{K}} + (1-\theta)M_{\mathcal{A}})C + \lambda)}{\lambda + \lambda_{\min}} \tag{83}$$

$$+(32\frac{B}{\zeta_{\min}}\sqrt{\frac{\ln\frac{d}{\rho}}{b}} + \frac{1}{8})C(\theta L_{\mathcal{K}} + (1-\theta)L_{\mathcal{A}} \tag{84}$$

It then suffices to bound the second term in Eq. (72). We have that:

$$\begin{aligned}
\left\|\tfrac{\tilde{\boldsymbol{H}}_{n,\lambda}^{-1}}{H}\nabla_{\tilde{\boldsymbol{w}}^*,\mathcal{K},\mathcal{A}}\right\|_2 &= \Big\|\big[(\boldsymbol{H}_{w^*,\mathcal{K},\mathcal{A}}+\lambda\boldsymbol{I})^{-1}-(\boldsymbol{H}_{w^*,\mathcal{K},\mathcal{A}}+\lambda\boldsymbol{I})^{-1} \\
&\qquad + \tfrac{\tilde{\boldsymbol{H}}_{n,\lambda}^{-1}}{H}\big]\nabla_{\tilde{\boldsymbol{w}}^*,\mathcal{K},\mathcal{A}}\Big\|_2 && (85)\\
&= \Big\|(\boldsymbol{H}_{w^*,\mathcal{K},\mathcal{A}}+\lambda\boldsymbol{I})^{-1}\nabla_{\tilde{\boldsymbol{w}}^*,\mathcal{K},\mathcal{A}} \\
&\qquad + \big(\tfrac{\tilde{\boldsymbol{H}}_{n,\lambda}^{-1}}{H}-(\boldsymbol{H}_{w^*,\mathcal{K},\mathcal{A}}+\lambda\boldsymbol{I})^{-1}\big)\nabla_{\tilde{\boldsymbol{w}}^*,\mathcal{K},\mathcal{A}}\Big\|_2 && (86)\\
&\le \|(\boldsymbol{H}_{w^*,\mathcal{K},\mathcal{A}}+\lambda\boldsymbol{I})^{-1}\|_2\,\|\nabla_{\tilde{\boldsymbol{w}}^*,\mathcal{K},\mathcal{A}}\|_2 \\
&\quad + \left\|\tfrac{\tilde{\boldsymbol{H}}_{n,\lambda}^{-1}}{H}-(\boldsymbol{H}_{w^*,\mathcal{K},\mathcal{A}}+\lambda\boldsymbol{I})^{-1}\right\|_2\|\nabla_{\tilde{\boldsymbol{w}}^*,\mathcal{K},\mathcal{A}}\|_2 && (87)\\
&\le \frac{G}{\lambda+\lambda_{\min}}+\Big(16\frac{B}{\zeta_{\min}}\sqrt{\tfrac{\ln(d/\rho)}{b}}+\tfrac{1}{16}\Big)G. && (88)
\end{aligned}$$

by definition of λ, Lemma E.7, and that $||\nabla_{\tilde{\boldsymbol{w}}^*,\mathcal{K},\mathcal{A}}||_2 \le G$.

Incorporating the above into Eq. (72), this yields that:

$$\begin{aligned}
\|\tilde{\boldsymbol{w}}-\tilde{\boldsymbol{w}}^*\|_2 &\le \frac{2C\big((\theta M_{\mathcal{K}}+(1-\theta)M_{\mathcal{A}})\,C+\lambda\big)}{\lambda+\lambda_{\min}} && (89)\\
&\quad + \Big(32\frac{B}{\zeta_{\min}}\sqrt{\frac{\ln(d/\rho)}{b}}+\tfrac{1}{8}\Big)C\Big(\theta L_{\mathcal{K}}+(1-\theta)L_{\mathcal{A}}+\frac{G}{\lambda+\lambda_{\min}} \\
&\qquad + \Big(16\frac{B}{\zeta_{\min}}\sqrt{\frac{\ln(d/\rho)}{b}}+\tfrac{1}{16}\Big)G\Big) && (90)\\
&= \frac{2C\big((\theta M_{\mathcal{K}}+(1-\theta)M_{\mathcal{A}})\,C+\mu\big)\;+\;G}{\mu+\mu_{\min}} && (91)\\
&\quad + \Big(16\frac{B}{\zeta_{\min}}\sqrt{\frac{\ln(d/\rho)}{b}}+\tfrac{1}{16}\Big)\big(2C(\theta L_{\mathcal{K}}+(1-\theta)L_{\mathcal{A}}+G)\big).
\end{aligned}$$

as desired.

□

E.9 Proof of Proposition F.1

Proof. By the same token as proposition 4.2 in Zhang et al. (2024), follow the proof of theorem D.5. □

E.10 Proof of Proposition 3.1

Proof. Fix any sampled $\mathcal{D}$. Since $\mathcal{M}_\theta(\mathcal{D})$ is taken to be the global risk minimizer, we have that:

$$\begin{aligned}
&\theta\mathcal{L}_{\mathcal{K}}(\mathcal{M}_\theta(\mathcal{D}),\mathcal{D}_f)+(1-\theta)\mathcal{L}_{\mathcal{A}}(\mathcal{M}_\theta(\mathcal{D}),\mathcal{D}_r) && (92)\\
&\le \theta\mathcal{L}_{\mathcal{K}}(\boldsymbol{w},\mathcal{D}_f)+(1-\theta)\mathcal{L}_{\mathcal{A}}(\boldsymbol{w},\mathcal{D}_r)\;\forall\boldsymbol{w}\in\mathcal{W} && (93)
\end{aligned}$$

subtracting $\frac{\lambda}{2}||\boldsymbol{w}||_2$ from both sides.

Let $\boldsymbol{w}_U$ be the parameter that results in a parameterized model $f_{\boldsymbol{w}_U}$ which outputs a uniform distribution; by Prop. 2.2, such a parameter exists. We then have that:

$$\mathcal{L}_{\mathcal{K}}(\boldsymbol{w}_U,\mathcal{D}_f)=\sum_{i=1}^{|\mathcal{D}_f|}D_{KL}(U[0,|\mathcal{Y}|])||U[0,|\mathcal{Y}|]=0 \tag{94}$$

and

$$\mathcal{L}_{\mathcal{A}}(\boldsymbol{w}_U, \mathcal{D}_r) = \sum_{i=1}^{|\mathcal{D}_r|} \mathbb{H}_{CE}(\boldsymbol{y}^{(i)}, U[0, |\mathcal{Y}|]) = -\sum_{i=1}^{|\mathcal{D}_r|} \sum_{j=1}^{|\mathcal{Y}|} \boldsymbol{y}_j^{(i)} \ln \frac{1}{|\mathcal{Y}|} = |\mathcal{D}_r| \ln |\mathcal{Y}| \tag{95}$$

where $\boldsymbol{y}$ is a one hot vector of length $\mathcal{Y}$ such that for $\boldsymbol{y}_j^{(i)}$, $j = 1, ..., |\mathcal{Y}|$,

$$\boldsymbol{y}_j^{(i)} = \begin{cases} 1 & \text{instance } i \text{ is labeled class } j \\ 0 & \text{instance } i \text{ is not labeled class } j \end{cases} \tag{96}$$

Incorporating the above into Eq. (93) yields:

$$\begin{aligned} \theta \mathcal{L}_{\mathcal{K}}(\mathcal{M}_\theta(\mathcal{D}), \mathcal{D}_f) + (1-\theta)\mathcal{L}_{\mathcal{A}}(\mathcal{M}_\theta(\mathcal{D}), \mathcal{D}_r) &\leq \theta \mathcal{L}_{\mathcal{K}}(\boldsymbol{w}_U, \mathcal{D}_f) + (1-\theta)\mathcal{L}_{\mathcal{A}}(\boldsymbol{w}_U, \mathcal{D}_r) && (97) \\ &\leq \theta(0) + (1-\theta)|\mathcal{D}_r| \ln |\mathcal{Y}| && (98) \\ &= |\mathcal{D}_r|(1-\theta) \ln |\mathcal{Y}| && (99) \end{aligned}$$

This then yields that:

$$\begin{aligned} \mathcal{L}_{\mathcal{K}}(\mathcal{M}_\theta(\mathcal{D}), \mathcal{D}_f) &\leq \frac{1-\theta}{\theta}(|\mathcal{D}_r| \ln |\mathcal{Y}| - \mathcal{L}_{\mathcal{A}}(\mathcal{M}_\theta(\mathcal{D}), \mathcal{D}_r) && (100) \\ &\leq \frac{1-\theta}{\theta}|\mathcal{D}_r| \ln |\mathcal{Y}| && (101) \end{aligned}$$

since the cross entropy is nonnegative, yielding that $-\mathcal{L}_{\mathcal{A}}(\mathcal{M}_\theta(\mathcal{D}), \mathcal{D}_r) \leq 0$.

Then, we have:

$$\begin{aligned} ||f_{\mathcal{M}_\theta(\mathcal{D})}(\mathcal{D}_f) - U[0, |\mathcal{Y}|]||_\infty &\leq ||f_{\mathcal{M}_\theta(\mathcal{D})}(\mathcal{D}_f) - U[0, |\mathcal{Y}|]||_1 && (102) \\ &\leq 2TV(f_{\mathcal{M}_\theta(\mathcal{D})}(\mathcal{D}_f) - U[0, |\mathcal{Y}|]) && (103) \\ &\leq 2\sqrt{\frac{1}{2} D_{KL}(f_{\mathcal{M}_\theta(\mathcal{D})}, ||U[0, |\mathcal{Y}|])}, \text{ Pinsker's inequality (Pinsker, 1964)} && (104) \\ &= \sqrt{2 D_{KL}(f_{\mathcal{M}_\theta(\mathcal{D})}, ||U[0, |\mathcal{Y}|])} && (105) \\ &= \sqrt{2\mathcal{L}_{\mathcal{K}}(\mathcal{M}_\theta(\mathcal{D}), \mathcal{D}_f)} && (106) \\ &\leq \sqrt{2|\mathcal{D}_r|(\frac{1-\theta}{\theta}) \ln |\mathcal{Y}|} && (107) \end{aligned}$$

by the above bound on $\mathcal{L}_{\mathcal{K}}$, as desired. □

E.11 Proof of Corollary 3.2

Proof. To have Eq. (9), by Prop. 3.1, it suffices to solve for θ in the bound obtained. This results in:

$$\sqrt{2(\frac{1-\theta}{\theta})|\mathcal{D}_r|\ln|\mathcal{Y}|} \leq \varepsilon \iff \frac{1-\theta}{\theta}|\mathcal{D}_r|\ln|\mathcal{Y} \leq \frac{\varepsilon^2}{2} \tag{108}$$

$$\iff \frac{|\mathcal{D}_r|\ln|\mathcal{Y}|}{\theta} - \frac{|\mathcal{D}_r|\ln|\mathcal{Y}|\theta}{\theta} \leq \frac{\varepsilon^2}{2} \tag{109}$$

$$\iff \frac{|\mathcal{D}_r|\ln|\mathcal{Y}|}{\theta} \leq \frac{\varepsilon^2}{2} + |\mathcal{D}_r|\ln|\mathcal{Y}| = \frac{\varepsilon^2 + 2|\mathcal{D}_r|\ln|\mathcal{Y}|}{2} \tag{110}$$

$$\iff \frac{\theta}{|\mathcal{D}_r|\ln|\mathcal{Y}|} \geq \frac{2}{\varepsilon^2 + 2|\mathcal{D}_r|\ln|\mathcal{Y}|} \tag{111}$$

$$\iff \theta \geq \frac{2|\mathcal{D}_r|\ln|\mathcal{Y}}{\varepsilon^2 + 2|\mathcal{D}_r|\ln|\mathcal{Y}|} \tag{112}$$

as desired.

□

E.12 Proof of Theorem 3.5

First, before we prove theorem 3.5, we note that we can use Lemma E.2 and that $||\boldsymbol{w}|| \leq 2$ to obtain a simple bound. Let:

$$|\alpha^* - \alpha(\theta)| = |\mathcal{L}_{\mathcal{A}}(\mathcal{A}(\mathcal{D}_r), \mathcal{D}_r) - \mathcal{L}_{\mathcal{A}}(\mathcal{M}_\theta(\mathcal{D}), \mathcal{D}_r)| \tag{113}$$

$$\leq \frac{L_{\mathcal{A}}}{2}||\mathcal{M}_\theta(\mathcal{D}) - \mathcal{A}(\mathcal{D}_r)||_2^2 + ||\nabla_{\mathcal{A}(\mathcal{D}_r),\mathcal{A}}||_2||\mathcal{M}_\theta(\mathcal{D}) - \mathcal{A}(\mathcal{D}_r)||_2 \tag{114}$$

$$\leq \frac{C^2 L_{\mathcal{A}}}{2} + \lambda C^2 \tag{115}$$

after applying the triangle inequality and rearranging the first order condition on $\mathcal{A}(\mathcal{D}_r)$.

However, this bound is vacuous and not tight; it does not incorporate any information about θ or most of the constants that appear in Asm. 3.3 and Asm. 3.4. Given this, we seek to construct a tighter, non-vacuous bound.

Proof. First, when $\theta = 0$, we have that:

$$\boldsymbol{w}_{\alpha^*} := \arg\min_{\boldsymbol{w}\in\mathcal{W}, ||\boldsymbol{w}||_2 \leq C} \mathcal{L}_{\mathcal{A}}(\boldsymbol{w}, \mathcal{D}_r) + \frac{\lambda}{2}||\boldsymbol{w}||_2^2 \tag{116}$$

which yields the first order condition:

$$\nabla_{\boldsymbol{w}_{\alpha^*},\mathcal{A}} + \lambda \boldsymbol{w}_{\alpha^*} = 0 \tag{117}$$

which, upon multiplying $1-\theta$ on both sides, yields:

$$(1-\theta)\nabla_{\boldsymbol{w}_{\alpha^*},\mathcal{A}} + (1-\theta)\lambda \boldsymbol{w}_{\alpha^*} = 0 \tag{118}$$

Then, when $\theta \in (0, 1)$, we have:

$$\boldsymbol{w}_{\alpha(\theta)} := \arg\min_{\boldsymbol{w}\in\mathcal{W}, ||\boldsymbol{w}||_2 \leq C} \theta\mathcal{L}_{\mathcal{K}}(\boldsymbol{w}, \mathcal{D}_f) + (1-\theta)\mathcal{L}_{\mathcal{A}}(\boldsymbol{w}, \mathcal{D}_r) + \frac{\lambda}{2}||\boldsymbol{w}||_2^2 \tag{119}$$

which yields the first order condition:

$$\theta\nabla_{\boldsymbol{w}_{\alpha(\theta)},\mathcal{K}} + (1-\theta)\nabla_{\boldsymbol{w}_{\alpha(\theta)},\mathcal{A}} + \lambda \boldsymbol{w}_{\alpha(\theta)} = 0 \tag{120}$$

Subtracting Eq. (118) from Eq. (120) yields:

$$\theta\nabla_{\boldsymbol{w}_{\alpha(\theta)},\mathcal{K}} + (1-\theta)\nabla_{\boldsymbol{w}_{\alpha(\theta)},\mathcal{A}} + \lambda\boldsymbol{w}_{\alpha(\theta)} - (1-\theta)\nabla_{\boldsymbol{w}_{\alpha^*},\mathcal{A}} - (1-\theta)\lambda\boldsymbol{w}_{\alpha^*} = 0 \tag{121}$$

which simplifies to:

$$\theta\nabla_{\boldsymbol{w}_{\alpha(\theta)},\mathcal{K}} + (1-\theta)(\nabla_{\boldsymbol{w}_{\alpha(\theta)},\mathcal{A}} - \nabla_{\boldsymbol{w}_{\alpha^*},\mathcal{A}}) + \lambda(\boldsymbol{w}_{\alpha(\theta)} - \boldsymbol{w}_{\alpha^*}) = -\theta\lambda\boldsymbol{w}_{\alpha^*} \tag{122}$$

The fundamental theorem of calculus then yields:

$$\int_0^1 \boldsymbol{H}_{\boldsymbol{w}_{\alpha^*}+t(\boldsymbol{w}_{\alpha(\theta)}+\boldsymbol{w}_{\alpha^*}),\mathcal{A}}(\boldsymbol{w}_{\alpha(\theta} - \boldsymbol{w}_{\alpha^*})dt = \nabla_{\boldsymbol{w}_{\alpha(\theta)},\mathcal{A}} - \nabla_{\boldsymbol{w}_{\alpha^*},\mathcal{A}} \tag{123}$$

and

$$\int_0^1 \boldsymbol{H}_{\boldsymbol{w}_{\alpha^*}+t(\boldsymbol{w}_{\alpha(\theta)}+\boldsymbol{w}_{\alpha^*}),\mathcal{K}}(\boldsymbol{w}_{\alpha(\theta)} - \boldsymbol{w}_{\alpha^*})dt = \nabla_{\boldsymbol{w}_{\alpha(\theta)},\mathcal{K}} - \nabla_{\boldsymbol{w}_{\alpha^*},\mathcal{K}} \tag{124}$$

We thus denote:

$$\bar{\boldsymbol{H}}_{\mathcal{K}} := \int_0^1 \boldsymbol{H}_{\boldsymbol{w}_{\alpha^*}+t(\boldsymbol{w}_{\alpha(\theta)}+\boldsymbol{w}_{\alpha^*}),\mathcal{K}}dt \tag{125}$$

$$\bar{\boldsymbol{H}}_{\mathcal{A}} := \int_0^1 \boldsymbol{H}_{\boldsymbol{w}_{\alpha^*}+t(\boldsymbol{w}_{\alpha(\theta)}+\boldsymbol{w}_{\alpha^*}),\mathcal{A}}dt \tag{126}$$

$$\Delta\boldsymbol{w} := \boldsymbol{w}_{\alpha(\theta)} - \boldsymbol{w}_{\alpha^*} \tag{127}$$

Incorporating Eq. (123) and Eq. (124) into Eq. (122) then yields:

$$\begin{aligned}
& \theta(\nabla_{\boldsymbol{w}_{\alpha^*},\mathcal{K}} + \bar{\boldsymbol{H}}_{\mathcal{K}}\Delta\boldsymbol{w}) + (1-\theta)(\nabla_{\boldsymbol{w}_{\alpha^*},\mathcal{A}} + \bar{\boldsymbol{H}}_{\mathcal{A}}\Delta\boldsymbol{w} - \nabla_{\boldsymbol{w}_{\alpha^*},\mathcal{A}}) + \lambda\Delta\boldsymbol{w} = -\theta\lambda\boldsymbol{w}_{\alpha^*} \\
\iff\quad & \theta\nabla_{\boldsymbol{w}_{\alpha^*},\mathcal{K}} + \theta\bar{\boldsymbol{H}}_{\mathcal{K}}\Delta\boldsymbol{w} + (1-\theta)\bar{\boldsymbol{H}}_{\mathcal{A}}\Delta\boldsymbol{w} + \lambda\Delta\boldsymbol{w} + \theta\lambda\boldsymbol{w}_{\alpha^*} = 0 \\
\iff\quad & \big(\theta\bar{\boldsymbol{H}}_{\mathcal{K}} + (1-\theta)\bar{\boldsymbol{H}}_{\mathcal{A}} + \lambda\boldsymbol{I}\big)\Delta\boldsymbol{w} = -\theta\big(\nabla_{\boldsymbol{w}_{\alpha^*},\mathcal{K}} + \lambda\boldsymbol{w}_{\alpha^*}\big) \\
\iff\quad & \big(\boldsymbol{H}_{\boldsymbol{w}_{\alpha^*},\mathcal{K},\mathcal{A}} + \lambda\boldsymbol{I} + \theta(\bar{\boldsymbol{H}}_{\mathcal{K}} - \boldsymbol{H}_{\boldsymbol{w}_{\alpha^*},\mathcal{K}}) + (1-\theta)(\bar{\boldsymbol{H}}_{\mathcal{A}} - \boldsymbol{H}_{\boldsymbol{w}_{\alpha^*},\mathcal{A}})\big)\Delta\boldsymbol{w} \\
& \quad = -\theta\big(\nabla_{\boldsymbol{w}_{\alpha^*},\mathcal{K}} + \lambda\boldsymbol{w}_{\alpha^*}\big) \\
\iff\quad & \big(\boldsymbol{H}_{\boldsymbol{w}_{\alpha^*},\mathcal{K},\mathcal{A}} + \lambda\boldsymbol{I}\big)\Delta\boldsymbol{w} = -\big(\theta(\bar{\boldsymbol{H}}_{\mathcal{K}} - \boldsymbol{H}_{\boldsymbol{w}_{\alpha^*},\mathcal{K}}) + (1-\theta)(\bar{\boldsymbol{H}}_{\mathcal{A}} - \boldsymbol{H}_{\boldsymbol{w}_{\alpha^*},\mathcal{A}})\big)\Delta\boldsymbol{w} \\
& \quad - \theta\big(\nabla_{\boldsymbol{w}_{\alpha^*},\mathcal{K}} + \lambda\boldsymbol{w}_{\alpha^*}\big).
\end{aligned} \tag{128}$$

Then, note that:

$$\begin{aligned}
||\bar{\boldsymbol{H}}_{\mathcal{K}} - \boldsymbol{H}_{\boldsymbol{w}_{\alpha^*},\mathcal{K}}||_2 &= ||\int_0^1 \boldsymbol{H}_{\boldsymbol{w}_{\alpha^*}+t\Delta\boldsymbol{w},\mathcal{K}}dt - \boldsymbol{H}_{\boldsymbol{w}_{\alpha^*},\mathcal{K}}||_2 && (129)\\
&\leq \int_0^1 ||\boldsymbol{H}_{\boldsymbol{w}_{\alpha^*}+t\Delta\boldsymbol{w},\mathcal{K}} - \boldsymbol{H}_{\boldsymbol{w}_{\alpha^*},\mathcal{K}}||_2 && (130)\\
&\leq \frac{M_{\mathcal{K}}}{2}||\Delta\boldsymbol{w}||_2 && (131)
\end{aligned}$$

by the same token as in Prop. D.3.

Similarly:

$$||\bar{\boldsymbol{H}}_{\mathcal{A}} - \boldsymbol{H}_{\boldsymbol{w}_{\alpha^*,\mathcal{A}}}||_2 \leq \frac{M_{\mathcal{A}}}{2}||\Delta \boldsymbol{w}||_2 \tag{132}$$

Also:

$$\begin{aligned} ||\nabla_{\boldsymbol{w}_{\alpha^*,\mathcal{K}}}||_2 &= ||\nabla_{\boldsymbol{w}_{\alpha^*,\mathcal{K}}} - \nabla_{\mathcal{K}(\mathcal{D}_f),\mathcal{K}}||_2 && (133)\\ &\leq L_{\mathcal{K}}||\boldsymbol{w}_{\alpha^*} - \boldsymbol{w}_{\mathcal{K}(\mathcal{D}_f)}||_2 && (134)\\ &\leq 2L_{\mathcal{K}}C && (135)\end{aligned}$$

by definition of the uniform learner $\mathcal{K}$, Lemma E.1, and the triangle inequality.

Additionally:

$$||\lambda \boldsymbol{w}_{\alpha^*}||_2 \leq \lambda C \tag{136}$$

By the triangle inequality, incorporating Eq. (131), Eq. (132), Eq. (135), and Eq. (136) into Eq. (128), we have that:

$$\begin{aligned} ||(\boldsymbol{H}_{\boldsymbol{w}_{\alpha^*,\mathcal{K},\mathcal{A}}} + \lambda \boldsymbol{I})\Delta \boldsymbol{w}||_2 &\leq (\theta||\bar{\boldsymbol{H}}_{\mathcal{K}} - \boldsymbol{H}_{\boldsymbol{w}_{\alpha^*,\mathcal{K}}}||_2 + (1-\theta)||\bar{\boldsymbol{H}}_{\mathcal{A}} - && (137)\\ &\quad \boldsymbol{H}_{\boldsymbol{w}_{\alpha^*,\mathcal{A}}}||_2)||\Delta \boldsymbol{w}||_2 + \theta||\nabla_{\boldsymbol{w}_{\alpha^*,\mathcal{K}}}||_2 + \theta||\lambda \boldsymbol{w}_{\alpha^*}||_2 && (138)\\ &\leq (\theta M_{\mathcal{K}} + (1-\theta)M_{\mathcal{A}})||\Delta \boldsymbol{w}||_2^2 + \theta C(2L_{\mathcal{K}} + \lambda) && (139)\end{aligned}$$

Note that we have, where $\sigma_{\min}(\cdot)$ denotes the minimum singular value:

$$\begin{aligned} ||(\boldsymbol{H}_{\boldsymbol{w}_{\alpha^*,\mathcal{K},\mathcal{A}}} + \lambda \boldsymbol{I})\Delta \boldsymbol{w}||_2 &\geq \sigma_{\min}(\boldsymbol{H}_{\boldsymbol{w}_{\alpha^*,\mathcal{K},\mathcal{A}}} + \lambda \boldsymbol{I})||\Delta \boldsymbol{w}||_2 \text{ by property of op. norm} && (140)\\ &= \lambda_{\min}(\boldsymbol{H}_{\boldsymbol{w}_{\alpha^*,\mathcal{K},\mathcal{A}}} + \lambda \boldsymbol{I})||\Delta \boldsymbol{w}||_2 \text{ by Lemma E.3} && (141)\end{aligned}$$

Furthermore, by Lemma E.1, we have that $||\boldsymbol{H}_{\boldsymbol{w}_{\alpha^*,\mathcal{K}}}||_2 \leq L_{\mathcal{K}}$ and $||\boldsymbol{H}_{\boldsymbol{w}_{\alpha^*,\mathcal{A}}}||_2 \leq L_{\mathcal{A}}$, which yields:

$$||\boldsymbol{H}_{\boldsymbol{w}_{\alpha^*,\mathcal{K},\mathcal{A}}}||_2 \leq \theta L_{\mathcal{K}} + (1-\theta)L_{\mathcal{A}} \tag{142}$$

which by Lemma E.3 yields:

$$\lambda_{\min}(\boldsymbol{H}_{\alpha^*,\mathcal{K},\mathcal{A}} + \lambda \boldsymbol{I}) \in [\lambda - \theta L_{\mathcal{K}} - (1-\theta)L_{\mathcal{A}}, \mu + \theta L_{\mathcal{K}} + (1-\theta)L_{\mathcal{A}}] \tag{143}$$

With Eq. (141), this yields that:

$$||(\boldsymbol{H}_{\boldsymbol{w}_{\alpha^*,\mathcal{K},\mathcal{A}}} + \lambda \boldsymbol{I})\Delta \boldsymbol{w}||_2 \geq (\lambda - \theta L_{\mathcal{K}} - (1-\theta)L_{\mathcal{A}})||\Delta \boldsymbol{w}||_2 \tag{144}$$

Incorporating this into Eq. (139) yields:

$$(\lambda - \theta L_{\mathcal{K}} - (1-\theta)L_{\mathcal{A}})||\Delta \boldsymbol{w}||_2 \leq (\theta M_{\mathcal{K}} + (1-\theta)M_{\mathcal{A}})||\Delta \boldsymbol{w}||_2^2 + \theta C(2L_{\mathcal{K}} + \lambda) \tag{145}$$

Simplifying yields the quadratic inequality:

$$(\theta M_{\mathcal{K}} + (1-\theta)M_{\mathcal{A}})||\Delta \boldsymbol{w}||_2^2 - (\lambda - \theta L_{\mathcal{K}} - (1-\theta)L_{\mathcal{A}})||\Delta \boldsymbol{w}||_2 + \theta C(2L_{\mathcal{K}} + \lambda) \geq 0 \tag{146}$$

This then yields that:

$$||\Delta \boldsymbol{w}||_2 \leq \frac{\lambda - L - \sqrt{(\lambda - L)^2 - 4\theta CM(2L_{\mathcal{K}} + \lambda)}}{2M} \tag{147}$$

This is only valid when:

$$(\lambda - L)^2 - 4\theta CM(2L_{\mathcal{K}} + \lambda) \geq 0 \tag{148}$$

$$\iff \lambda^2 - 2L\lambda + L^2 - 4\theta C2L_{\mathcal{K}}M - 4\theta C\lambda M \geq 0 \tag{149}$$

$$\iff \lambda^2 - 2L\lambda - 4\theta CM\lambda + L^2 - 8\theta CL_{\mathcal{K}}M \geq 0 \tag{150}$$

$$\iff \lambda^2 - (2L + 4\theta CM)\lambda + (L^2 - 8\theta CL_{\mathcal{K}}M) \geq 0 \tag{151}$$

$$\impliedby \lambda \geq L + 2\theta CM + \sqrt{2\theta CM(L + 2\theta CM + 8L_{\mathcal{K}}} \tag{152}$$

which holds by assumption. Note that all components of $2\theta CM + \sqrt{2\theta CM(L + 2\theta CM + 8L_{\mathcal{K}}}$ are nonnegative, rendering this valid. Incorporating Eq. (147) into Lemma E.2 yields the final bound as desired. □

F Online Algorithm

We also consider the online setting, where users send requests in sequential order (Nguyen et al., 2022). Here, we denote $\mathcal{D}_{f_k}$ as the forget set after the k-th request and the associated retain set as $\mathcal{D}_{r_k} = \mathcal{D} \setminus \cup_{i=1}^{k} \mathcal{D}_{f_i}$. Letting $\tilde{\boldsymbol{w}}_0 = \mathcal{A}(\mathcal{D})$, we estimate $\tilde{\boldsymbol{w}}_k$ recursively as $\tilde{\boldsymbol{w}}_k = \tilde{\boldsymbol{w}}_{k-1} - \frac{\tilde{\boldsymbol{H}}^{-1}_{n,\lambda,k-1}}{H} \nabla_{\tilde{\boldsymbol{w}}_{k-1},\mathcal{K},\mathcal{A}}$, where $\tilde{\boldsymbol{H}}^{-1}_{n,\lambda,k-1}$ is an estimator for $(\boldsymbol{H}_{\tilde{\boldsymbol{w}}_{k-1},\mathcal{K},\mathcal{A}} + \lambda \boldsymbol{I})^{-1}$ with respect to $\mathcal{D}_{f_k}$ and $\mathcal{D}_{r_k}$. $\nabla_{\tilde{\boldsymbol{w}}_{k-1},\mathcal{K},\mathcal{A}}$ is also computed with respect to $\mathcal{D}_{f_k}$ and $\mathcal{D}_{r_k}$. Adding noise to $\tilde{\boldsymbol{w}}_k$ as stipulated in theorem D.1 yields a $\boldsymbol{w}_k^-$ satisfying Def. 2.6. Furthermore, we have that:

Proposition F.1. *Let $\lambda_{\min}$ be the smallest eigenvalue of $\boldsymbol{H}_{\tilde{\boldsymbol{w}}_{k-1},\mathcal{K},\mathcal{A}}$, $\lambda > ||\boldsymbol{H}_{\boldsymbol{w}^*,\mathcal{K},\mathcal{A}}||_2$, and $||\nabla_{\tilde{\boldsymbol{w}}_k,\mathcal{K},\mathcal{A}}||_2, ||\nabla_{\tilde{\boldsymbol{w}}_k,\mathcal{K},\mathcal{A}}||_2 \leq G$ for all k, all evaluated with respect to $\mathcal{D}_{f_k}$ and $\mathcal{D}_{r_k}$. Then, the bound in theorem D.5 is identical in the online setting.*

Proof: See Sec. E.9.

In the online setting, Prop. F.1 yields Alg. 4.

Note that, for simplicity, we set $b = 1$. However, they can be added similarly to Alg. 3 if the user desires.

G Eliminating Hyperparameters in Certified Algorithms

Here, we summarize how to eliminate hyperparameters in Alg. 2, Alg. 3, and Alg. 4.

- $\lambda_{\min}$ can be chosen as 0 by convex approximation, or it can be estimated using simple algorithms like Gershgorin's circle theorem or inverse power iteration.
- By Lemma E.1, λ can be chosen as $\theta L_K + (1 - \theta)L_A$
- Similarly, by Lemma E.1, H can be chosen as 2λ
- In practice, since $\frac{B}{\lambda + \lambda_{\min}}$ offers a bound on $\hat{\kappa}_l$ by Lemma E.6, $\zeta_{\min}$ can be chosen as $\lambda + \lambda_{\min}$
- By Lemma E.7, n can be chosen as $n = 2\frac{B}{\lambda + \lambda_{\min}} \ln(\frac{B}{\lambda + \lambda_{\min}} b)$
- G can be approximated by computing $||\nabla_{\boldsymbol{w}^*,\mathcal{K},\mathcal{A}}||_2$.
- θ can be chosen with Cor. 3.2 to satisfy a particular closeness to uniformity.
- In practice, we find that C can be chosen as 10, 20, or 100.
- b can be chosen to satisfy a particular concentration on the estimator, so we let it be free. However, one can set $b = 1$.

Algorithm 4 Online $(\varepsilon, \delta, \theta)$-certified uniformity with DP

Require: Dataset $\mathcal{D}$; forget sets $\{\mathcal{D}_{f_1}, ..., \mathcal{D}_{f_k}\}$; pretrained model $\boldsymbol{w}^* = \mathcal{A}(\mathcal{D})$; privacy budgets ε and δ; ; privacy-utility tradeoff coefficient θ; sample size n; local convex coefficient λ; norm upper bound C; cumulative Hessian upper bound H; individual Hessian minimum eigenvalue upper bound $\zeta_{\min}$; bound looseness probability ρ.
$\tilde{\boldsymbol{w}}_0 \leftarrow \boldsymbol{w}^*$
$\mathcal{D}_{r_0} \leftarrow \mathcal{D}$
for $i = 1, ..., k$ **do**
  $\mathcal{D}_{r_i} \leftarrow \mathcal{D}_{r_{i-1}} \setminus \mathcal{D}_{f_i}$
  $\boldsymbol{P}_{0,\lambda} \leftarrow \nabla_{\tilde{\boldsymbol{w}}_{\boldsymbol{i-1}},\mathcal{K},\mathcal{A}}$
  for $t = 1, ..., n$ **do**
    Sample X_{t_i} from D_{f_i} with probability θ or sample X_{t_i} from D_r with probability $1 - \theta$
    if $X_{t_i} \sim D_f$ **then**
      $\boldsymbol{H}_{t,\lambda,i} \leftarrow \nabla^2_{\boldsymbol{w}} \mathcal{L}_{\mathcal{K}}(\boldsymbol{w}^*, X_{t_i}) + \frac{\lambda \boldsymbol{I}}{2\theta}$
    else if $X_i \sim D_r$ **then**
      $\boldsymbol{H}_{t,\lambda} \leftarrow \nabla^2_{\boldsymbol{w}} \mathcal{L}_{\mathcal{A}}(\boldsymbol{w}^*, X_{t_i}) + \frac{\lambda \boldsymbol{I}}{2(1-\theta)}$
    end if
   $\boldsymbol{P}_{t,\lambda,i} = \boldsymbol{P}_{0,\lambda,i} + (\boldsymbol{I} - \frac{\boldsymbol{H}_{t,\lambda,i}}{H})\boldsymbol{P}_{t-1,\lambda,i}$.
  end for
  $\tilde{\boldsymbol{w}}_{\boldsymbol{i}} \leftarrow \tilde{\boldsymbol{w}}_{i-1} - \frac{\boldsymbol{P}_{n,\lambda,i}}{H}$
end for
Compute Δ as the bound in Eq. (23).
$\sigma = \frac{\Delta}{k\varepsilon}\sqrt{2\ln(1.25/\delta)}$
$\boldsymbol{w}^- \leftarrow \tilde{\boldsymbol{w}}_k + Y$ where $Y \sim \mathcal{N}(\boldsymbol{0}, \sigma^2 \boldsymbol{I})$
return $\boldsymbol{w}^-$

- Common heuristics for ε and δ are available in the differential privacy literature.
- In practice, following what is common in certified unlearning e.g. in (Zhang et al., 2024), the Lipchitz constants in Asm. 3.3 and Asm. 3.4 are treated as hyperparameters. However, in practice, they can all be set to 1.

H Intuition for Early Stopping

Firstly, recall that random vectors are nearly orthogonal in high dimensions (Vershynin, 2018). In particular, for larger models, the gradients will conflict i.e. point in opposite directions more strongly, since their parameter space is very large. Second, every gradient step of our Alg. 1 is given by $\theta \nabla_{\mathbf{w}} \mathcal{L}_{\mathcal{K}}(\mathbf{w}, \mathcal{D}_f) + (1-\theta)\nabla_{\mathbf{w}} \mathcal{L}_{\mathcal{A}}(\mathbf{w}, \mathcal{D}_r)$.

In what follows, consider a large model e.g. CIFAR10 ResNet50.

When we begin finetuning the pretrained model with Alg. 1, θ is large, $\mathcal{L}_{\mathcal{A}}$ is small, and $\mathcal{L}_{\mathcal{K}}$ is large. Thus, $\nabla_{\mathbf{w}} \mathcal{L}_{\mathcal{K}}$ significantly dominates $\nabla_{\mathbf{w}} \mathcal{L}_{\mathcal{A}}$. For large models, since the gradients are nearly orthogonal, we will move very fast in the direction of the forget gradient.

As finetuning continues, we reach a point where θ is large, $\mathcal{L}_{\mathcal{K}}$ is small, and $\mathcal{L}_{\mathcal{A}}$ is large. At this point, the $\nabla_{\mathbf{w}} \mathcal{L}_{\mathcal{A}}$ begins to dominate, albeit less significantly since θ is large. For large models, since the gradients are nearly orthogonal, we will move fast in the direction of the retain gradient. However, due to our choice of large θ, the retain gradient will be reduced in magnitude. Thus, we will move more slowly at this stage.

We must stop shortly after this, otherwise the forget loss will climb back up to a point where the model is no longer reasonably uniform.

Importantly, since smaller models (e.g. CIFAR10 ResNet8) have smaller parameter spaces, the gradients do not conflict as much. Thus, when we begin finetuning the model, while we do increase in retain loss initially, after the uniform loss is minimized we can minimize the retain loss freely. As such, we can move in a direction that minimizes both the forget and retain gradients, and do not need to stop early.

I Experimental Details

I.1 Dataset Details

MNIST: The MNIST dataset contains 70k 28x28 greyscale images of hand-drawn digits in 10 classes (Deng, 2012). We conduct our experiments with 49k training images and 21k test images. The classes are mutually exclusive.

Kuzushiji-MNIST: The Kuzushiji-MNIST (KMNIST) dataset contains 70k 28x28 greyscale images of Japanese kanji in 10 classes (Clanuwat et al., 2018). We conduct our experiments with 49k training images and 21k test images. The classes are mutually exclusive.

CIFAR10: The CIFAR10 dataset consists of 60k 32x32 color images in 10 classes. The classes are mutually exclusive and include airplanes, automobiles, birds, cats, deer, dogs, frogs, horses, ships, and trucks (Krizhevsky et al., 2009).

CIFAR-100: The CIFAR-100 dataset is similar to CIFAR-10 but contains 100 classes, each with 600 images, making a total of 60k 32x32 color images. The 100 classes are grouped into 20 superclasses, and each image comes with a "fine" label (the class to which it belongs) and a "coarse" label (the superclass to which it belongs) (Krizhevsky et al., 2009).

SVHN: The Street View House Numbers (SVHN) dataset contains images of double-digit numbers on house walls as colored 32x32 images. We load SVHN with 100 classes, corresponding to 10 * 10 for each digit. There are 73k training images, 26k testing images.

I.2 Model Details

LogReg: A logistic regression model that has a single linear layer between inputs and outputs, followed by a softmax output function.

MLP: A two-layer ReLU feedforward neural network.

ResNet8: A [1,1,1,0] residual network, , with standard convolutional blocks, as described in (He et al., 2016).

ResNet18: A [2,2,2,2] residual network, with standard convolutional blocks, as described in (He et al., 2016).

ResNet50: A [3, 4, 6, 3] residual network, with bottleneck convolutional blocks, as described in (He et al., 2016).

ViT_S_16: A vision transformer with ≈ 20 million parameters, as detailed in (Dosovitskiy et al., 2021).

ViT_B_16: A vision transformer with ≈ 80 million parameters, as detailed in (Dosovitskiy et al., 2021).

I.3 Baseline Details

We implement several baselines and provide the rationale for their use below:

Pretrained: This is simply the pretrained model corresponding to whichever model and benchmark is specified. The rationale for using this is to demonstrate that we alter uniformity significantly from before without tarnishing accuracy for either the retain or test sets.

Retrained: This is a model retrained over the retain set, performing exact unlearning. The rationale for using this is to demonstrate that our methods mimic unlearning in how we preserve accuracy, but induce uniformity in a way that unlearning does not.

Synthetic: This method proceeds as follows: for each instance in the forget set, sample k instances from the ε-ball, with respect to the ℓ_2 norm, around that instance. Then, assign these k instances random labels from the label space, choosing labels uniformly at random. Do this for all forget set instances, yielding $|\mathcal{D}_f|k$ new instances. Then, append this to the retain set and retrain over this augmented dataset. This provides strong accuracy for simple baselines like MNIST while also

inducing uniformity, providing an alternative, simple algorithm to compare our method against in terms of time elapsed.

Label Differential Privacy: Specifically, we use the multi-stage training method of Ghazi et al. (2021) to obtain a model which is differentially private with respect to the labels–that is, an adversary cannot be sure whether the label they obtain is the true label. This is related to our work, albeit addresses a different threat model, as described in Sec. B. Still, we believe it is important to demonstrate that our method achieves privacy while not sacrificing utility to the extend that label differential privacy does, since it is a well-known method in the privacy literature that addresses a similar problem.

I.4 Hyperparameter Details

Please note that, throughout, we do not do extensive hyperparameter optimization, which may lead to improved performance.

We use a standard train-test split of 70-30 throughout. Pretraining and synthetic training have the same hyperparameters as pretraining, unless mentioned otherwise. We use ADAM, with standard PyTorch hyperparameters aside from learning rate and weight decay, throughout. A batch size of 128 is used for pretraining and also for the retain set in Alg. 1 throughout. For all Alg. 1 experiments and Alg. 2 experiments, we use a forget set size of 100 with a batch size (when loading the forget set into the finetuning in Alg. 1) of 10. We perform Alg. 1 for 100 epochs and finetune Alg. 2 for 50 epochs before running the certified Newton step. We generally use the forward KL divergence between model softmax outputs and the uniform distribution for $\mathcal{L}_{\mathcal{K}}$ and the cross entropy between model predictions and ground truth labels for $\mathcal{L}_{\mathcal{A}}$. For LogReg, we instead use the square loss between the uniform softmax probabilities and the model softmax outputs, since the forward KL is not necessarily convex in $\boldsymbol{w}$ in this case, while the square loss is; this allows us to use Alg. 2 with small λ. For our synthetic baseline, we use $\varepsilon = 8/255$ throughout, where ε is the size of the ε-ball where we sample instances to assign random labels for retraining. For the LabelDP baseline, we use the multi-stage training algorithm of Ghazi et al. (2021) throughout.

Early stopping is implemented by saving the model which first meets the early stopping conditions, and continuing to see if any model performs better in terms of confidence distance while still meeting the early stopping conditions specified below.

Compute: We use two RTX 6000 Ada Generation NVIDIA GPUs throughout. The most resource intensive experiments are the LabelDP experiments, which take up most of the memory on both GPUs. Besides those, the other experiments take up at most a fourth of the compute resources available on one GPU. No experiments ran required more compute than these two GPUs provide.

MNIST, LogReg Pretraining: Epochs: 25. Learning rate: 0.01.

MNIST, MLP Pretraining: Epochs: 5. Learning rate: 0.01.

MNIST, ResNet18 Pretraining: Epochs: 2. Learning rate: 0.001.

MNIST, LogReg Alg. 1: Learning rate: 0.01

MNIST, MLP Alg. 1: Learning rate: 0.01

MNIST, ResNet18 Alg. 1: Learning rate: 0.001. Early stopping criterion of a confidence distance < 0.32 and a retain accuracy of $> 90\%$.

MNIST, LogReg Alg. 2: $M = 1$. $C = 10$, pretrained with PGD with the same hyperparameters as the standard pretraining. Since the losses are convex in $\boldsymbol{w}$, $\lambda_{\min} = 0$. $\lambda = 0.0001$. Following Zhang et al. (2024), we use the variance σ^2 as a hyperparameter, corresponding to a broad range of choices of ε and δ. We choose $\sigma = 0.001$. This results in large ε and δ, as typical in differential privacy (Dwork et al., 2014) and certified unlearning (Qiao et al., 2025). However, we still observe good induced uniformity.

MNIST, LogReg Synthetic Baseline: Sampled k instances for each forget set instance: 5.

MNIST, ResNet18 Synthetic Baseline: Sampled k instances for each forget set instance: 500.

MNIST, LogReg LabelDP Baseline: Epochs: 200. Batch size: 256. Random flip, random left-right flip, and random cutout (8). SGD with learning rate 0.4 with momentum 0.9. $\varepsilon = 2.0$. Mixup for stage 1: 16. Mixup for stage 2: 8. Data split evenly between the two stages. Piecewise constant learning rate scheduler. These hyperparameters are chosen to match those in the best results of Ghazi et al. (2021). See Ghazi et al. (2021) for more details on these hyperparameters.

MNIST, ResNet18 LabelDP Baseline: Same as the MNIST LogReg LabelDP hyperpameters, except with a weight decay of 0.0005 throughout.

KMNIST, LogReg Pretraining: Epochs: 100. Learning rate: 0.01.

KMNIST, MLP Pretraining: Epochs: 100. Learning rate: 0.001.

KMNIST, ResNet18 Pretraining: Epochs: 12 Learning rate: 0.002.

KMNIST, LogReg Alg. 1: Same as pretraining.

KMNIST, MLP Alg. 1: Learning rate: 0.01.

KMNIST, ResNet18 Alg. 1: Learning rate: 0.002. Early stopping criterion of a confidence distance < 0.32 and a retain accuracy of $> 99\%$.

KMNIST, ResNet18 Synthetic Baseline: Sampled k instances for each forget set instance: 500.

KMNIST, ResNet18 LabelDP Baseline: Same as the MNIST ResNet18 LabelDP hyperparameters.

SVHN, ResNet50 Pretraining: Epochs: 150. Learning rate: 0.001. Weight decay: 0.00005.

SVHN, ResNet50 Alg. 1: Same as pretraining.

SVHN, ResNet50 Synthetic Baseline: Sampled k instances for each forget set instance: 500.

SVHN, ResNet50 LabelDP Baseline: Same as MNIST ResNet18 LabelDP hyperparameters.

CIFAR10, ResNet18 Pretraining: Epochs: 200 with SGD with a momentum of 0.9. Learning rate: 0.1. Weight decay: 0.0005.

CIFAR10, ResNet18 Alg. 1: Same as pretraining. Early stopping criterion of a confidence distance < 0.42 and a retain accuracy of $> 87\%$.

CIFAR10, ResNet50 Pretraining: Same as CIFAR10 ResNet18.

CIFAR10, ResNet50 Alg. 1: Same as pretraining. Early stopping criterion of a confidence distance < 0.42 and a retain accuracy of $> 87\%$.

CIFAR10, ResNet8 Pretraining: Same as CIFAR10 ResNet18.

CIFAR10, ResNet8 Alg. 1: Same as CIFAR10 ResNet18.

CIFAR10, ResNet18 Synthetic Baseline: Sampled k instances for each forget set instance: 5000.

CIFAR10, ResNet50 Synthetic Baseline: Sampled k instances for each forget set instance: 5000.

CIFAR10, ResNet18 LabelDP Baseline: Same as MNIST ResNet18 LabelDP hyperparameters, except with a batch size of 512.

CIFAR10, ResNet50 LabelDP Baseline: Same as CIFAR10 ResNet18 LabelDP.

CIFAR10, ViT_S_16 Finetuning: 8 epochs. Learning rate 0.0001 with AdamW.

CIFAR10, ViT_B_16 Finetuning: 10 epochs. Learning rate 0.0001 with AdamW.

CIFAR100, ResNet50 Pretraining: Same as CIFAR10 ResNet18.

CIFAR100, ResNet50 Alg. 1: Same as pretraining. Early stopping criterion of a confidence distance < 0.42 and a retain accuracy of $> 87\%$.

CIFAR100, ResNet8 Pretraining: Same as CIFAR100 ResNet50.

CIFAR100, ResNet8 Alg. 1: Same as CIFAR100 ResNet50.

CIFAR100, ResNet50 Synthetic Baseline: Sampled instances: 5000.

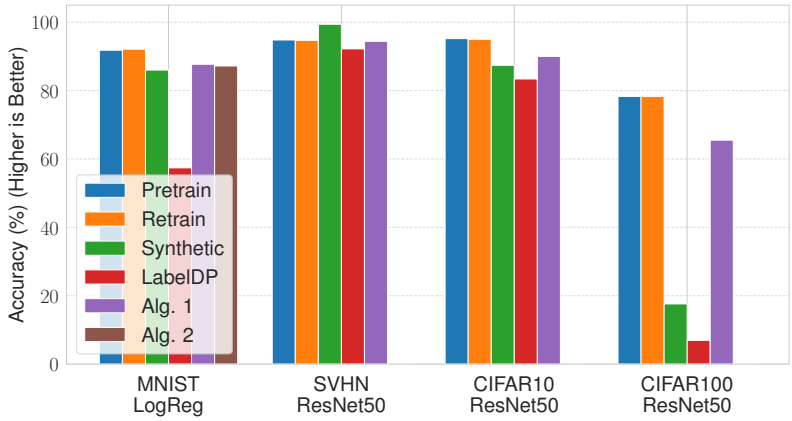

Figure 5: Accuracy on test set for baselines as well as Alg. 1 and Alg. 2 with $\theta = 0.75$.

CIFAR100, ResNet50 LabelDP Baseline: Same as CIFAR10 ResNet18 LabelDP.

CIFAR100, ViT_S_16 Finetuning: 15 epochs. Learning rate 0.0001 with AdamW.

CIFAR100, ViT_S_16 Alg. 1: 100 epochs. Learning rate 0.001 with SGD.

CIFAR100, ViT_B_16 Finetuning: 10 epochs. Learning rate 0.0001 with AdamW.

CIFAR100, ViT_B_16 Alg. 1: Same as CIFAR100 ViT_S_16.

TinyImageNet, ViT_S_16 Finetuning: 30 epochs. Learning rate 0.0001, momentum 0.9, and weight decay 0.01 with SGD.

TinyImageNet, ViT_S_16 Alg. 1: Same as CIFAR100 ViT_S_16.

TinyImageNet, ViT_B_16 Finetuning: 50 epochs. Learning rate 0.0001, momentum 0.9, and weight decay 0.01 with SGD.

TinyImageNet, ViT_B_16 Alg. 1: Same as CIFAR100 ViT_S_16.

Attacks: $\alpha = 0.0001$. PGD learning rate: 0.001. PGD steps: 50.

Test-Set Finetuning: Finetune pretrained model for 20 more epochs with the same hyperparameters as pretraining, then run Alg. 1 with the same hyperparameters as the original run of Alg. 1. For CIFAR10/CIFAR100, finetune for 100 epochs.

J Additional Experiments

J.1 Test Set Accuracies for Main Paper Experiments

We provide a figure, similar to Fig. 2a, for the test set in Fig. 5. We observe similar results as one does on the retain set, with test accuracies preserved by Alg. 1 and Alg. 2.

J.2 Tables for Main Paper Experiments

The tables for Fig. 2 are in Tab. 1 and Tab. 2. We include results for MNIST and KMNIST ResNet18 as well. We see that Alg. 1 induces uniformity without great damage to utility, while all other baselines–including the synthetic baseline–fail to do so without critically harming utility. Furthermore, we observe that ResNet50 performs better than ResNet18, providing more credibility to the claim in Sec. 4 that larger models tend to perform better when used in Alg. 1. Next, we observe that Alg. 1 can actually provide better retain and test accuracy than the pretrained model, as observed for ResNet50 over CIFAR100; this is because we also minimize the retain accuracy during finetuning. We similarly have to use early stopping for Alg. 1, as discussed in Sec. 4, since we use large models. Finally, we observe that LabelDP can induce uniformity, albeit at the cost of retain and test accuracy, but does so

Table 1: Results for Alg. 1, used in Fig. 2. We find that we are able to induce uniformity while only slightly decreasing retain and test accuracy. $\theta = 0.75$ throughout.

Dataset	Model	Method	Retain Acc.	Test Acc.	Conf. Dist. (Lower Better)
MNIST	ResNet18	Pretrain	98.0%	98.1%	0.877
		Retrain	97.3%	97.1%	0.876
		Synthetic	100.0%	99.1%	0.010
		LabelDP	98.8%	98.8%	0.593
		Alg. 1	99.6%	99.1%	0.070
KMNIST	ResNet18	Pretrain	98.2%	92.1%	0.880
		Retrain	98.4%	92.4%	0.884
		Synthetic	99.9%	96.7%	0.019
		LabelDP	98.9%	96.1%	0.530
		Alg. 1	99.1%	94.7%	0.257
SVHN	ResNet50	Pretrain	99.6%	94.8%	0.980
		Retrain	99.3%	94.7%	0.964
		Synthetic	99.9%	99.4%	0.013
		LabelDP	92.0%	92.2%	0.282
		Alg. 1	99.5%	94.4%	0.280
CIFAR10	ResNet18	Pretrain	100.0%	95.3%	0.898
		Retrain	100.0%	95.3%	0.891
		Synthetic	94.0%	89.7%	0.844
		LabelDP	85.8%	83.6%	0.359
		Alg. 1	89.6%	83.1%	0.377
	ResNet50	Pretrain	100.0%	95.2%	0.900
		Retrain	100.0%	95.0%	0.891
		Synthetic	91.4%	87.4%	0.818
		LabelDP	85.5%	83.4%	0.334
		Alg. 1	94.7%	90.0%	0.270
CIFAR100	ResNet50	Pretrain	100.0%	78.3%	0.902
		Retrain	100.0%	78.3%	0.765
		Synthetic	17.7%	17.6%	0.189
		LabelDP	8.41%	6.95%	0.203
		Alg. 1	91.4%	65.5%	0.298

Table 2: Results for Alg. 2 for logistic regression trained over MNIST, used in Fig. 2. $\theta = 0.75$ throughout.

Method	Retain Acc.	Test Acc.	Conf. Dist. (Lower Better)
Pretrain	92.1%	91.8%	0.807
Retrain	92.0%	92.1%	0.807
Synthetic	86.4%	86.0%	0.313
LabelDP	57.1%	57.4%	0.125
Alg. 1	87.8%	87.7%	0.180
Alg. 2	87.1%	87.2%	0.280

not only on the forget set but also the retain set; for a comparison of the confidence distances across the retain, test, and forget sets for LabelDP and our method, please see Tab. 4. Additionally, for larger, more complex datasets like CIFAR100, LabelDP fails entirely. Please note that we do not perform extensive hyperparameter optimization during pretraining or retraining.

We observe similar results for Alg. 2 in Tab. 2.

Table 3: Results for Alg. 1 for TinyImageNet ViT_S_16, CIFAR100 ViT_S_16, and CIFAR100 ViT_B_16.

Dataset	Model	Method	Retain Acc.	Test Acc.	Conf. Dist. (Lower Better)
TinyImageNet	ViT_S_16	Pretrain	86.7%	84.4%	0.698
		Alg. 1	84.2%	81.4%	0.057
TinyImageNet	ViT_B_16	Pretrain	95.0%	91.7%	0.822
		Alg. 1	91.8%	88.3%	0.037
CIFAR100	ViT_S_16	Pretrain	98.0%	84.7%	0.970
		Alg. 1	93.6%	80.1%	0.067
CIFAR100	ViT_B_16	Pretrain	97.0%	80.7%	0.972
		Alg. 1	92.6%	77.3%	0.038

Table 4: A comparison of the confidence distances on the retain, test, and forget sets between Alg. 1 and LabelDP. In general, we induce uniformity on only the forget set, while maintaining confidently correct predictions on the retain and test sets, while LabelDP falls short. Note that this is only for one experiment run.

Dataset	Model	Method	Retain Conf. Dist. (Higher Better)	Test Conf. Dist. (Higher Better)	Forget Conf. Dist. (Lower Better)
MNIST	ResNet18	LabelDP	0.579	0.577	0.593
		Alg. 1	0.503	0.509	0.070
KMNIST	ResNet18	LabelDP	0.495	0.466	0.530
		Alg. 1	0.870	0.828	0.257
SVHN	ResNet50	LabelDP	0.288	0.285	0.282
		Alg. 1	0.888	0.855	0.280
CIFAR10	ResNet18	LabelDP	0.371	0.365	0.359
		Alg. 1	0.724	0.690	0.377
	ResNet50	LabelDP	0.366	0.361	0.334
		Alg. 1	0.725	0.701	0.270
CIFAR100	ResNet50	LabelDP	0.182	0.156	0.203
		Alg. 1	0.576	0.470	0.298

J.3 Additional Experiments on TinyImageNet & ViT

We provide experimental results for Alg. 1 for TinyImageNet ViT_S_16, CIFAR100 ViT_S_16, and CIFAR100 ViT_B_16 in Tab. 3, observing similar behavior–in fact significantly lower confidence distance with little retain or test accuracy reduction–when compared to in Tab. 1.

J.4 LabelDP and Alg. 1 Confidence Distances for Retain, Test, and Forget Sets

Here, we present Tab. 4, which details the confidence distances for the retain, test, and forget sets of our method vs. LabelDP. Not only do we achieve better retain and test accuracy, but also we induce uniformity on *only* the forget set, while LabelDP induces uniformity on the forget, retain, and test sets altogether, functionally the same as adjusting the temperature. This does not suffice for our threat model, since we want to preserve confident predictions on the retain and test sets.

J.5 Pareto Frontier Main Paper Table

The results which correspond to Fig. 3a, Fig. 3b, and Fig. 6 are included in Tab. 5.

J.6 Optimization Dynamics Main Paper Table

Results as used in Fig. 4b, Fig. 4a, and Fig. 7 are included in Tab. 6.

Table 5: Results for Alg. 1 and Alg. 2 as we explore the Pareto frontier over MNIST, single run for Fig. 3a, Fig. 3b, and Fig. 6.

Model	θ	Retain Acc.	Test Acc.	Conf. Dist. (Lower Better)
LogReg	0.0	93.7%	92.9%	0.817
	0.25	92.9%	92.4%	0.178
	0.5	92.4%	92.1%	0.342
	0.75	91.6%	91.2%	0.263
	0.95	89.2%	89.1%	0.169
Cert. LogReg	0.0	92.5%	92.2%	0.738
	0.25	91.6%	91.5%	0.324
	0.5	90.5%	90.6%	0.300
	0.75	87.1%	87.2%	0.280
	0.95	85.0%	85.7%	0.092
MLP	0.0	100.0%	98.1%	0.893
	0.25	99.8%	97.4%	0.068
	0.5	99.5%	97.1%	0.037
	0.75	97.5 %	95.7%	0.037
	0.95	91.3%	90.0%	0.029
ResNet18	0.0	99.6%	99.4%	0.896
	0.25	97.2%	97.5%	0.427
	0.5	97.0%	97.0%	0.357
	0.75	97.0%	97.0%	0.151
	0.95	93.6%	94.0%	0.288

J.7 Evaluating Test-Time Privacy Attacks

In what follows, we assume a test-time privacy (TTP) adversary with white-box model access.

Our first simple algorithm is to add a small amount of uniformly sampled Gaussian noise, presented in Alg. 5. We find that this is not very effective in increasing confidence distance, as demonstrated in Tab. 7 and Tab. 8. When it brings the confidence distances from low to moderate, the model is usually confidently wrong, as demonstrated in Tab. 9.

One way to more optimally attack the TTP of a pretrained model is by finding instances in a ϕ-ball around the forget set instances that maximize the prediction confidence. To design such an attack, suppose we have a pretrained classifier $f_{\boldsymbol{w}^*} : \mathcal{X} \to \Delta_{|\mathcal{Y}|}$. Here, $f_{\boldsymbol{w}}(\boldsymbol{x}) = \text{softmax}(\boldsymbol{z}(\boldsymbol{x}))$, for $\boldsymbol{x} \in \mathcal{X}$, where $\boldsymbol{z}$ is a vector of logits. For a forget set instance, we begin by adding a small amount of uniform noise to break symmetry and obtain a nonzero gradient. We then want to obtain the worst-case perturbation over the logits by solving the optimization problem:

$$\max_{\phi} \max_{j} \boldsymbol{z}^{(j)}_{\boldsymbol{w}^*}(\boldsymbol{x} + \phi), \tag{153}$$

$$\text{s.t. } ||\phi||_\infty \leq \gamma. \tag{154}$$

Since the $\max$ function is not differentiable everywhere, we use LogSumExp to approximate it. Denote $\rho(f_{\boldsymbol{w}}(\boldsymbol{x} + \boldsymbol{\phi})) = \log \sum_{j=1}^{|\mathcal{Y}|} \boldsymbol{z}^j_{\boldsymbol{w}}(\boldsymbol{x} + \phi)$. This yields the optimization problem:

$$\max_{\phi} \rho(f_{\boldsymbol{w}^*}(\boldsymbol{x} + \delta)), \tag{155}$$

$$\text{s.t. } ||\phi||_\infty \leq \gamma. \tag{156}$$

Following the Fast Gradient Sign Method (FGSM), a simple white-box attack used to generate adversarial examples (Goodfellow et al., 2015), we design an attack as Alg. 6. Intuitively, we take a single linear step towards maximizing the function. We design also design stronger attack based on

Table 6: Studying the optimization dynamics of Alg. 1. Used in Fig. 4.

Dataset	Model	Epoch	Retain Acc.	Test Acc.	Conf. Dist. (Lower Better)
CIFAR10	ResNet8	0	98.9%	90.8%	0.883
		10	88.9%	80.4%	0.713
		20	90.8%	83.1%	0.539
		30	92.9%	85.3%	0.386
		40	95.4%	87.3%	0.295
		50	96.5%	88.9%	0.263
		60	97.3%	89.9%	0.261
		70	97.9%	90.0%	0.295
		80	98.2%	90.4%	0.270
		90	98.6%	90.5%	0.276
		100	98.9%	90.9%	0.245
CIFAR10	ResNet50	0	100.0%	95.2%	0.899
		10	72.5%	66.4%	0.593
		20	77.9%	75.0%	0.176
		30	88.8%	85.3%	0.131
		40	92.9%	88.7%	0.231
		50	96.1%	91.1%	0.394
		60	98.0%	92.5%	0.459
		70	98.9%	93.2%	0.579
		80	99.4%	93.7%	0.636
		90	99.6%	94.0%	0.665
		100	99.7%	94.0%	0.665
CIFAR100	ResNet8	0	96.4%	67.8%	0.515
		10	84.9%	59.2%	0.112
		20	89.5%	63.4%	0.063
		30	93.0%	67.3%	0.048
		40	94.6%	68.5%	0.046
		50	95.2%	69.0%	0.038
		60	95.6%	69.4%	0.036
		70	95.9%	69.5%	0.031
		80	96.0%	69.8%	0.030
		90	96.1%	70.0%	0.026
		100	96.2%	70.2%	0.026
CIFAR100	ResNet50	0	100.0%	78.3%	0.906
		10	64.9%	50.8%	0.170
		20	83.6%	65.6%	0.348
		30	93.1%	71.7%	0.419
		40	96.9%	74.4%	0.467
		50	98.7%	75.5%	0.505
		60	99.4%	76.4%	0.519
		70	99.7%	76.7%	0.530
		80	99.8%	76.5%	0.546
		90	99.8%	76.8%	0.555
		100	99.9%	77.3%	0.561

Algorithm 5 Gaussian Noise White-Box Test Time Privacy Attack

Require: Forget set $\mathcal{D}_f$; pretrained model $\boldsymbol{w}^* = \mathcal{A}(\mathcal{D})$; adversarial γ
  $\mathcal{D}_f^{adv} = []$
  for $i = 1, ..., |\mathcal{D}_f|$ **do**
    $\boldsymbol{x}_{adv} = \mathcal{D}_f^{(i)} + \beta$, $\beta \sim \mathcal{N}(0, \gamma \boldsymbol{I})$
    $\mathcal{D}_f^{adv,(i)} = \boldsymbol{x}_{\text{adv}}$
  end for
    return $\mathcal{D}_f^{\text{adv}}$

Algorithm 6 FGSM-Style White-Box Test Time Privacy Attack

Require: Forget set $\mathcal{D}_f$; pretrained model $\boldsymbol{w}^* = \mathcal{A}(\mathcal{D})$; adversarial γ; symmetry breaking α
  $\mathcal{D}_f^{adv} = []$
  for $i = 1, ..., |\mathcal{D}_f|$ **do**
    $\boldsymbol{x}_0 = \mathcal{D}_f^{(i)} + \beta$, $\beta \sim U([-\alpha\gamma, \alpha\gamma])$
    $\boldsymbol{x}_{\text{adv}} = \mathcal{D}_f^{(i)} + \gamma \text{sign}(\nabla_{\boldsymbol{x}} \rho(f_{\boldsymbol{w}^*}(\boldsymbol{x}))\Big|_{\boldsymbol{x}=\boldsymbol{x}_0})$
    $\mathcal{D}_f^{adv,(i)} = \boldsymbol{x}_{\text{adv}}$
  end for
    return $\mathcal{D}_f^{\text{adv}}$

Projected Gradient Descent (PGD) (Madry et al., 2018) as Alg. 7, taking 40 steps while incrementally maximizing the confidence function while projecting back to the ball around the original instance.

The results are in Tab. 7 and Tab. 8. We see that our method effectively defends against it for various choices of γ in most scenarios. In our choices of γ, we follow the adversarial robustness literature, choosing γ sufficiently small such that the perturbation is invisible to the naked eye, but sufficiently large such that our attack is effective. However, in some cases, the attacks succeed despite the use of our method. Still, as demonstrated in Tab. 9, we find that our algorithm renders the forget accuracy very low in these cases. As such, the adversary cannot be confidently correct–rather, in most cases, they can at best be confidently wrong.

J.8 Robustness of Alg. 1 Classifier on Neighboring Test Instances

To illustrate what happens for the finetuned classifier on neighboring test instances, we run an experiment evaluating accuracy and average confidence distance on test instances which are nearest neighbors to forget instances. Specifically, for each forget instance $\mathbf{x} \in \mathcal{D}_f$, we found the nearest

Algorithm 7 PGD-Style White-Box Test Time Privacy Attack

Require: Forget set $\mathcal{D}_f$; pretrained model $\boldsymbol{w}^* = \mathcal{A}(\mathcal{D})$; adversarial γ; symmetry breaking α; step count N
  $\mathcal{D}_f^{adv} = []$
  for $i = 1, ..., |\mathcal{D}_f|$ **do**
    $\boldsymbol{x}_{adv}^0 = \mathcal{D}_f^{(i)} + \beta$, $\beta \sim U([-\alpha\gamma, \alpha\gamma])$
    for $j = 1, ..., N$ **do**
      $\boldsymbol{x}_{adv}^j = \boldsymbol{x}_{adv}^{j-1} + \beta \text{sign}(\nabla_{\boldsymbol{x}} \rho(f_{\boldsymbol{w}^*}(\boldsymbol{x}))\Big|_{\boldsymbol{x}=\boldsymbol{x}_0})$
      $\boldsymbol{x}_{adv}^j = \prod_{\mathcal{B}_\gamma(\mathcal{D}_f^{(i)})}(\boldsymbol{x}_{adv})$
    end for
    $\mathcal{D}_f^{adv,(i)} = \boldsymbol{x}_{\text{adv}}^N$
  end for
    return $\mathcal{D}_f^{\text{adv}}$

Table 7: Confidence distances over the forget set after Alg. 5, Alg. 6, and Alg. 7 are applied to pretrained models and models finetuned with Alg. 1 for MNIST and KMNIST. Lower is better.

Dataset	Model	γ	Method	Attack	Prior Conf. Dist. (Lower Better)	Attack Conf. Dist. (Lower Better)
MNIST	MLP	$\frac{2}{255}$	Pretrain	Alg. 6	0.879	0.884
			Alg. 1	Alg. 5	0.037	0.043
				Alg. 6	0.037	0.054
				Alg. 7	0.037	0.185
		$\frac{5}{255}$	Pretrain	Alg. 6	0.879	0.888
			Alg. 1	Alg. 5	0.037	0.064
				Alg. 6	0.037	0.089
				Alg. 7	0.037	0.488
		$\frac{8}{255}$	Pretrain	Alg. 6	0.879	0.891
			Alg. 1	Alg. 5	0.037	0.091
				Alg. 6	0.037	0.125
				Alg. 7	0.037	0.632
	ResNet18	$\frac{2}{255}$	Pretrain	Alg. 6	0.895	0.896
			Alg. 1	Alg. 5	0.070	0.075
				Alg. 6	0.070	0.133
				Alg. 7	0.070	0.133
		$\frac{5}{255}$	Pretrain	Alg. 6	0.895	0.897
			Alg. 1	Alg. 5	0.070	0.088
				Alg. 6	0.070	0.164
				Alg. 7	0.070	0.350
		$\frac{8}{255}$	Pretrain	Alg. 6	0.895	0.898
			Alg. 1	Alg. 5	0.070	0.116
				Alg. 6	0.070	0.248
				Alg. 7	0.070	0.638
KMNIST	ResNet18	$\frac{2}{255}$	Pretrain	Alg. 6	0.858	0.865
			Alg. 1	Alg. 5	0.257	0.258
				Alg. 6	0.257	0.302
				Alg. 7	0.257	0.317
		$\frac{5}{255}$	Pretrain	Alg. 6	0.858	0.872
			Alg. 1	Alg. 5	0.257	0.259
				Alg. 6	0.257	0.370
				Alg. 7	0.257	0.420
		$\frac{8}{255}$	Pretrain	Alg. 6	0.858	0.878
			Alg. 1	Alg. 5	0.257	0.259
				Alg. 6	0.257	0.433
				Alg. 7	0.257	0.520

neighbor of $\mathbf{x}$ in the test set. We evaluated this nearest neighbor in pixel space with respect to the ℓ_2 distance.

Results are in Tab. 10. We notice that the classifier works as intended. That is, we obtain high accuracy as well as high confidence distance on the test set, including for nearby instances. While we do observe a drop for CIFAR100 ResNet50, we also observe that the confidence distance is still much higher than the 0.298 confidence distance on the forget set.

J.9 Ensuring Test-Time Privacy for Test Instances

In our paper, we focus on training data examples because this is the basis for scenarios addressed by the GDPR, HIPAA, etc. Providing the same guarantee for non-training (test) data is an equally important problem. However, the proposed method can be extended to cover this new case without loss of generality. One can just finetune on test instances highlighted to be corrupted and then run Alg. 1. In Tab. 11, we find that finetuning with test instances yields similar performance to using our algorithm over just the training instances.

Table 8: Confidence distances over the forget set after Alg. 5, Alg. 6, and Alg. 7 are applied to pretrained models and models finetuned with Alg. 1 for SVHN, CIFAR10, and CIFAR100. Lower is better.

Dataset	Model	γ	Method	Attack	Prior Conf. Dist. (Lower Better)	Attack Conf. Dist. (Lower Better)
SVHN	ResNet50	$\frac{1}{255}$	Pretrain	Alg. 6	0.972	0.886
			Alg. 1	Alg. 5	0.289	0.519
				Alg. 6	0.289	0.571
				Alg. 7	0.289	0.582
		$\frac{2}{255}$	Pretrain	Alg. 6	0.972	0.904
			Alg. 1	Alg. 5	0.289	0.519
				Alg. 6	0.289	0.613
				Alg. 7	0.289	0.640
CIFAR10	ResNet18	$\frac{1}{255}$	Pretrain	Alg. 6	0.898	0.898
			Alg. 1	Alg. 5	0.377	0.300
				Alg. 6	0.377	0.353
				Alg. 7	0.377	0.356
		$\frac{2}{255}$	Pretrain	Alg. 6	0.898	0.822
			Alg. 1	Alg. 5	0.377	0.301
				Alg. 6	0.377	0.397
				Alg. 7	0.377	0.408
	ResNet50	$\frac{1}{255}$	Pretrain	Alg. 6	0.900	0.806
			Alg. 1	Alg. 5	0.270	0.336
				Alg. 6	0.270	0.374
				Alg. 7	0.270	0.378
		$\frac{2}{255}$	Pretrain	Alg. 6	0.900	0.827
			Alg. 1	Alg. 5	0.270	0.336
				Alg. 6	0.270	0.407
				Alg. 7	0.270	0.425
CIFAR100	ResNet50	$\frac{1}{255}$	Pretrain	Alg. 6	0.906	0.587
			Alg. 1	Alg. 5	0.298	0.275
				Alg. 6	0.298	0.360
				Alg. 7	0.298	0.373
		$\frac{2}{255}$	Pretrain	Alg. 6	0.906	0.652
			Alg. 1	Alg. 5	0.298	0.276
				Alg. 6	0.298	0.421
				Alg. 7	0.298	0.468

J.10 New Metric for Uniformity Evaluation

The ℓ_2 metric $||f(\mathbf{x}) - \frac{\vec{1}}{K}||_2$ has similar utility to our presented metric. However, it is slightly less interpretable and may accidentally overpenalize uncertain outputs. For example, if one class has no probability but the other 9 classes are uniform. Still, as demonstrated in Tab. 12, we find that we minimize this metric as well for the same models and datasets. This holds similarly for other potential metrics e.g. the ℓ_1 metric.

J.11 Tightness of Bound in Theorem 3.5

To evaluate how tight our bound is, we run an experiment for MNIST logistic regression. We use the notation of theorem 3.5 in Tab. 13. We find that our constant bound is fairly tight as $\theta \to 1$; we leave using more advanced techniques to ensure better tightness to future work.

J.12 Proportions of Time Elapsed in Alg. 1

Results are reported in Tab. 14.

Table 9: Accuracies over the forget set after Alg. 6 and Alg. 7 are applied to pretrained models and models finetuned with Alg. 1 for SVHN, CIFAR10, and CIFAR100. We see that Alg. 1 significantly lowers forget set accuracy.

Dataset	Model	γ	Method	Attack	Prior. Forget Acc. (Lower Better)	Atk. Forget Acc. (Lower Better)
MNIST	MLP	$\frac{5}{255}$	Pretrain	Alg. 7	97.0%	96.0%
			Alg. 1	Alg. 7	71.0%	43.0%
		$\frac{8}{255}$	Pretrain	Alg. 7	98.3%	96.0%
			Alg. 1	Alg. 7	71.0%	41.0%
	ResNet18	$\frac{8}{255}$	Pretrain	Alg. 7	98.9%	100.0%
			Alg. 1	Alg. 7	28.0%	54.0%
KMNIST	ResNet18	$\frac{8}{255}$	Pretrain	Alg. 7	96.0%	96.0%
			Alg. 1	Alg. 7	50.0%	55.0%
SVHN	ResNet50	$\frac{1}{255}$	Pretrain	Alg. 6	97.0%	66.0%
			Alg. 1	Alg. 5	40.0%	53.0%
				Alg. 6	40.0%	52.0%
				Alg. 7	40.0%	52.0%
		$\frac{2}{255}$	Pretrain	Alg. 6	97.0%	66.0%
			Alg. 1	Alg. 5	40.0%	52.0%
				Alg. 6	40.0%	53.0%
				Alg. 7	40.0%	53.0%
CIFAR10	ResNet18	$\frac{1}{255}$	Pretrain	Alg. 6	100.0%	61.0%
			Alg. 1	Alg. 5	60.0%	35.0%
				Alg. 6	60.0%	34.0%
				Alg. 7	60.0%	34.0%
		$\frac{2}{255}$	Pretrain	Alg. 6	100.0%	61.0%
			Alg. 1	Alg. 5	60.0%	35.0%
				Alg. 6	60.0%	33.0%
				Alg. 7	60.0%	32.0%
	ResNet50	$\frac{1}{255}$	Pretrain	Alg. 6	100.0%	56.0%
			Alg. 1	Alg. 5	55.0%	33.0%
				Alg. 6	55.0%	30.0%
				Alg. 7	55.0%	30.0%
		$\frac{2}{255}$	Pretrain	Alg. 6	100.0%	56.0%
			Alg. 1	Alg. 5	55.0%	30.0%
				Alg. 6	55.0%	30.0%
				Alg. 7	55.0%	32.0%
CIFAR100	ResNet50	$\frac{1}{255}$	Pretrain	Alg. 6	100.0%	32.0%
			Alg. 1	Alg. 5	48.0%	11.0%
				Alg. 6	48.0%	10.0%
				Alg. 7	48.0%	11.0%
		$\frac{2}{255}$	Pretrain	Alg. 6	100.0%	32.0%
			Alg. 1	Alg. 5	48.0%	11.0%
				Alg. 6	48.0%	10.0%
				Alg. 7	48.0%	11.0%

J.13 Warmup Values for MNIST LogReg

Results are contained in Tab. 15. We find that after applying the certified Newton step in Alg. 2, we obtain better retain and test accuracy, at small cost to uniformity. Thus, warming up is not the only component of achieving good results in Alg. 2.

J.14 Results for KMNIST LogReg and MLP

Results are contained in Tab. 16. As mentioned in Sec. 4, one can see that a small model for a more complex benchmark, logistic regression on KMNIST, fails to induce uniformity, since the pretrained

Table 10: Accuracies and confidence distances for test instances which are nearest neighbors (with respect to ℓ_2 distance) of forget set instances. We observe that models continue to confidently and correctly classify nearby test instances after finetuning with Alg. 1.

Dataset	Model	Method	Acc.	Conf. Dist. (Higher Better)
MNIST	MLP	Pretrain	100.0%	0.894
		Alg. 1	93.0%	0.754
	ResNet18	Pretrain	100.0%	0.896
		Alg. 1	100.0%	0.875
KMNIST	ResNet18	Pretrain	99.0%	0.871
		Alg. 1	99.0%	0.850
SVHN	ResNet50	Pretrain	95.0%	0.982
		Alg. 1	95.0%	0.939
CIFAR10	ResNet18	Pretrain	98.0%	0.876
		Alg. 1	85.0%	0.538
	ResNet50	Pretrain	96.0%	0.884
		Alg. 1	90.0%	0.700
CIFAR100	ResNet50	Pretrain	78.0%	0.778
		Alg. 1	66.0%	0.484

model is too small to generalize. However, on a bigger model i.e. an MLP trained over KMNIST, since it is large enough to generalize, one can induce uniformity over it. Thus, larger models which generalize well are preferred for our method, in line with the goals of ML.

J.15 Ablation Study on Forget Set Size

Throughout our experiments, we use a forget set size of 100. We do so because for our use case, it is likely that a data controller would want to induce uniformity only for a small number of instances. In Tab. 17, we provide experiments on MLP trained over MNIST for Alg. 1 and logistic regression trained over MNIST for Alg. 2. We observe that as one increases the forget set size, it becomes harder to induce uniformity with the same hyperparameters. Still, for Alg. 1, we are able to obtain strong uniformity with good retain and test accuracy for significantly larger forget set sizes. Furthermore, we observe that Alg. 2 fails for sufficiently large forget set size; this is likely because Hessian matrix is significantly larger (in norm) for a larger forget set, resulting in a catastrophically large Newton step. Mitigating this phenomenon is left to future work, where Hessian-free techniques like those of Qiao et al. (2025) may be advantageous.

J.16 Ablation Study on Synthetic Baseline Sample Size

Below, we study what we happen if we increase the number of samples sampled in the ε-ball in the synthetic baseline. For each forget set instance, we sample k instances from the ε-ball around the forget set, and then assign random labels to these instances, yielding an additional $|\mathcal{D}_f|k$ instances in the training data. We then retrain the model over the retain set along with these new $|\mathcal{D}_f|k$ instances. For a MLP trained over MNIST, we observe better performance as we increase sample size. However, for a ResNet18 trained over CIFAR10, even if we have a very large sample size. This is presented in Tab. 18. Thus, since Alg. 1 can induce uniformity as shown in Tab. 1, without great cost to retain or test accuracy, it is better than the synthetic baseline.

J.17 Test Accuracy Plot for Pareto Frontier Experiments

We provide a plot characterizing test accuracy for Alg. 1 and Alg. 2 applied on MNIST for various choices of θ in Fig. 6.

Table 11: Finetuning on test instances and running Alg. 1. Here, "pretrain" denotes the initially pretrained model (no additional test instances), while other rows correspond to finetuning on the specified number of test instances.

Dataset	Model	% Forget Size	Method	Retain Acc.	Test Acc.	Conf. Dist. (Lower Better)
MNIST	MLP	0	Pretrain	98.3%	97.0%	0.879
			Alg. 1	97.5%	95.7%	0.037
		1/5	Pretrain	99.1%	97.3%	0.892
			Alg. 1	96.4%	93.9%	0.147
		1/2	Pretrain	99.0%	97.1%	0.896
			Alg. 1	96.2%	93.4%	0.157
	ResNet18	0	Pretrain	99.2%	98.9%	0.879
			Alg. 1	99.6%	99.1%	0.070
		1/5	Pretrain	98.9%	98.5%	0.884
			Alg. 1	99.6%	98.9%	0.181
		1/2	Pretrain	99.4%	100.0%	0.897
			Alg. 1	99.5%	98.7%	0.243
KMNIST	ResNet18	0	Pretrain	98.2%	92.1%	0.880
			Alg. 1	99.1%	94.7%	0.257
		1/5	Pretrain	100.0%	97.5%	0.900
			Alg. 1	99.7%	96.5%	0.301
		1/2	Pretrain	100.0%	97.7%	0.895
			Alg. 1	99.5%	96.9%	0.233
SVHN	ResNet50	0	Pretrain	99.5%	94.4%	0.971
			Alg. 1	99.0%	94.4%	0.280
		1/5	Pretrain	99.7%	94.6%	0.974
			Alg. 1	99.2%	94.4%	0.184
		1/2	Pretrain	99.5%	94.5%	0.986
			Alg. 1	99.8%	95.1%	0.391
CIFAR10	ResNet18	0	Pretrain	100.0%	95.3%	0.898
			Alg. 1	89.6%	83.1%	0.377
		1/5	Pretrain	100.0%	98.4%	0.894
			Alg. 1	89.4%	85.6%	0.358
		1/2	Pretrain	100.0%	93.5%	0.887
			Alg. 1	87.9%	83.7%	0.494
	ResNet50	0	Pretrain	100.0%	95.2%	0.900
			Alg. 1	94.7%	90.0%	0.270
		1/5	Pretrain	99.9%	93.4%	0.896
			Alg. 1	91.6%	87.1%	0.392
		1/2	Pretrain	99.8%	93.6%	0.894
			Alg. 1	89.1%	86.7%	0.390
CIFAR100	ResNet50	0	Pretrain	100.0%	78.3%	0.902
			Alg. 1	91.4%	65.5%	0.298
		1/5	Pretrain	100.0%	79.0%	0.880
			Alg. 1	93.5%	69.1%	0.021
		1/2	Pretrain	99.9%	78.2%	0.860
			Alg. 1	97.9%	72.8%	0.221

J.18 Test Accuracy Plot for Optimization Dynamics Experiments

We provide a plot characterizing how test accuracy for Alg. 1 and Alg. 2 applied on CIFAR10 and CIFAR100 for $\theta = 0.75$ changes over 100 epochs in Fig. 7 for ResNet8 and ResNet50. We observe similar behavior to retain accuracy.

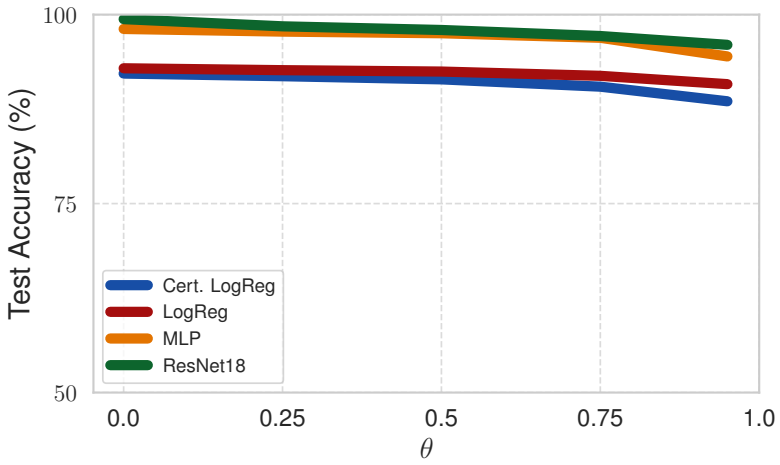

Figure 6: Test Accuracy vs. θ, MNIST. This has similar behavior to Fig. 3b.

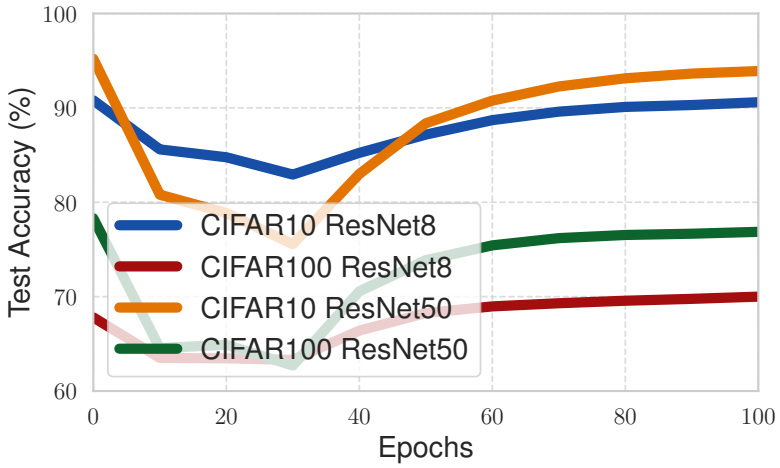

Figure 7: Test Accuracy vs. Epochs, $\theta = 0.75$, MNIST. This has similar behavior to Fig. 4b

Table 12: ℓ_2 confidence distances for models finetuned with Alg. 1.

Dataset	Model	Conf. Dist. Type	Pretrained (Lower Better)	Alg. 1 (Lower Better)
MNIST	MLP	Paper	0.879	0.037
		ℓ_2	0.930	0.053
	ResNet18	Paper	0.895	0.070
		ℓ_2	0.944	0.070
KMNIST	ResNet18	Paper	0.880	0.257
		ℓ_2	0.911	0.302
SVHN	ResNet50	Paper	0.972	0.289
		ℓ_2	0.979	0.298
CIFAR10	ResNet18	Paper	0.898	0.377
		ℓ_2	0.947	0.435
	ResNet50	Paper	0.900	0.270
		ℓ_2	0.948	0.323
CIFAR100	ResNet50	Paper	0.902	0.298
		ℓ_2	0.911	0.311

Table 13: Comparison of bounds

$\alpha^* - \alpha(1)$	**O(1) bound size**
1.678	3.374

K Broader Impacts

Potential positive impacts are motivated by the threat model as discussed in Sec. 1 and Sec. A ; per our example provided in the introduction, violations of test-time privacy constitute a real threat for ML safety. Hence, providing the defense that we do constitutes a positive societal impact. However, we acknowledge the potential danger in providing a new threat model–it is possible that potential adversaries had not thought of this before. Still, we provide a way to address this threat.

Table 14: Time proportions of each step in Alg. 1.

Dataset	Model	Retain Grad.	Forget Grad.	Surgery	Reg. Grad.	Step
MNIST	MLP	0.967	0.033	0.000	0.000	0.000
	ResNet18	0.984	0.016	0.0010	0.000	0.000
KMNIST	ResNet18	0.989	0.011	0.000	0.000	0.000
SVHN	ResNet50	0.980	0.020	0.000	0.000	0.000
CIFAR10	ResNet18	0.989	0.011	0.000	0.000	0.000
	ResNet50	0.992	0.008	0.000	0.000	0.000
CIFAR100	ResNet50	0.993	0.006	0.000	0.000	0.000

Table 15: Warmup values for Alg. 2 for logistic regression trained over MNIST, contrasted with the values after Alg. 2 is applied.

θ	**Method**	**Retain Acc.**	**Test Acc.**	**Conf. Dist. (Lower Better)**
0.0	Warmup	91.4%	91.6%	0.765
0.0	Alg. 2	92.5%	92.2%	0.738
0.25	Warmup	90.1%	90.4%	0.283
0.25	Alg. 2	91.6%	91.5%	0.324
0.50	Warmup	89.3%	89.7%	0.215
0.50	Alg. 2	90.5%	90.6%	0.300
0.75	Warmup	88.4%	88.6%	0.154
0.75	Alg. 2	87.1%	87.2%	0.280
0.95	Warmup	85.4%	86.0%	0.097
0.95	Alg. 2	85.0%	85.7%	0.092

Table 16: Results for Alg. 1 applied to logistic regression and MLP trained over KMNIST, $\theta = 0.75$ for Alg. 1.

Model	**Method**	**Retain Acc.**	**Test Acc.**	**Conf. Dist. (Lower Better)**
LogReg	Pretrain	81.4%	66.4%	0.775
	Retrain	80.9%	65.3%	0.770
	Alg. 1	77.4%	63.4%	0.770
MLP	Pretrain	100%	88.4%	0.900
	Retrain	100%	88.5%	0.887
	Alg. 1	92.8%	80.3%	0.039

Table 17: Results on applying Alg. 1 and Alg. 2 on various forget set sizes over MNIST. We observe that, while Alg. 1 still works well, confidence distance increases as forget set size does; please see Sec. J.15 for a discussion on Alg. 2. $\theta = 0.75$ throughout.

Method	**Model**	**Forget Size**	**Retain Acc.**	**Test Acc.**	**Conf. Dist. (Lower Better)**
Alg. 1	MLP	100	97.5%	95.7%	0.037
		250	97.6%	95.1%	0.010
		500	95.8%	93.8%	0.121
		1000	94.8%	93.3%	0.162
		5000	96.6%	95.0%	0.420
Alg. 2	LogReg	100	92.1%	91.8%	0.258
		250	85.4%	85.2%	0.243
		500	5.7%	5.9%	0.824
		1000	4.4%	4.6%	0.891
		5000	2.4%	2.5%	0.899

Table 18: Results for the synthetic baseline applied with various sampled k on a MLP over MNIST and a ResNet18 over CIFAR10. We observe that increasing k yields better performance, but nevertheless even very large k (an additional 50k instances, with a forget set size of 100) fails to induce uniformity for CIFAR10.

Dataset	**Model**	**Sampled k**	**Retain Acc.**	**Test Acc.**	**Conf. Dist. (Lower Better)**
MNIST	MLP	5	99.4%	97.1%	0.541
		25	99.0%	96.4%	0.183
		125	99.4%	96.8%	0.105
		250	98.6%	96.0%	0.066
		500	99.6%	96.3%	0.003
CIFAR10	ResNet18	5	99.0%	91.0%	0.683
		25	99.2%	91.3%	0.865
		125	98.8%	90.9%	0.856
		250	98.4%	90.7%	0.869
		500	98.3%	91.1%	0.852
		5000	94.0%	89.7%	0.844

L SYMBOL TABLE

Symbols	
f	A pretrained classifier
f_u	A pretrained classifier after unlearning has been conducted over $\boldsymbol{x}_p$
$\boldsymbol{x}_p$	A data instance corresponding to person p
$\mathcal{X}$	A sample space, subset of $\mathbb{R}^d$
$\mathcal{Y}$	A label space, subset of $\mathbb{R}^o$
$\mathcal{Z}$	The Cartesian product of a sample space and a label space. This is the space where a dataset is drawn from.
$\mathcal{D}$	A dataset, subset of $\mathcal{Z}^n$, which is the n-fold Cartesian product of $\mathcal{Z}$. This represents a set of n data instances.
$\mathcal{D}_f$	A forget set, a subset of a dataset $\mathcal{D}$
$\mathcal{D}_r$	A retain set, the complement of the forget set in $\mathcal{D}$
$\mathcal{W}$	A space of parameters, subset of $\mathbb{R}^p$
$\mathcal{A}$	A function that maps datasets to parameters; this represents the learning algorithm that a ML model provider uses throughout our paper.
$\mathcal{H}_{\mathcal{W}}$	A set of functions which map samples in $\mathcal{X}$ to the probability simplex $\Delta_{\lvert\mathcal{Y}\rvert}$, parameterized by a $\boldsymbol{w} \in \mathcal{W}$.
$\lvert\lvert\boldsymbol{w}\rvert\rvert_2$	The ℓ_2 norm of a vector $\boldsymbol{w}$
$\lvert\lvert A\rvert\rvert_2$	The 2 operator norm of a matrix $\boldsymbol{A}$
$\lambda_{\min}(\boldsymbol{A})$	The minimum eigenvalue of a matrix $\boldsymbol{A}$
$\mathcal{K}$	A uniform learner, which maps samples to parameters which, when one parametrizes a function by any such parameter, a uniform distribution over all possible labels, $U[0, \lvert\mathcal{Y}\rvert]$ is outputted.
$f_{\boldsymbol{w}}$	A classifier parameterized by a parameter $\boldsymbol{w} \in \mathcal{W}$
$\mathcal{L}_{\mathcal{A}}$	A loss function to yield accurate predictions e.g. the cross entropy loss between model predictions and labels
$\mathcal{L}_{\mathcal{K}}$	A loss function to yield accurate uniformity e.g. the Kullback-Liebler divergence between softmax outputs and uniform distribution
θ	A trade off parameter in $(0, 1)$ between utility and uniformity
$\mathcal{M}_\theta$	A map between datasets and parameters that is the minimizer of a Pareto objective between $\mathcal{L}_{\mathcal{A}}$ and $\mathcal{L}_{\mathcal{K}}$, where θ spans the (convex) Pareto frontier

Symbols

λ	A regularization/weight decay parameter added to the objective of $\mathcal{M}_\theta$ for local convex approximation
C	A bound on the model weights
$L_\mathcal{K}$	The Lipschitz constant for the gradients of $\ell_\mathcal{K}$, the component loss functions of $\mathcal{L}_\mathcal{K}$, from Asm. 3.3
$L_\mathcal{A}$	The Lipschitz constant for the gradients of $\ell_\mathcal{A}$, the component loss functions of $\mathcal{L}_\mathcal{A}$, from Asm. 3.3
$M_\mathcal{K}$	The Lipschitz constant for the Hessians of $\ell_\mathcal{K}$, the component loss functions of $\mathcal{L}_\mathcal{K}$, from Asm. 3.4
$M_\mathcal{A}$	The Lipschitz constant for the Hessians of $\ell_\mathcal{A}$, the component loss functions of $\mathcal{L}$, from Asm. 3.4
L	A convex combination of $L_\mathcal{K}$ and $L_\mathcal{A}$ with respect to θ
M	A convex combination of $M_\mathcal{K}$ and $M_\mathcal{A}$ with respect to θ
$\mathcal{N}(0, \sigma^2 \boldsymbol{I})$	The standard normal distribution with an isotropic covariance matrix
$\nabla_{\boldsymbol{w}^*,\mathcal{K},\mathcal{A}}$	The gradient of the Pareto objective evaluated at $\boldsymbol{w}^*$, used in the main paper with regularization
$\boldsymbol{H}_{\boldsymbol{w}^*,\mathcal{K},\mathcal{A}}$	The Hessian of the Pareto objective evaluated at $\boldsymbol{w}^*$, used in the main paper without regularization